

Structure and function of K_{ATP} -channels in inspiratory neurons of mice

Dissertation
zur Erlangung des Doktorgrades
der Mathematisch-Naturwissenschaftlichen Fakultäten
der Georg-August-Universität zu Göttingen

vorgelegt von
Mirjam Haller
aus Hannover

Göttingen 2000

D7

Referent: Prof. Dr. W. Felsch

Korrefferent: Prof. Dr. D.W. Richter, Prof. Dr. E. Neher

Tag der mündlichen Prüfung: 27.4.2000

Table of contents

1	Introduction.....	1
1.1	K _{ATP} -channel structure.....	1
1.2	K _{ATP} -channel drugs.....	3
1.3	K _{ATP} -channel gating kinetics	5
1.4	Physiological role of K _{ATP} -channels in pancreas and heart	7
1.5	The respiratory network.....	8
1.6	Purinoceptors.....	10
1.7	K _{ATP} -channels in respiratory neurons	11
1.8	Measurements of the intrinsic optical signal	12
1.9	Tasks and aims of the present experiments	14
2	Materials and methods	15
2.1	Slice preparation.....	15
2.2	Solutions.....	16
2.3	Experimental setup	17
2.4	Electrophysiological recordings	20
2.5	Fluorescent indicator dye measurements.....	20
2.6	Flash photolysis.....	22
2.7	Imaging of the intrinsic optical signal	23
2.8	Molecular biology	24
3	Data analysis.....	26
3.1	K _{ATP} -channel kinetics	26
3.2	K _{ATP} -channel modulation	26
4	Results.....	29
4.1	Molecular biology of K _{ATP} -channels	29
4.2	Channel kinetics	31
4.3	Effects of K _{ATP} -channel drugs on rhythmic activity.....	40
4.4	Functional modulation of K _{ATP} -channel openings.....	42
4.4.1	Estimates of fluctuations in [ATP] _i	45
4.4.2	Exceptions from p _{open} modulation.....	47
4.4.3	Variation of cycle length.....	50
4.4.4	Effect of hypoxia on K _{ATP} -channel modulation	52
4.5	Estimation of [ATP] _i based on fluorometric measurements	54
4.6	Effect of purinoceptor activation.....	60
4.7	Flash photolysis of caged-Ca ²⁺ and caged-ATP	64
4.8	Measurements of the intrinsic optical signal (IOS)	66
4.8.1	IOS during cell swelling and hypoxia.....	66
4.8.2	The hypoxic IOS response	70
4.8.3	IOS response following application of K _{ATP} -channel drugs.....	73

5	Discussion	75
5.1	K_{ATP} -channel structure and gating kinetics.....	75
5.2	K_{ATP} -channel drugs and rhythmic activity.....	76
5.3	Periodic modulation of K_{ATP} -channel activity	76
5.4	Estimation of $[ATP]_i$ during hypoxia.....	79
5.5	Purinoreceptor activation modulates the respiratory rhythm	80
5.6	Flash photolysis	80
5.7	Intrinsic optical signal.....	81
5.7.1	Changes in cell volume	81
5.7.2	Regional differences in IOS	82
5.7.3	Mechanisms underlying the hypoxic IOS response	82
5.7.3.1	Effect of neurotransmitters on IOS.....	82
5.7.3.2	Na^+/K^+ -pump and neuronal activity.....	83
5.7.4	Involvement of mitochondrial K_{ATP} -channels in IOS generation.....	85
5.8	Conclusion and perspectives.....	86
6	Summary	89
7	Appendix.....	91
8	Abbreviations	93
9	References.....	94
	Acknowledgements	104
	Lebenslauf	105

1 Introduction

ATP-sensitive K^+ -channels (K_{ATP} -channels) are characterized by a strong inhibition of channel activity by intracellular adenosine 5'-triphosphate (ATP). When ATP, which serves as a cellular energy store, is depleted K_{ATP} -channels open to hyperpolarize the cell. Thus, they couple cell metabolism to the electrical excitability of cells modulating a variety of cellular functions, including insulin secretion from pancreatic β -cells, K^+ recycling in renal epithelia, and cytoprotection in cardiac and brain ischemia (Ashcroft, 1988; Cook et al., 1988; Misler and Giebisch, 1992; Terzic et al., 1995). They are normally closed and open only when the cell metabolism is impaired; thereby the cell is held in the resting state, which saves ATP that remains available for the processes contributing to protection of the cell. There are, however, exceptions to this rule such as the pancreatic β -cells (Ashcroft and Ashcroft, 1990; Smith et al., 1990b) or hippocampal (Trafton et al., 1996) and respiratory (Pierrefiche et al., 1996) neurons, where channels are open during the normal functioning of the cell. K_{ATP} -channels were first discovered in cardiomyocytes (Noma, 1983) and later found in a variety of other tissues, including pancreatic β -cells (Ashcroft et al., 1984; Cook and Hales, 1984), skeletal muscle (Spruce et al., 1985) and smooth muscle (Standen et al., 1989). In addition, they were described in several neurons in the brain, e.g. in the hippocampus (Zawar et al., 1999), cortex (Jiang and Haddad, 1997) and brainstem (Pierrefiche et al., 1996; Karschin et al., 1998; Xia and Haddad, 1991). In general, they can be expected to be present in cells, in which electrical activity is linked to metabolism, glucose concentration, or oxygen levels.

1.1 K_{ATP} -channel structure

K_{ATP} -channels are heteromeric structures consisting of two types of subunits (Sakura et al., 1995; Inagaki et al., 1995a): an inwardly rectifying K^+ -channel subunit (termed *Kir6.1* or *Kir6.2*) and a sulphonylurea receptor subunit (*SUR*), which is a member of the family of ATP-binding cassette (ABC) transporter proteins (Figure 1). Two different Kir6 subunit genes have been described, Kir6.1 and Kir6.2 (Sakura et al., 1995; Inagaki et al., 1995a), and the two closely related genes encoding the sulphonylurea receptors SUR1 (high affinity receptor)

and SUR2 (low affinity receptor) have also been cloned (Aguilar-Bryan et al., 1995; Inagaki et al., 1996; Isomoto et al., 1996). Three different splice variants of SUR2 were identified: SUR2A (Inagaki et al., 1996), SUR2B (Isomoto et al., 1996) and SUR2C (Chutkow et al., 1996) (following the nomenclature proposed in Ashcroft and Gribble (1998)).

Each of the Kir-channel subunits has two putative transmembrane segments and a K⁺-ion pore-forming region (H5) (Jan and Jan, 1994). Both Kir6.1 and Kir6.2 contain several potential protein kinase A- and protein kinase C-phosphorylation sites (Inagaki et al., 1995a; Inagaki et al., 1995b) as indicated in Figure 1A.

Although the SUR subunits were originally thought to have 13 transmembrane segments, a 17-transmembrane-segment model (Figure 1) was more recently proposed by Tusnady et al. (1997). SUR is thought to have three transmembrane domains, which consist of five, six and six transmembrane segments, respectively (Figure 1A). It is further assumed to contain N-linked glycosylation sites, protein kinase A- and protein kinase C-dependent phosphorylation sites, as well as two nucleotide binding folds (NBFs). Each NBF contains the Walker A and B motifs (Virsolvy-Vergine et al., 1992), which are thought to be important for nucleotide regulation of the functional activity of ABC proteins (Higgins, 1995).

The various Kir and SUR subunits combine to form functional K_{ATP}-channels with different sensitivities to nucleotides and K_{ATP}-channel drugs (see chapter 1.2). K_{ATP}-channels are the first example of a heteromultimeric complex assembled by an ion channel and a receptor that are structurally unrelated to each other. Comparison of the properties of cloned and wild-type K_{ATP}-channels suggests that the pancreatic β -cell and neuronal K_{ATP}-channels are composed of Kir6.2 and SUR1, the cardiac type of Kir6.2 and SUR2A, the smooth muscle type of Kir6.2 and SUR2B and the vascular smooth muscle type of Kir6.1 and SUR2B (Sakura et al., 1995; Inagaki et al., 1995a; Aguilar-Bryan et al., 1995; Inagaki et al., 1996; Isomoto et al., 1996; Chutkow et al., 1996; Yamada et al., 1997). An ATP-insensitive, but MgGDP-activated, channel is observed when Kir6.1 and SUR2B are coexpressed. Such a channel might correspond to the nucleotide-activated channel found in some smooth muscle cells (Yamada et al., 1997). As depicted in Figure 1B both subunits are required to coassemble in a 4:4 stoichiometry in order to form a functional channel (Clement et al., 1997; Inagaki et al., 1997; Shyng and Nichols, 1997).

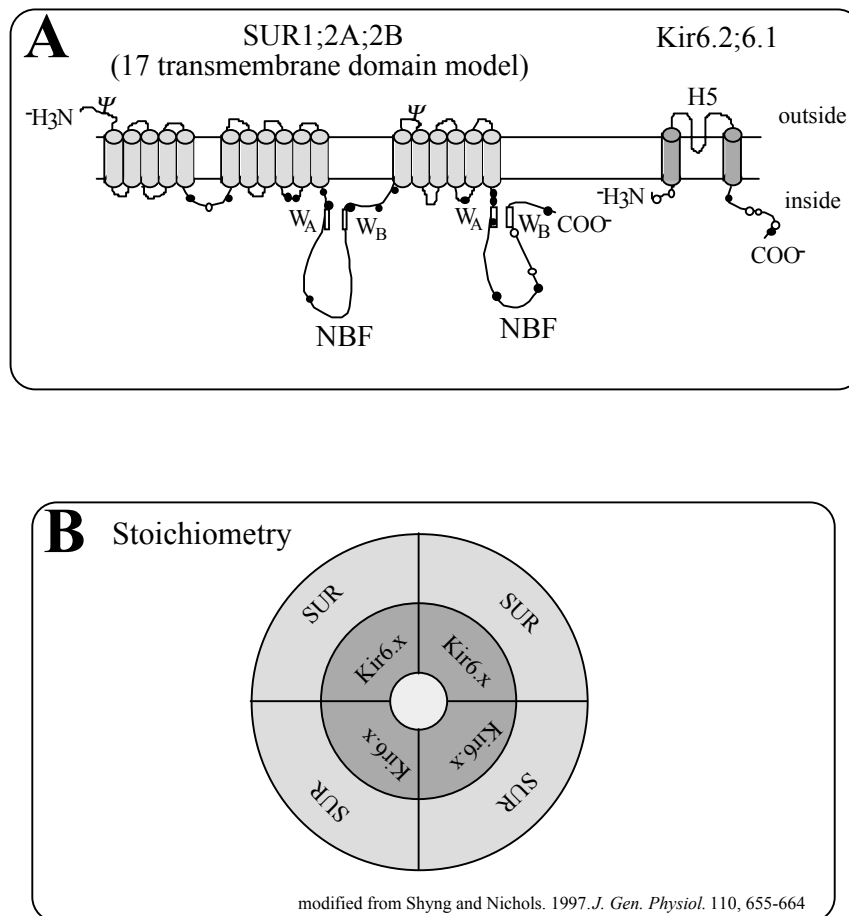


Figure 1: The K_{ATP} -channel as a complex of Kir and SUR subunits. (A) Proposed membrane topology of SUR1; 2A; 2B and Kir6.2; Kir6.1. Locations of Walker A motif (W_A) and Walker B motif (W_B) are shown by boxes. Approximate location of potential protein kinase A- and protein kinase C-dependent phosphorylation sites as well as N-linked glycosylation sites (in Kir6.2 and SUR1) are indicated by open circles, filled circles and Ψ , respectively. (B) A model for the structure of a K_{ATP} -channel, which are assumed to be hetero-octamers assembled from four Kir6.1/Kir6.2 subunits forming the K^+ ion-permeable domain and four SUR1/SUR2 subunits.

1.2 K_{ATP} -channel drugs

Excised patch experiments showed that K_{ATP} -channels in the pancreatic β -cell are inhibited by ATP, with a half-maximal inhibitory concentration (IC_{50}) ranging from 15 to 40 μM (Ashcroft and Kakei, 1989; Cook and Hales, 1984; Ohno-Shosaku et al., 1987; Rorsman et al., 1989). However, perforated patch recordings have revealed that a certain number of K_{ATP} -channels ($\sim 10\%$) could be active under resting conditions at a normal intracellular ATP

concentration that would close the channels in excised patches (Ashcroft and Ashcroft, 1990; Smith et al., 1990b). Such findings indicate that other regulators in addition to ATP govern the activity of K_{ATP} -channels. Table 1 lists the most important regulators of K_{ATP} -channels and their sites of action.

Regulator	Action	Site of action
Nucleotide triphosphates (dual action)		
1. Ligand action (ATP)	inhibition	Kir subunit
2. Hydrolysis-dependent action; phosphorylation (MgATP)	stimulation/maintenance	SUR subunit
Nucleotide diphosphates (MgADP, MgGDP)	stimulation	SUR subunit
K^+ - channel opening drugs (pinacidil, diazoxide, cromakalim)	stimulation	SUR subunit
Sulfonylurea compounds (glibenclamide, tolbutamide)	inhibition	SUR subunit
G-protein (G_α) PKA, PKC, PKG	modulation	Kir subunit and SUR subunit
pH	modulation	
Free radicals	modulation	
Disruption of cytoskeleton	stimulation	SUR subunit

Table 1: Major regulators of K_{ATP} -channels.

In contrast to the inhibition produced by ATP (ligand action), K_{ATP} -channel activity disappears gradually in ATP free conditions – a phenomenon, which is called run-down. Run-down was found to be reversed to some extent by reexposure to ATP. This action required Mg^{2+} , which suggests that MgATP maintains the channel activity through phosphorylation, i.e. through a hydrolysis-dependent action (Furukawa et al., 1994; Ohno-Shosaku et al., 1987; Takano et al., 1990). Nucleotide diphosphates, such as ADP, UDP and GDP, were discovered to exert a stimulatory effect on K_{ATP} -channels in pancreatic, cardiac and vascular smooth muscle tissues, especially in the presence of Mg^{2+} (Beech et al., 1993a; Beech et al., 1993b; Dunne and Petersen, 1986; Findlay, 1987; Kajioka et al., 1991; Terzic et al., 1994a). Several compounds that bind to the SUR subunit and stimulate K_{ATP} -channels are

collectively called K^+ -channel openers (KCOs) (Edwards and Weston, 1993; Terzic et al., 1995). Examples include diazoxide, pinacidil and cromakalim. K_{ATP} -channels are inhibited by sulphonylurea compounds such as glibenclamide and tolbutamide, which act on a different binding site on the SUR subunit. It was further reported that K_{ATP} -channels were modulated by G proteins (Kirsch et al., 1990; Terzic et al., 1994b; Mironov et al., 1999), by phosphorylation through protein kinase A (PKA), protein kinase G (PKG) and protein kinase C (PKC) (Hu et al., 1996; Light et al., 1996; Liu et al., 1996; Mironov and Richter, 2000) as well as by low acidosis or alkalosis (Cuevas et al., 1991; Koyano et al., 1993; Lederer and Nichols, 1989; Proks et al., 1994) and oxygen free radicals (Tokube et al., 1996). The channels are also modulated through the disruption of the cytoskeleton, which impairs the ability of sulphonylureas to inhibit the channel (Brady et al., 1996; Yokoshiki et al., 1997). As an underlying mechanism for this effect, it was suggested that actin filaments might connect directly or through a linking protein with the SUR subunit and that the disruption of this connection might result in the dissociation of the SUR subunit from the channel pore, thereby effectively blocking any inhibitory signal from the SUR subunit (Baines et al., 1999; Metzger et al., 1997; Yokoshiki et al., 1997; Loffler-Walz and Quast, 1998; Mironov and Richter, 2000).

1.3 K_{ATP} -channel gating kinetics

Studies of the kinetics of K_{ATP} -channels in skeletal and cardiac muscles, pancreas and neurons suggest that their kinetic behavior is complex, with one or two open and several closed states, and that channel openings are grouped into bursts separated by longer closed periods (Gillis et al., 1989; Karschin et al., 1998; Alekseev et al., 1997; Trapp et al., 1998; Davies et al., 1992; Davies, 1990; Davies et al., 1991). A number of different kinetic gating schemes have been proposed for K_{ATP} -channels. Davies et al. (1992) and Spruce et al. (1987) suggested a model for K_{ATP} -channels in frog skeletal muscle containing at least four closed and two open states (Figure 2A). Some rate constants governing the transitions to the closed states of the scheme were increased by ATP, while some rate constants governing transitions to the open states were found to decrease by ATP-binding. An alternative model containing one open (O_2) and three closed states (C_1 , C_3 , and C_4) as depicted in Figure 2B was proposed for the pancreatic

β -cell by Gillis et al. (1989). Dwell time in state C_1 corresponds to intraburst gaps, in C_3 to interburst gaps and in C_4 to gaps between clusters of bursts.

A complex kinetic model of the ATP-dependent regulation of channel activity based on the assumption of four sequential ATP-binding steps was suggested by Nichols et al. (1991) for rat ventricular myocytes. The model assumes one ATP-independent closed state, one ATP-independent open state, one ATP-dependent open state as well as four ATP-dependent closed states reflecting the sequential binding of four ATP-molecules to the channel. The binding of the first ATP-molecule is assumed to close the channel and subsequent ATP-binding might then stabilize the blocked channel. Recently, Trapp et al. (1998) proposed another model for the pancreatic β -cell (Figure 2C). In this model, C_1 represents the short closed state observed within a burst of openings, and C_2 represents the long closed state as observed in the absence of ATP, which governs the interburst duration. In the presence of ATP, two additional closed states were found labeled C_2 (ATP) and C_3 (ATP).

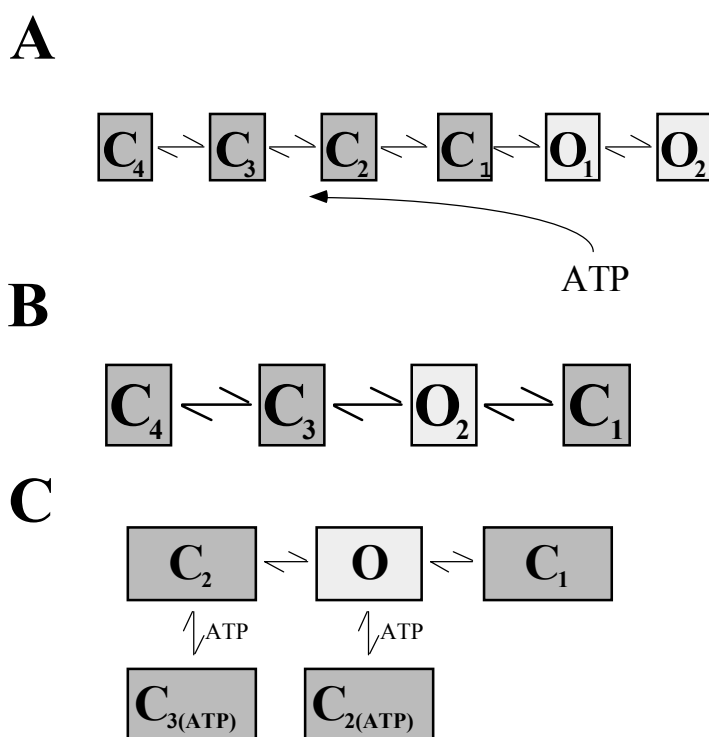


Figure 2: Kinetic gating schemes for K_{ATP} -channels. Models proposed by Spruce et al. (1987), Gillis et al. (1989) and Trapp et al. (1998) are illustrated in (A), (B) and (C), respectively. Closed states are depicted by ‘C’ and open states by ‘O’.

1.4 Physiological role of K_{ATP} -channels in pancreas and heart

The functional significance of K_{ATP} -channels is well understood in the pancreas and the heart. In the pancreas, K_{ATP} -channels act as a major regulator of insulin secretion. Hyperglycemia resulting in an ATP-increase and antidiabetic sulphonylureas, such as glibenclamide, close K_{ATP} -channels, thereby causing membrane depolarization, Ca^{2+} influx and insulin secretion.

K_{ATP} -channels are usually active in the resting pancreatic β -cells during fasting (2 - 3 mM blood glucose). The electromotive force of the K^+ current hyperpolarizes the cell, which leads to closure of Ca^{2+} -channels and a low intracellular Ca^{2+} concentration, which means a low rate of insulin secretion. On the other hand, an increase in glucose following a meal raises the intracellular ATP concentration via the Krebs cycle and results in K_{ATP} -channel closure and thus membrane depolarization. Ca^{2+} -influx through voltage-activated Ca^{2+} -channels is then stimulated leading to a rise of $[Ca^{2+}]_i$ and insulin secretion (Smith et al., 1990b; Faehling and Ashcroft, 1997; Mislner et al., 1992).

K_{ATP} -channels have likewise been found at high densities in plasma membranes of cardiac cells, where they modulate cardiac contractions during metabolic impairment (Terzic et al., 1995). Specifically during ischemia, their opening protects against cellular damage of the myocardium, limits infarct size and improves recovery of cardiac function during reperfusion, acting as a cardioprotective mechanism (Hiraoka, 1997). Mitochondrial K_{ATP} -channels are also associated with a mechanism termed *ischemic preconditioning*, which refers to the increased myocardial tolerance against infarction following the exposure of myocytes to periods of 3 - 10 min transient ischaemia (Liang, 1996; Yabe et al., 1995; Yao and Gross, 1994; Baines et al., 1999).

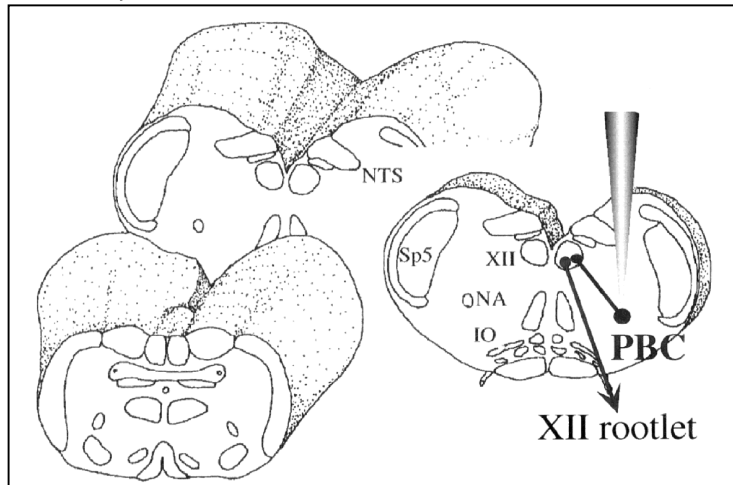
Oscillatory variations of K_{ATP} -conductances (gK_{ATP}) and membrane potentials were observed both in pancreatic β -cells (Larsson et al., 1996) and in cardiomyocytes (O'Rourke et al., 1994). In the pancreas a modulatory role is assigned to these fluctuations in gK_{ATP} in shaping the firing pattern of these cells (Kinard et al., 1999), or it was proposed that oscillations in K_{ATP} -channel activity themselves are the cause of oscillations in electrical activity causing $[Ca^{2+}]_i$ -fluctuations during glucose stimulation (Larsson et al., 1996). Similar behavior was observed in cardiomyocytes (O'Rourke et al., 1994), where metabolic stress induced after substrate deprivation initiated cyclic activation of K_{ATP} -channels and simultaneous

suppression of depolarization-induced $[Ca^{2+}]_i$ -transients. Such oscillations of K_{ATP} -currents were completely blocked by the K_{ATP} -channel blocker glibenclamide and modulated by changes in glucose metabolism, indicating that the oscillations were mediated by alterations in glycolysis.

1.5 *The respiratory network*

The main function of respiration is an exchange of gases between the external and the internal milieu of the organism. This gas exchange is a result of coordinated actions of the respiratory and cardiovascular systems. The respiratory system controls ventilation of the lung, whereas the cardiovascular system transports O_2 and CO_2 between the pulmonary and systemic capillaries. Ventilation of the lung is caused by periodic movements of respiratory muscles. The spinal motoneurons, which innervate these muscles, are activated by a rhythm-generating network in the lower brainstem. This neuronal network is located in and near the nucleus ambiguus, the pre-Bötzinger and Bötzinger complexes which together comprise the ventral respiratory group (Schwarzacher et al., 1995; Smith et al., 1991).

The *rhythmic slice preparation* (Figure 3) contains this network and allows the investigation of generation and modulation of the respiratory rhythm through electrophysiological tools. By correlating neuronal activity with phrenic or hypoglossal nerve discharges (Richter, 1982; Smith et al., 1990a; Ezure, 1990), respiratory neurons can be subdivided into several groups: early-inspiratory, augmenting-inspiratory, late-inspiratory, post-inspiratory, augmenting-expiratory and pre-inspiratory. Each group performs a specific function for rhythm generation and pattern formation (Bianchi et al., 1995). The rhythmic activity of respiratory neurons is a result of permanent afferent inputs that are summed to periodic excitatory or inhibitory *synaptic drive* currents. Thus, during ongoing network activity the cell membrane potential does not remain constant but rather fluctuates periodically, giving rise to oscillations of $[K^+]_e$ (Richter et al., 1978), $[H^+]_i$ (Ballanyi et al., 1994) and $[Ca^{2+}]_i$ (Frermann et al., 1999). The neurotransmitters and neuromodulators involved in synaptic regulation of the respiratory rhythm are glutamate (Greer et al., 1992), glycine and GABA (Champagnat et al., 1982; Schmid et al., 1996; Pierrefiche et al., 1993) and – most importantly – serotonin, adenosine and endorphines (Richter et al., 1999).

*In vitro mouse**Rhythmic Brainstem Slice*

IR Visualization

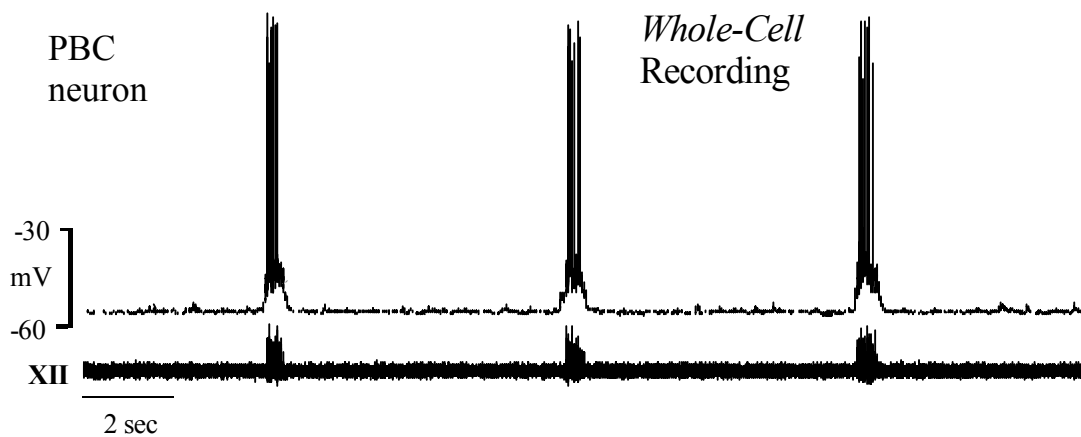
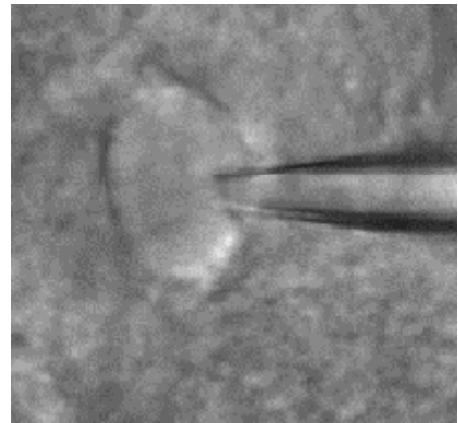


Figure 3: Rhythmic slice preparation. The upper panel on the left shows the rhythmic slice preparation of the *in vitro* mouse. Note the location of the nucleus hypoglossus (XII) and the nucleus ambiguus (NA). The right-hand panel displays the infrared (IR) image of a respiratory neuron from the pre-Bötzinger complex (PBC) during a patch-clamp experiment. The respiratory rhythm as recorded from hypoglossal nerve (XII) activity is depicted below together with a voltage-clamp recording from an inspiratory neuron.

1.6 Purinoceptors

Recently, there was evidence that in the respiratory network ATP is not only functioning as energy storage, but also as a co-released neurotransmitter acting via purinergic receptors, also termed *purinoceptors* (Thomas and Spyer, 2000; Thomas et al., 1999). Purinoceptors can be subdivided into the adenosine-sensitive (P_1 , subclasses: A_1 and A_2) and the ATP/ADP-sensitive (P_2) types (Abbracchio and Burnstock, 1994). Neurons are known to express both types of purinoceptors (Blazynski and Perez, 1991; Sawynok, 1998; Housley, 1998; Rudolphi et al., 1992; Krishtal et al., 1988; Illes and Norenberg, 1993; Edwards, 1994; Zimmermann, 1994). Similar to GABA, glutamate, adenosine and 5-HT receptors, P_2 purinoceptors either function via fast ligand-gated channels or as G-protein coupled metabotropic receptors. Thus, they are further subdivided into ionotropic P_{2X} receptors (P_{2X1} - P_{2X7}) and metabotropic P_{2Y} receptors (Abbracchio and Burnstock, 1998; King et al., 1998). One way of distinguishing between P_2 purinoceptor subtypes is through their agonist potency order, which is α,β -methylene ATP (α,β -MeATP) > ATP = 2-methylthio-ATP for P_{2X} receptors and 2-methylthio-ATP > ATP > α,β -MeATP for P_{2Y} receptors (for a summary of purinoceptor structure and properties see North and Barnard (1997)).

Metabotropic P_{2Y} receptors modulate inward-rectifying Kir3.0-channels (Mosbacher et al., 1998), muscarinic (K_{ACH}) channels (Matsuura and Ehara, 1996), delayed K^+ -channels (Thomas and Hume, 1993) and high-voltage activated Ca^{2+} -channels (Lim et al., 1997). There is some discussion as to whether the effects are mediated indirectly by intracellular Ca^{2+} changes (Mironov, 1994), PKC activity (Nishizaki and Ikeuchi, 1996), or directly via G-proteins and phospholipase C (PLC) or phospholipase A_2 (PLA_2) (Illes and Norenberg, 1993; Zimmermann, 1994; Abbracchio and Burnstock, 1998). P_{2Y} receptors were also found to affect adenylyl cyclase (Murayama et al., 1998) and the cytoskeleton (Vaziri and Downes, 1992). All these factors are known to modulate the activity and ATP-sensitivity of K_{ATP} -channels. Thus, it is a reasonable question to ask whether K_{ATP} -channels are modulated by purinoceptor activation. In contrast to adenosine A_1 and A_2 receptors, which were found to activate K_{ATP} -channels (Miura and Tsuchida, 1999; Kim et al., 1997; Tang et al., 1999; Mironov et al., 1999), little is known about the effect of P_{2X} and P_{2Y} receptor activation on K_{ATP} -channel activity.

1.7 K_{ATP} -channels in respiratory neurons

K_{ATP} -channels in respiratory neurons were first reported in expiratory neurons of the anaesthetized cat (Pierrefiche et al., 1996), where intracellular injection of ATP reversibly depolarized neurons during all phases of the respiratory cycle. Application of diazoxide/tolbutamide led to membrane hyperpolarization/depolarization of most neurons and extracellular application of tolbutamide blocked a persistent outward current during voltage-clamp experiments. This indicates that K_{ATP} -channels are partly activated during normal conditions, which might be due to ongoing electrical activity in these rhythmically active neurons.

In inspiratory neurons of the brainstem slice preparation, K_{ATP} -channels of 75 pS conductance were found that were inhibited by tolbutamide and glibenclamide and activated by diazoxide (Mironov et al., 1998).

In other neurons, research on the functional significance of K_{ATP} -currents has so far mostly concentrated on the modulatory effect on overall activities of cells rather than the periodic activation of single K_{ATP} -channels. For this reason *inspiratory* neurons, which are persistently active and every 3 - 4 sec discharge bursts of action potentials that last for 1 - 2 sec constitute ideal probes for the study of periodic modulation of single K_{ATP} -channels. Since restoration of ion distribution during their intense neuronal activity implies a high metabolic demand of cells, K_{ATP} -channels can be expected to be rhythmically modulated contributing to the periodic cell potential variations.

During *hypoxia* (i.e. reduction of oxygen supply to the tissue below physiological levels) oscillations of the membrane potential of respiratory neurons are initially enhanced. The respiratory network responds to hypoxia in a biphasic manner. An initial augmentation (i.e. frequency and amplitudes of rhythmic activity increase) is followed by a secondary depression (i.e. frequency and amplitudes of rhythmic activity decrease) as described by Cherniack et al.(1970) and Richter et al.(1991). K_{ATP} -channels have been found to be activated during such hypoxic depression of the metabolism and presumably contribute to the depression of electrical activity (Mironov et al., 1998). Such activation could be due to a

variety of mechanisms, such as a hypoxia-induced increase in ATP-consumption (Kass and Lipton, 1982; Wilken et al., 1998) and/or a fall in intracellular pH during hypoxia (Findlay, 1992). In addition, glutamate, serotonin, adenosine and GABA, which are known to contribute to the initial hypoxic response of the respiratory network (Richter et al., 1999), might play a role. Agonists of their respective receptors as well as activators of the α -subunit of G-proteins were found to modulate K_{ATP} -channels (Mironov et al., 1999; Mironov and Richter, 2000), indicating that K_{ATP} -channels are modulated by G-proteins that are activated by metabotropic receptors. Cells are also known to swell during hypoxia (Patel et al., 1998; Haller et al., 1998b) due to a water influx following the intracellular accumulation of ions (Na^+ , Ca^{2+} , Cl^-) during enhanced neuronal activity. The resulting mechanical stress to the cytoskeleton might lead to an additional swelling-induced activation of K_{ATP} -channels.

1.8 Measurements of the intrinsic optical signal

Activity-induced cell swelling such as that occurring during hypoxia can be monitored through changes in infrared light transmittance, termed the *intrinsic optical signal* (IOS). The IOS provides a non-invasive technique for imaging “neuronal functions” in the living brain. It originates from changes in the refractory indices of the cytoplasm and the extracellular space that determine light transmittance and/or scattering. Thus, as the signal arises from endogenous properties of the tissue it does not require cell labeling and is not subject to bleaching and similar disadvantages of fluorescent dyes. The IOS imaging technique has been applied to the intact brain as well as to slice preparations. IOSs have been employed in the intact brain, e. g. to map the spatial distribution of neuronal activity patterns and propagation of seizures (Federico et al., 1994). The technique was also used to examine slices from hippocampus, neocortex and the retina in various pathological conditions.

The IOS has been shown to reflect changes in neuronal activity (Holthoff and Witte, 1998) such as spreading depression in the retina (Fernandes de Lima et al., 1997; Ulmer et al., 1995) and the hippocampus (Obeidat and Andrew, 1998; Muller and Somjen, 1998) or excitotoxicity originating from enhanced release of excitatory neurotransmitters (Andrew et al., 1999).

The origin of the complex mechanisms underlying the IOS is, however, not yet completely clear. There are strong indications that a large part of the IOS is determined by changes in cell volume (Polischuk and Andrew, 1996; Andrew et al., 1996), which might originate from neuronal swelling due to Na^+ , Ca^{2+} , Cl^- accumulation and concomitant water fluxes through the cell membranes (Andrew and MacVicar, 1994) or from swelling of adjacent glial cells buffering extracellular K^+ that is released during neuronal activity (MacVicar and Hochman, 1991).

However, there is also evidence that not all aspects of the IOS can be explained in terms of cell volume changes. Buchheim et al. (1999) found that electrical hyperactivity in hippocampal-entorhinal slices of rat leads to diverse changes in the IOS during shrinkage of the extracellular space, indicating the presence of another, cell volume-independent mechanism of IOS change. Similarly, in hippocampal slices (Aitken et al., 1999) light transmittance was found to increase during moderate hypotonia and decrease during severe hypotonia even though cells continued to swell. Another puzzling piece of evidence is that spreading depression, occurring during both normoxic and hypoxic conditions, leads to a decrease in the intensity of transmitted light.

A possible explanation for all these phenomena could be that apart from cell volume changes IOS is also affected by morphological changes of the distribution or volume of intracellular organelles. Candidates for mechanisms leading to an increase in light scattering are mitochondrial swelling (Aitken et al., 1999; Andrew et al., 1999) and/or dendritic beading (Andrew et al., 1999), i.e. alterations in the dendritic shape that are typically a result of excitotoxic injury (Hasbani et al., 1998).

1.9 Tasks and aims of the present experiments

The aim of this work was to study K_{ATP} -channels in respiratory neurons of the pre-Bötzinger complex (PBC). More specifically, the tasks were

1. to determine the molecular structure of K_{ATP} -channels, i.e. to identify the combination of subunits (Kir6.1/Kir6.2 and SUR1/SUR2) present in respiratory neurons,
2. to analyze the gating kinetics of the channel and to propose a kinetic gating model based on the log-likelihood method,
3. to analyze rhythmic modulation of ongoing channel activity and identify factors responsible for it,
4. to investigate the effect on rhythmic modulation of factors that are known to affect the respiratory rhythmicity such as elevation of $[K^+]_e$ and hypoxia,
5. to analyze the effect of extracellular ATP, acting via purinoceptors on K_{ATP} -channel activity,
6. to give estimates of submembraneous $[ATP]_i$ -fluctuations that are based on open probability kinetics as well as on measurements with the ratiometric dyes mag-fura-2 and fura-2 and simulations of intracellular ion concentration changes, and
7. to examine the response of the respiratory network to hypoxia and especially the involvement of mitochondrial K_{ATP} -channels using measurements of the intrinsic optical signal (IOS).

2 Materials and methods

2.1 Slice preparation

Experiments were performed on the medullary slice preparation from neonatal NMRI-mice (P5 - P8) containing the core of the spontaneously active respiratory center. Tissue isolation followed the approach developed for rats and mice (Smith et al., 1991; Mironov et al., 1998). All animals were housed, cared for and euthanized in accordance to the recommendations of the European Commission (No. L 358, ISSN 0378-6978), and protocols were approved by the Committee for Animal Research, Göttingen University.

The brainstem-spinal cord was isolated in ice-cold artificial cerebrospinal fluid (ACSF, composition listed below) and a single 700 μm thick transverse slice containing the pre-Bötzing complex was cut from the brainstem, transferred to the recording chamber and mounted on the stage of an upright microscope (Axioscope, Zeiss, Oberkochen, Germany). The slice was fully submerged in a continuously flowing ACSF (28 °C, 40 - 50 ml/min) that was gassed with carbogen (95 % O₂ and 5 % CO₂). To prevent loss of the dissolved gases, the perfusing solution was fed to the experimental chamber via stainless steel tubing. The respiratory rhythm was stabilized by elevating network activity through increased levels of [K⁺]_e at 8 - 12 mM.

All drugs were added directly to the bath and arrived at the experimental chamber after a delay of 8 - 12 sec. Drug wash-out was obtained by perfusing 400 - 500 ml fresh solution containing control [K⁺]_e. In order to induce hypoxic conditions in the slice, bath gassing was changed from carbogen to 95 % N₂ and 5 % CO₂. Tissue oxygen pressure was measured using oxygen-sensitive electrodes (Diamond Electro-Tech Inc., Ann Arbor, MI, USA) as described previously (Mironov et al., 1998). A P_{O₂} electrode was placed 100 ± 25 μm below the slice surface, in a region where respiratory neurons were located. Some 15 - 20 sec after oxygen in the perfusing solution was replaced by nitrogen, extracellular P_{O₂} fell from 232 ± 39 to 6 ± 4 mmHg and remained constant ($n = 15$, $P < 0.05$) thereafter.

2.2 Solutions

The ACSF solution was composed of (in mM concentrations): 128 NaCl, 3 KCl, 1.5 CaCl₂, 1.0 MgSO₄, 21 NaHCO₃, 0.5 NaH₂PO₄, and 30 D-glucose. Solutions with elevated K⁺ were obtained by replacing NaCl with KCl.

The standard patch pipette solution contained (in mM concentrations): 140 K-gluconate, 1 CaCl₂, 2 MgCl₂, 10 Hepes, 11 EGTA, 0.5 Na₂ATP

The following intracellular solutions were used (in mM concentrations) for optical measurements with the ratiometric dyes fura-2 or mag-fura-2: 140 K-gluconate, 1 CaCl₂, 2 MgCl₂, 10 Hepes, 11 EGTA, 2 Na₂ATP, 1 mag-fura-2 or 0.3 fura-2.

Flash photolysis solutions for photolytic Ca²⁺ release were prepared as described in Haller et al. (1998a) (in mM concentrations): 5 Na₄DM-nitrophen (1-(2-nitro-4,5-dimethoxyphenyl)-1,2-diaminoethane-N,N,N',N'-tetraacetic acid, tetrasodium salt), 96 Cs-glutamate, 40 Cs-Hepes, 0.3 GTP, 4.5 mM CaCl₂, 1 MgATP, 4 NaATP, 0.3 fura-2.

For flash photolysis of caged-ATP, the solution contained (in mM concentrations): 140 K-gluconate, 1 CaCl₂, 2 MgCl₂, 10 Hepes, 11 EGTA, 10 caged-ATP.

EGTA was ethylene glycol-bis(beta-aminoethyl ether)-N,N,N',N'-tetraacetic acid. Caged-ATP was either 3-O-(1-(2-nitrophenyl)ethyl)adenosine-5'-triphosphate (NPE-caged-ATP), 3-O-(1-(4,5-dimethoxy-2-nitrophenyl)ethyl) adenosine-5'-triphosphate (DMNPE-caged-ATP) or adenosine 5'-triphosphate, P²-(1,2-diphenyl-2-oxo)ethyl ester, ammonium salt (desyl-caged-ATP).

The pH of the solutions was adjusted to 7.4 with KOH. The solutions' osmolarity ranged from 280 to 300 mosm. All caged substances and fluorescent dyes were obtained from Molecular Probes (Leiden, Netherlands) and the other reagents were obtained from Sigma-Aldrich (Deisenhofen, Germany).

2.3 *Experimental setup*

The experimental setup allowed recordings in the whole-cell and cell-attached patch-clamp modes, recordings of hypoglossal nerve (XII) activity and served for microfluorometric and imaging measurements as well as the application of UV-flashes in flash photolysis experiments (Figure 4).

Brainstem slices were placed into the recording chamber that was mounted on the stage of an upright microscope (Axioscope, Zeiss, Oberkochen, Germany), which could be moved in X-Y directions with a manipulator (Spindler & Hoyer, Göttingen). Hypoglossal activity was recorded with a blunt suction electrode from the central end of XII rootlets to monitor central respiratory rhythmicity. XII activity was amplified 5,000 - 10,000 times, bandpass filtered (0.25 - 1.5 kHz), rectified and integrated (Paynter filter with a time constant of 50 - 100 ms). Electrical signals were measured with an EPC-7 patch-clamp amplifier (ESF, Friedland, Germany) and together with hypoglossal rootlet activity stored with a MacLab acquisition system (WissTech GmbH, Spechbach, Germany). Voltage pulses were applied either via the voltage output function of the MacLab-system or by the WinTida-system (Heka, Lambrecht, Germany) via an ITC16 (Heka, Lambrecht, Germany).

For imaging and microfluorometric measurements, a CCD-Camera System (MicroMax, Visitron Systems GmbH, Puchheim, Germany) was used which was controlled by the software 'Winview' (Visitron Systems GmbH, Puchheim, Germany). The system could either be operated in an 'imaging mode' to obtain cell images at a slow rate (2 - 3 images of maximum size (768 x 512 pixels) per 10 sec) or in a faster-paced 'photomultiplier-like mode'. In the second mode, 'regions of interest' (ROIs) could be selected, and in the case of a single approximately cell-sized ROI sample rates of ~ 1 - 5 Hz were reached. The microscope was equipped with epifluorescent optics and a monochromator (T.I.L.L. Photonics, Planegg, Germany) to allow fluorescence excitation at different wavelengths as well as a flash photolysis system (Cairn Research Ltd., Faversham, UK) to provide high-intensity UV-flashes.

The monochromator was controlled by 'Winview' via an AD-card. Operation of the camera and monochromator could be started and terminated via a TTL-pulse from the MacLab-system and was thus synchronized with electrophysiological recordings. The flash photolysis system could also be operated from the MacLab-system through TTL-pulses.

The excitation light from the monochromator and the flash photolysis unit was coupled into the microscope through a two port epifluorescence condenser (T.I.L.L. Photonics, Planegg,

Germany). Both light beams are combined by a sapphire window mounted at an angle of 45° to both light paths, which reflects 20% and transmits 80% of all incident light. They then pass through a filter set designed for fura-2 measurements containing a bandpass excitation filter (D 365 / 40), a beam-splitter (400 DCLP, which reflects the excitation light below 400 nm onto the specimen plane and allows transmission of emitted light above 400 nm) and a bandpass emission filter (D 510 / 40) (AFanalysentechnik, Tübingen, Germany). To reduce background fluorescence and to select the ROI, the light of both monochromator and flash lamp was attenuated by adjustable diaphragms situated in front of the sapphire window reducing the diameter of the illumination field in the object plane to 30 μm . Neurons were positioned approximately in the center of the illumination field. A 63 x Achroplan objective (Zeiss, Oberkochen, Germany) was used for microfluorometric measurements and either a 10 x Achroplan or 2.5 x Plan-Neofluar objective (Zeiss, Oberkochen, Germany) for measurements of the intrinsic optical signal (IOS) of the network region.

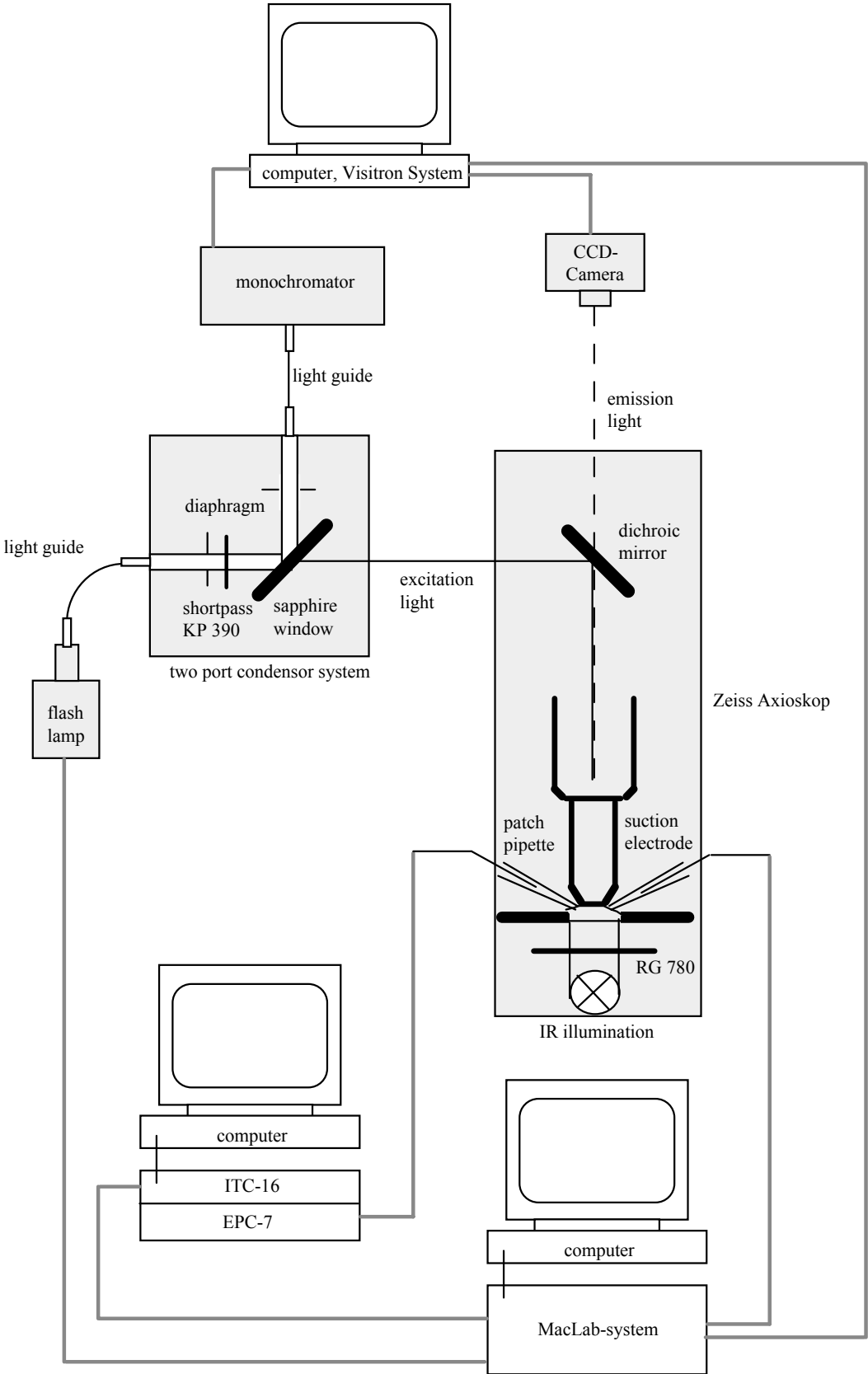


Figure 4: Experimental setup

2.4 Electrophysiological recordings

Electrodes for patch-clamp recordings were obtained from borosilicate glass (Clarke Electromedical, Pangbourne, UK) using a horizontal electrode puller (Zeitz, Munich, Germany). They had tip openings of 1 - 2 μm and a DC resistance of 2 - 4 $\text{M}\Omega$. Pipettes were typically filled with approximately 15 μl intracellular solution but only with approximately 2 μl when the cell cytosol was harvested for PCR analysis. Electrodes with an imposed internal hyperbaric pressure of were inserted into the slice with a *PatchMan* micromanipulator (Eppendorf-Netheler-Hinz GmbH, Hamburg, Germany). Cells were either patched under visual control or 'blindly' by advancing the pipette slowly through the tissue until an increase in pipette series resistance indicated contact with a cell. Following the formation of a *gigaseal* (generally higher than 2 $\text{G}\Omega$), cells were identified as inspiratory by correlating their spontaneous action potential discharge with rhythmic XII activity. Channel activity and spike discharges were then recorded in the cell-attached mode (usually at an applied potential of +40 mV that would correspond to a membrane potential of -100 mV assuming a resting potential of -60 mV). A sample frequency of 4 kHz and a 1 kHz hardware filter were used for single-channel recordings of long duration. For kinetic analysis, short time periods were sampled at 10 kHz with a 3 kHz filter. To establish whole cell configuration, the patch membrane was broken by negative pressure. Series resistance (approximately 10 - 20 $\text{M}\Omega$) was compensated by more than 80 %.

2.5 Fluorescent indicator dye measurements

The fluorescent indicator dyes fura-2 (Grynkiewicz et al., 1985) and mag-fura-2 (Konishi et al., 1991) were used to measure intracellular Ca^{2+} and Mg^{2+} . Both indicators absorb ultraviolet light (< 400 nm) and emit light at maximal intensity around 510 nm (fura-2) or 490 nm (mag-fura-2). Upon ion binding, the fluorescence spectrum changes, allowing an accurate estimate of intracellular ion activities with the aid of ratiometric measurements. This shift in absorption following the binding of Ca^{2+} (fura-2) or Mg^{2+} (mag-fura-2) can be visualized by scanning the excitation spectrum between 250 and 450 nm, while monitoring the emission at 510 nm and 490 nm, respectively (Figure 5).

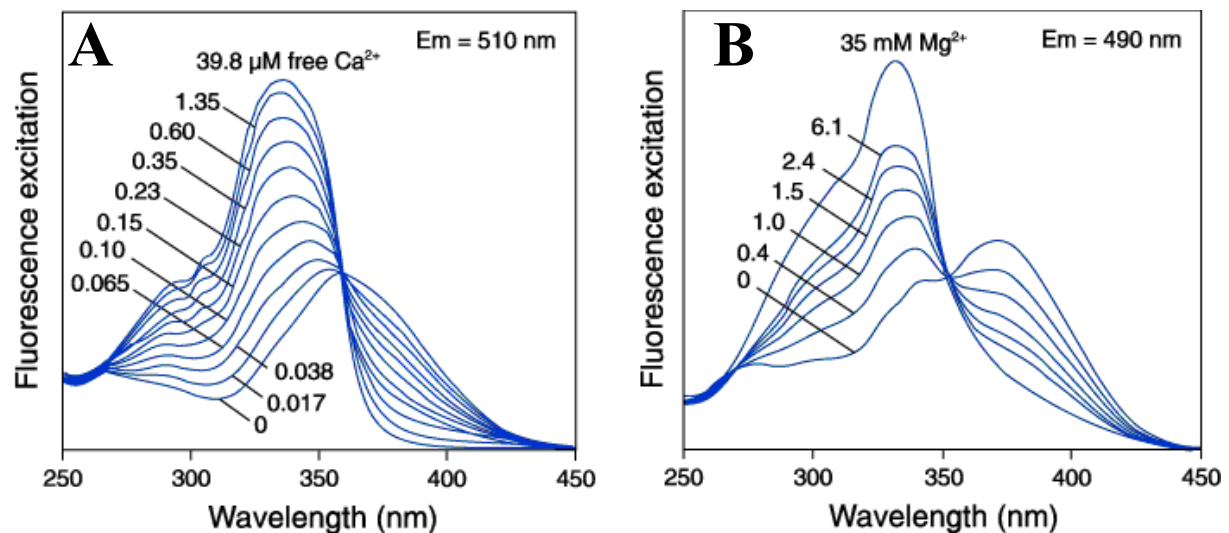


Figure 5: Fluorescence excitation spectra of fura-2 (A) and mag-fura-2 (B). Modified from the Molecular Probes Catalog (Molecular Probes, Leiden, Netherlands)

When considering the ratios of emission intensities of different excitation wavelengths a number of factors that perturb ion measurements based on single wavelength measurements are eliminated. Specifically, ion-independent variables affecting the signal intensity such as non-uniform distribution of dye concentration, dye bleaching and cell volume changes, are cancelled since these parameters have a similar effect on emission intensities at both wavelengths.

For measurements with fura-2 and mag-fura-2, cells were illuminated with alternating wavelengths at their respective isosbestic points, where the fluorescence intensity is independent of Ca^{2+} or Mg^{2+} concentration, and at 380 nm. The isosbestic wavelengths for Ca^{2+} binding to fura-2 and for Ca^{2+} and Mg^{2+} binding to mag-fura-2 are 360 nm (Grynkiewicz et al., 1985), 346 nm and 347 nm (Raju et al., 1989), respectively. Prior to establishment of the whole-cell configuration, the background light was recorded, which originates primarily from the illuminated portion of the patch pipette and the autofluorescence of the slice. Values for both wavelengths were subtracted from the fluorescence signal offline.

Emission light was recorded with a CCD-camera.

The intracellular free Ca^{2+} concentration was determined through fura-2 measurements as

$$[\text{Ca}^{2+}] = K_{\text{eff}} \cdot \frac{R - R_0}{R_1 - R}, \quad (1)$$

where R = measured fluorescence ratio (emission 360 nm divided by emission at 380 nm), R_1 and R_0 = fluorescent ratios at very high and low Ca^{2+} concentrations, and K_{eff} = effective

dissociation constant. To determine R_0 , R_I and K_{eff} an in-vitro calibration was performed following the procedures described in Grynkiewicz et al. (1985) and Poenie and Tsien (1986). For the experimental setup R_0 , R_I and K_{eff} were found to be 0.29, 5.10 and 1.75 μM , respectively.

2.6 Flash photolysis

Flash photolysis of photoactivatable or *caged* compounds allows the rapid and controlled release of specific reagents (Kaplan and Ellis-Davies, 1988). The caging moiety is designed to interfere with the binding or activity of the probe. It is detached when subjecting the caged complex to brief UV-flashes at < 360 nm (Figure 6). This method was employed to elevate the intracellular concentration of Ca^{2+} and ATP in inspiratory neurons. Caged- Ca^{2+} and caged-ATP solutions were prepared (see chapter 2.2) following the procedures described by Heinemann et al. (1994) and Haller et al. (1998a). Cells were loaded with the *caged substance* via the patch-pipette in the whole-cell mode and subjected to short pulses from a flash photolysis system (Cairn Research Ltd., Faversham, UK). The photolysis efficiency of the flash lamp was found to be 55 % for a medium flash of ~ 250 μs duration (flash lamp capacitor with capacitance 3000 μF charged to 350 V) based on the calibration procedures described in Heinemann et al. (1994).

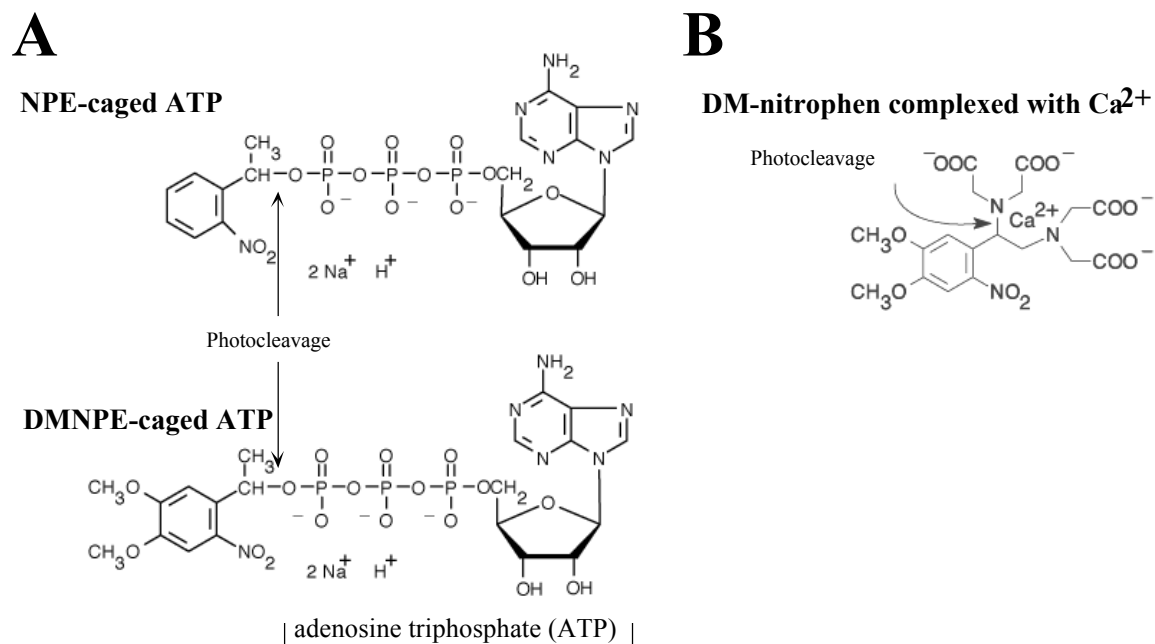


Figure 6: Caged probes. (A) NPE-caged-ATP (top) and DMNPE-caged-ATP (bottom) are ATP-analogs in which the terminal phosphate is esterified with a blocking group, rendering the molecule biologically inactive. The caging group is removed photolytically by UV illumination. (B) Upon illumination, the Ca^{2+} -DM-nitrophen complex is cleaved to yield free Ca^{2+} and two iminodiacetic acid photoproducts. The affinity of the photoproducts for Ca^{2+} is $\sim 600,000$ times lower than that of DM-nitrophen.

2.7 Imaging of the intrinsic optical signal

For measurements of the intrinsic optical signal (IOS), slices were transilluminated using a tungsten lamp that was controlled by a voltage-regulated power supply (Zeiss, Oberkochen, Germany). Infrared illumination was obtained using a highpass filter (RG 780) which cut off the light below 780 nm (Figure 4). Objective lenses of different magnification (2.5 x, 10 x) were used to obtain images of the whole slice or distinct nuclei. Images were collected with a CCD-camera (Visitron Systems GmbH, Puchheim, Germany) at the rates of up to 1 frame/s following the procedure described by Andrew and MacVicar (1994). First, control images were recorded, ROIs were defined and average light transmission for each ROI was used as control value, T_0 . The data collected afterwards were transformed into relative changes (in percent) given by $\text{IOS} = (\Delta T/T_0) 100\%$. Images were presented using a pseudocolor intensity scale.

2.8 *Molecular biology*

In order to harvest cytosol for RT-PCR analysis, cells were patched and identified as inspiratory neurons in the cell-attached configuration. After the whole-cell configuration was established, constant suction was applied for 1 - 2 min to aspirate the cytoplasm, while the access resistance was monitored to verify that the gigaseal formation remained intact.

aRNA amplification from single respiratory neurons was performed according to the procedure described in detail by Eberwine et al. (1992). In brief, 2.5 mM dNTPs, 2 ng/ μ l T7-oligo-d(T)₂₄ primer and 0.5 U/ μ l avian myeloblastosis virus (AMV) reverse transcriptase (Roche Diagnostics, Mannheim, Germany) were mixed with the cytosol and incubated at 37 °C for 60 - 90 min for reverse transcription. Second-strand synthesis was performed with T4 DNA polymerase and Klenow fragment (1 U/ μ l each), followed by treatment with S1 nuclease (1 U/ μ l) and subsequently Klenow enzyme (1 U/ μ l) to remove hairpin loops and to produce blunt ends of the cDNA. After aRNA amplification with 100 U/ μ l T7 RNA polymerase, a second round of amplification, including the final synthesis of double-stranded cDNA, was conducted to yield adequate amounts of template for the expression profiling of different mRNAs from a single respiratory neuron. All amplification steps were conducted under RNase-free conditions. In the mouse both SUR1 and SUR2 genes contain multiple introns, but the Kir6 isoforms are intronless. To exclude contaminations by genomic DNA, control experiments were performed without AMV reverse transcriptase, or amplified aRNA was incubated after each amplification with RNase-free DNase I at 37 °C for 1 h. Polymerase chain reaction (PCR) analysis was performed using as template (i) 1/50 of the total volume of the final aRNA amplification product, and (ii) alternatively, mRNA from single neurons that had been reverse transcribed for 60 min using 2.5 mM dNTPs, 25 μ M random hexamer primers, 10 mM dithiothreitol, 2 U/ μ l RNase inhibitor and 10 U/ μ l M-MuLV reverse transcriptase (Roche Diagnostics). Kir6 and SUR core fragments were amplified with primers based on the cDNA sequences of Kir6.1 (Yamada et al., 1997), Kir6.2 (Sakura et al., 1995), SUR1 (Aguilar-Bryan et al., 1995) and SUR2 (Isomoto et al., 1996). Sense and antisense primers were chosen to specifically amplify fragments of 539 - 865 bp in length:

mKir6.1 (Genbank accession number D88159, 865 bp),

sense primer 5'-GAAGATGCTGGCCAGGAAGAG-3',

antisense primer 5'-CAGCCACTGACCTTGTC AACC-3';

mKir6.2 (MMU73626; 553 bp),

sense primer 5'-GGAGAGGAGGGCCCGCTTCGTGTC-3',
antisense primer 5'-GGCGCTAATGATCATGCTTTTTTCGGAGGTC-3';
rSUR1 (L40624, 539 bp),
sense primer 5'- GCAGCCGAGAGCGAGGAAGATGA-3',
antisense primer 5'-ACAGCCAGGGCGGAGACACAGAGTA-3';
mSUR2 (D86037, 603 bp),
sense primer 5'-CGCGGCGGTCATCGTGCTC-3',
antisense primer 5'-CGCCGCGCCTGCTCGTAGTT-3' (conserved for SUR2A and SUR2B).

PCR amplifications were run with *taq* polymerase (Qiagen, Hilden, Germany) for 35 cycles at 95 °C denaturing, 52 - 58 °C annealing, and 72 °C extension for 1.5 min each, with a final extension of 15 min at 72 °C. Amplified fragments were purified from agarose gels, digested at terminal restriction sites or blunt ends produced, and ligated into pBluescriptSKII vector (Stratagene, La Jolla, CA, USA). Double-stranded sequencing of the PCR products was performed on both strands using the prism sequenase dye terminator kit on an automatic sequencer (Perkin Elmer, Weiterstadt, Germany).

3 Data analysis

3.1 K_{ATP} -channel kinetics

Data evaluation of K_{ATP} -channel data was performed offline. For single-channel analysis of cell-attached recordings, action potential signals were removed. Channel kinetics were analyzed with the QuB Software Suite developed by Qin, F., Auerbach, A. and Sachs, F. (version: 24th July, 1999). These programs fit open and closed time histograms constructed from idealized data to sums of exponentials using a *maximum likelihood estimation* algorithm as described by Qin et al. (1996) and Qin et al. (1997). They yield estimates of the log-likelihood as well as molecular rate constants. For a brief description of the method of maximum likelihood estimation see Appendix.

Events that were shorter than a fixed *dead time* were not considered for analysis. Theoretically, the minimal dead time is given by: $dead\ time = 0.18 / (filter\ cut-off\ frequency)$ (p. 500, Sakmann and Neher, (1995)) and was thus estimated to be 180 μ s / 60 μ s for sampling with a 1 kHz / 3 kHz cut-off frequency. Empirically, it was found that a slightly larger dead time of 200 μ s had to be implemented to reliably estimate rate constants. No other correction for short interval durations was used.

The QuB Software Suite further allowed the simulation of single-channel currents based on the previously obtained rate constants.

3.2 K_{ATP} -channel modulation

Time windows of fixed durations of cell-attached channel recordings containing inspiratory bursts (Figure 7A) were selected and then exported for analysis to Igor Pro (WaveMetrics, Inc., Lake Oswego, USA). ‘Macros’ for analysis were written in the Igor Pro macro programming language. An inspiratory burst consisted of 3 to 15 action potentials (APs). Figure 7B shows an example of a selected time window of 3 sec duration. In order to avoid artifacts, action potential (AP) discharges were first removed and the current values averaged over the 5 ms before and after each AP were determined. The data during the AP were then replaced by the smaller one of the two values (Figure 7C and D). Thus, channel openings occurring during an AP-discharge were deleted and the open probability was consequently underestimated during the respiratory burst. However, other methods – such as subtraction of

a predetermined AP-template – were not feasible due to the variation in shape and amplitude of APs even within a single burst. The duration of AP-discharges varied between experiments – from 6 to 18 ms. The channel activity was isolated from background noise by setting all points within a defined noise window (± 5 pA) to baseline levels (Figure 7B, C, lowest traces). In cases where the background noise was analyzed the window discriminator was narrowed to ± 1 pA. P_{open} was determined by averaging up to 200 such traces, dividing the resulting trace by the unitary current and the number of open channels that were identified, and finally smoothing with a ‘box smoothing algorithm’.

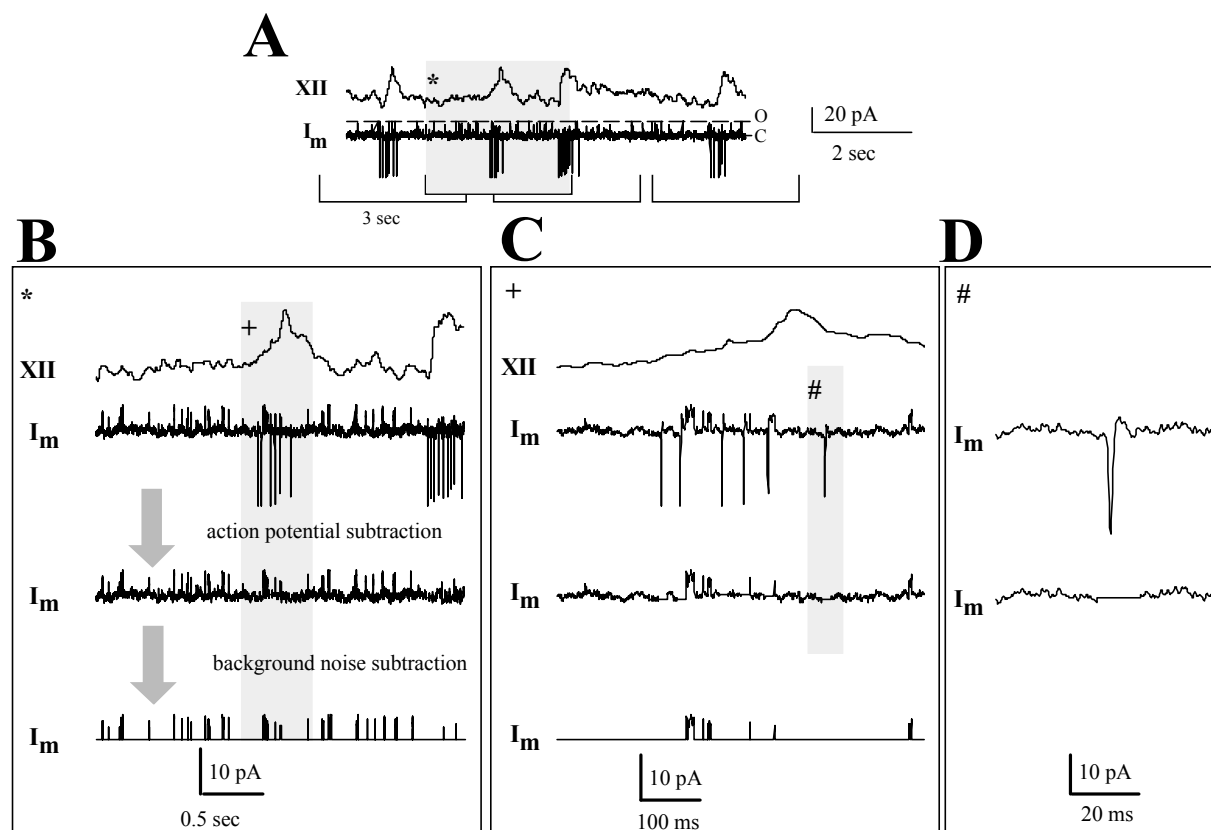


Figure 7: Analysis of rhythmic modulation of K_{ATP} -channels. (A) Sample trace of hypoglossal (XII) nerve and cell-attached recording (I_m). 3 sec windows were selected around the respiratory peaks and then subjected to two steps of analysis as indicated in (B). First, APs were removed and second, background noise was subtracted. To demonstrate AP subtraction, the marked sections were presented at an extended scale (C and D).

4 Results

4.1 Molecular biology of K_{ATP} -channels

As a first step the molecular composition of K_{ATP} -channels expressed in the medullary inspiratory neurons of the mouse was identified. Cytoplasm from identified inspiratory neurons was harvested through the patch electrode while the gigaseal formation was maintained. The cytosolic material was either processed for aRNA/cDNA amplification or directly reverse-transcribed for subsequent PCR analysis. Using primers for the Kir channel subunits Kir6.1 and Kir6.2, and the SUR receptor subunits SUR1 and SUR2, and 1/50 of the total volume of the amplified cDNA product in each reaction yielded high levels of both Kir6.2 subunit- and SUR1 receptor-fragments (Figure 8). All Kir6 and SUR primers used were tested for functionality and sensitivity with 0.05 - 0.1 ng of original cloned cDNA as template (and 50 ng of mouse tissue DNA). Amplified fragments of the neurofilament middle protein (NF-M) confirmed that the cytosol had been aspirated from neurons (action potential discharges) and not from glial cells (silent cells; data not shown). Moreover, adequate H₂O controls performed for all primer combinations were found to be negative.

Figure 8 shows the Kir6/SUR expression profiling after aRNA processing for two inspiratory neurons. The primer pair that was designed to amplify a Kir6.1 fragment amplified a strong 865 bp band from the vector template, but not from the cDNAs of the single respiratory neurons (using 1/50 of the total aRNA amplification product). Likewise, the primer combination that successfully amplified a 603 bp SUR2 fragment from atrial cDNA (50 ng) failed to yield detectable amplification products from the single cell source. In contrast, clearly detectable fragments were observed using Kir6.2 (552 bp) and SUR1 (539 bp) primers with cDNA from the two nerve cells. The same expression pattern, i.e. strong expression of Kir6.2/SUR1 and absence of Kir6.1/SUR2 signals, was detected in four additional inspiratory neurons directly processed for RT-PCR after recording. When subcloned, grown to a large scale and sequenced on both strands, the amplified fragments were always completely identical to the published cDNA sequences. Thus, PCR analysis of unprocessed and T7 RNAPolymerase-amplified RNA with specific primers suggests that SUR1 and Kir6.2 isoforms translate to form the major subtype of K_{ATP} -channel in brainstem respiratory neurons.

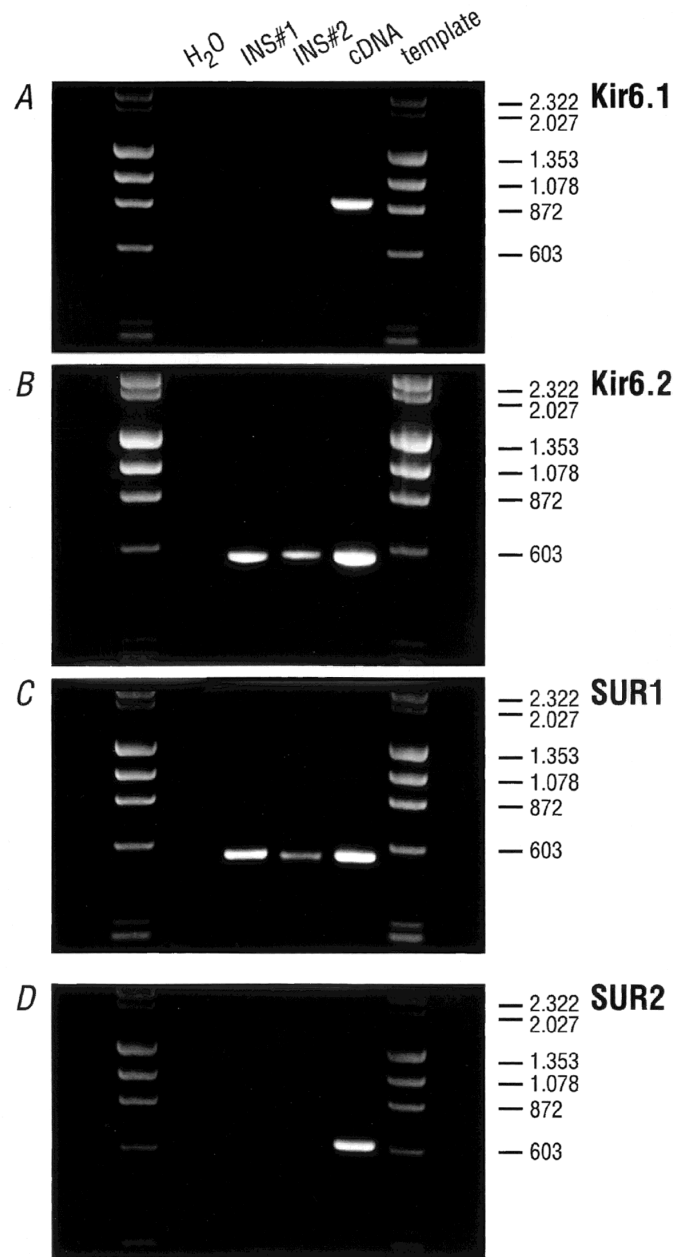


Figure 8: PCR analysis of amplified aRNA from single respiratory brainstem neurons. DNA fragments are amplified with primer pairs specific to Kir6.1 (A), Kir6.2 (B), SUR1 (C) and SUR2 (D). The first lanes next to the molecular weight marker (λ HindIII- Φ XHaeIII digest) are H₂O controls, templates in lanes 2 and 3 were of two different inspiratory neurons (INS#1, INS#2), and lanes 4 used 0.1 ng of plasmid cDNA as positive control (except in (D) where 50 ng of atrial cDNA were used). Primers were sensitivity-tested to amplify fragments of 865 bp (Kir6.1), 553 bp (Kir6.2), 539 bp (SUR1) and 603 bp (SUR2). Fragment sizes of the molecular marker are indicated on the right. Note that fragments amplified from single respiratory neurons can only be detected for Kir6.2 and SUR1.

4.2 Channel kinetics

K_{ATP} -channels in respiratory neurons were found to be active during normoxia. They were identified by their conductance and gating characteristics as well as by specific K_{ATP} -channel blockers (glibenclamide, tolbutamide) or openers (diazoxide, pinacidil) as described by Mironov et al.(1998) (see Figure 9).

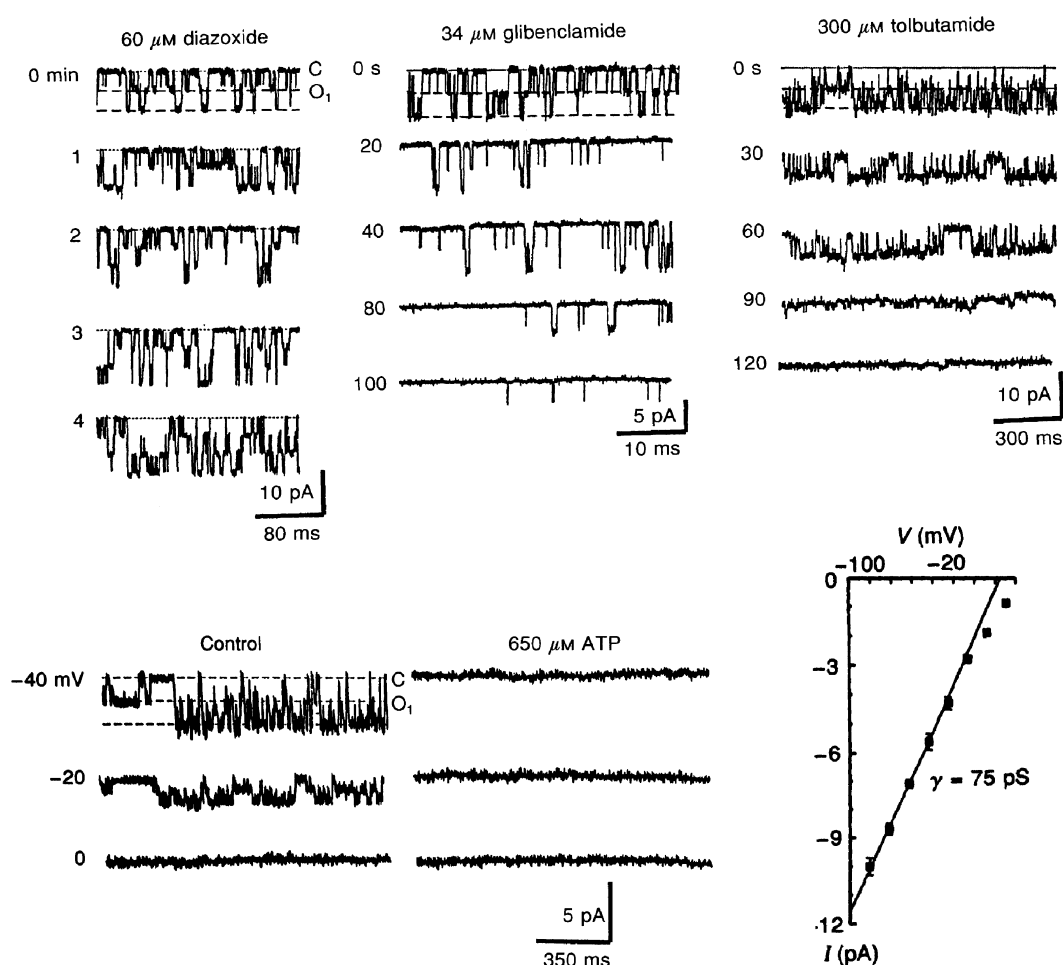


Figure 9: Properties of K_{ATP} -channels in inspiratory neurons. Inspiratory neurons express K_{ATP} -channels of 75 pS conductance that are spontaneously active. They can be blocked by glibenclamide and tolbutamide, activated by diazoxide and inhibited by $[\text{ATP}]_i$ (modified from Mironov et al. (1998)).

Figure 10A depicts the effects of pinacidil on K_{ATP} -channel activity in the cell-attached recording mode. Each point corresponds to the open probability, p_{open} , obtained from sweeps of 2s duration chosen to surround one inspiratory burst. p_{open} -values were calculated by dividing the mean current by the unitary current and the number of open channels in a given experiment. With pinacidil application, p_{open} increased from 0.004 ± 0.004 to 0.011 ± 0.009 ($P < 0.01$).

Interestingly, some data sweeps displayed a much higher p_{open} -value. This is due to a transition of the channel to a second gating mode with higher activity. Figure 10B illustrates the two different modes of channel activity exhibited in inspiratory neurons. The most common mode was one with low p_{open} (upper and lower pair of traces in Figure 10B). The middle pair of traces depicts a high p_{open} activity mode. All cell-attached recordings lasting longer than 20 minutes displayed episodes of high activity with a mean duration of 5.36 ± 4.92 sec ($n = 30$, 5 different cells). The frequency of occurrence, number and duration of these episodes varied between experiments. Due to these variations and the limited number of episodes, the high activity data was not analyzed in more detail. However, it seems important to note that the transition into the high activity mode was found to occur more frequently during hypoxia, with the transition probability increasing from $9.7 \pm 3.1 \cdot 10^{-3}$ sec⁻¹ at normoxia to $3.9 \pm 0.6 \cdot 10^{-3}$ sec⁻¹ at hypoxia as depicted in Figure 10C.

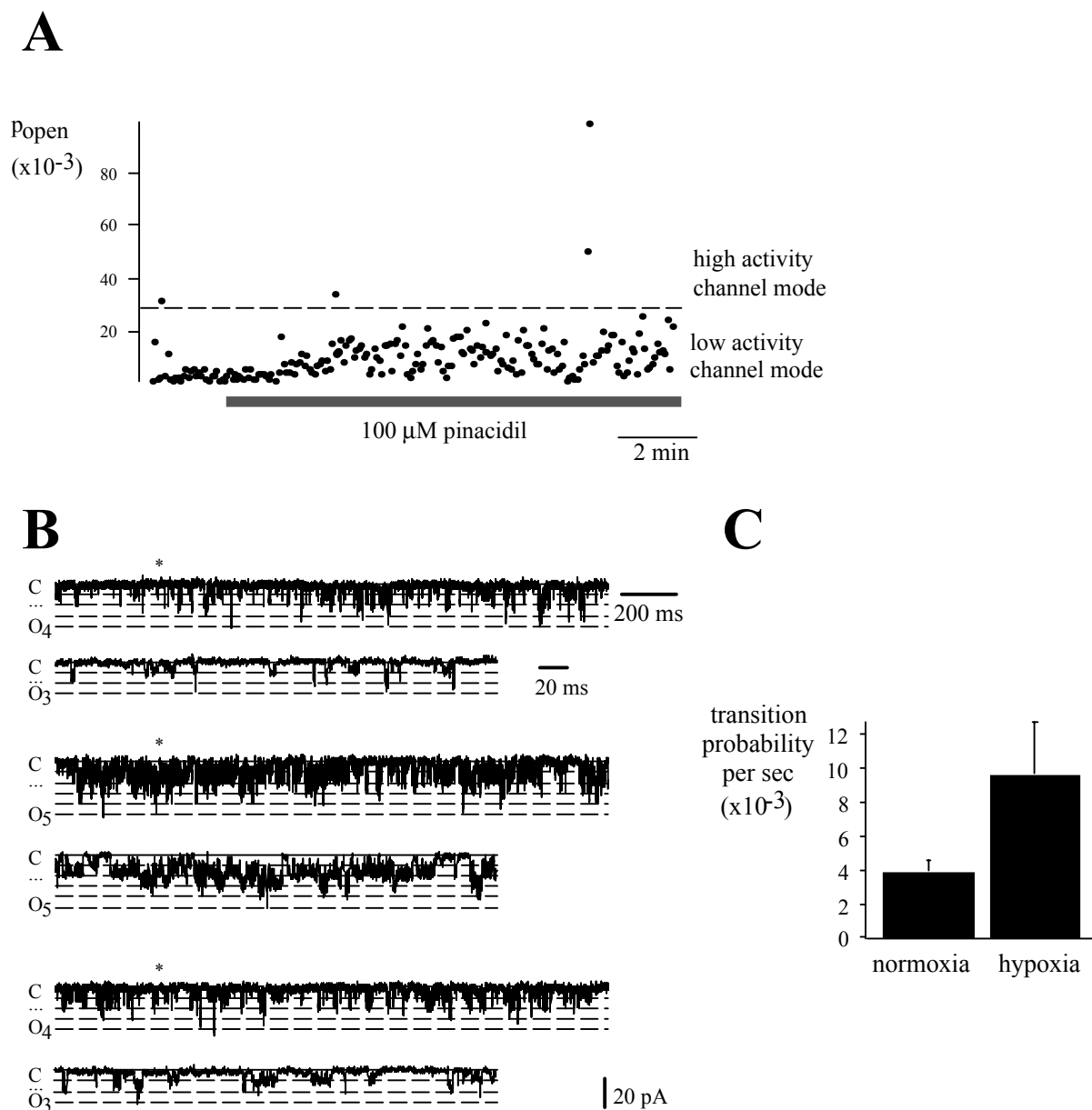


Figure 10: Two gating modes of the K_{ATP} -channel. (A) shows the changes in p_{open} of a typical experiment after application of 100 μ M pinacidil. Each point represents the mean open probability measured during time periods surrounding an inspiratory burst. For computation of p_{open} , individual action potentials and background noise were eliminated as described in chapter 3.2. Note that channel activity increases after pinacidil application. The channel normally persists in a low activity mode and occasionally displays a mode of higher open probability. (B) Consecutive cell-attached recordings at pipette potential -40 mV (sections marked by * are displayed underneath with a higher time resolution) show an example of the channel entering and exiting from a mode of high activity (middle traces). (C) Probability of transition from the low activity mode to the high activity mode per second of normoxia or hypoxia duration. Note the increase in the transition probability during hypoxia (4 cells).

Before subjecting single-channel recordings to the log-likelihood analysis it was verified that channels opened independently of each other. This is the case when the probability of seeing 1, 2, 3,..., N channels is very close to that predicted by the binomial distribution

$$P(n) = \frac{N!}{n!(N-n)!} P_{open}^n (1 - P_{open})^{N-n}, \quad (2)$$

where $P(n)$ is the probability that n channels are open out of a total of N . As can be seen in Figure 11 very good fits were observed when only two channels were detected in the patch ($n = 4$). In the case of multichannel recordings corresponding to the high activity gating mode ($n = 3$) the fit was less good, possibly due to less accurate idealization of the channel data. Previously, K_{ATP} -channels in inside-out recordings were reported to open independently only in the absence of ATP and could not be fitted to a binomial distribution in the presence of ATP (Spruce et al., 1987). No indication of such behavior was found here.

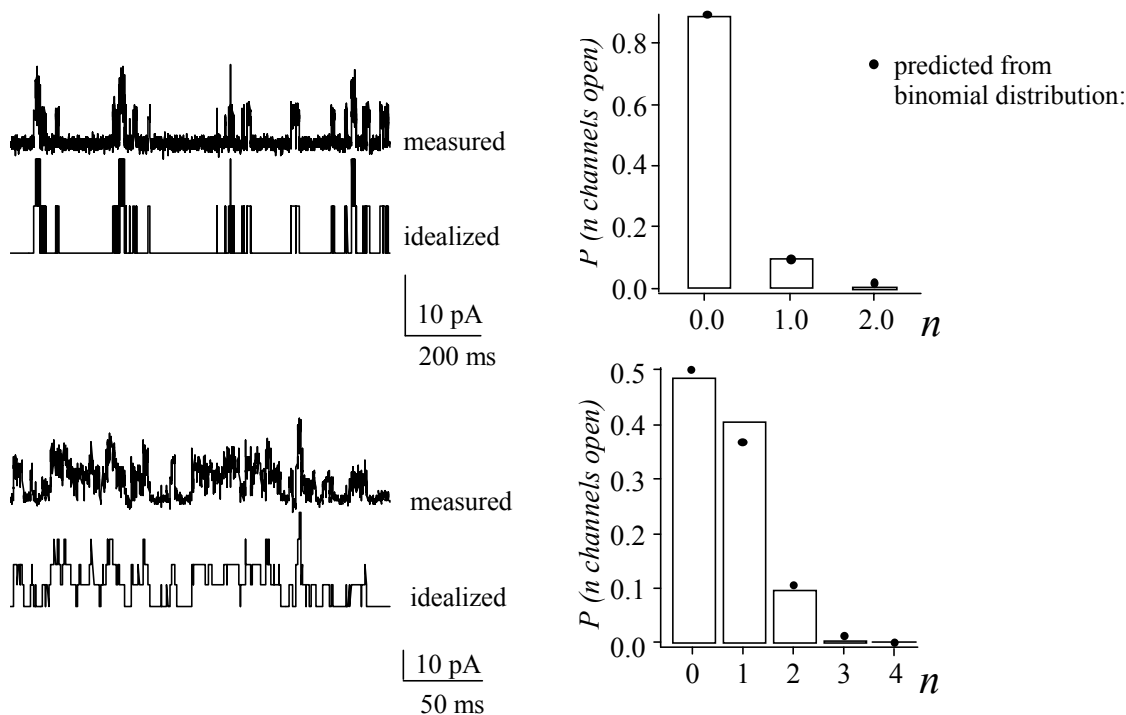
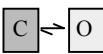
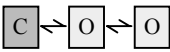
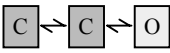
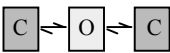
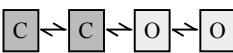
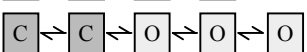
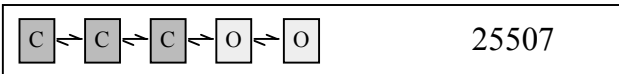
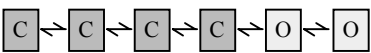


Figure 11: Binomial analysis of cell-attached recordings. The left-hand side shows two short samples (both raw and idealized traces) of the 10 sec recordings that were analyzed. Right-hand side: the ordinate represents the probability, P , that a given number, n , of channels are open, the abscissa the number of open channels, n . The histograms show the experimental probabilities for a patch containing two channels (top) and a patch that was detected for four channels (bottom). • represent the probabilities predicted by the binomial theorem, using the measured p_{open} -values for each channel. In the case of the multichannel patch the best fit was obtained when five channels were assumed to be present in the patch, even though only four were observed in the recording.

A kinetic scheme describing the behavior of K_{ATP} -channels in cell-attached recording of inspiratory neurons was obtained using the maximum likelihood approach as described in chapter 3.1. This method allows comparison of a number of kinetic models containing different numbers of open and closed states by calculating a model-specific parameter – termed the *log-likelihood* – which reflects the respective probability of the model. Figure 12 displays the log-likelihoods for a variety of kinetic models as depicted on the left-hand side. It can be seen that the log-likelihood reaches a maximum value for a model containing three closed and two open states. In two of five analyzed cells a very small increase in log-likelihood could be observed when a fourth open state was added. This indicates that a fourth open state might be present but is not resolvable in all instances.

When the log-likelihood values of models of different ‘connectivities’ were compared, two distinct classes of gating models emerged. For instance, the most simple version of the ‘five states-model’ (three closed, two open states), as marked by a box in Figure 12A, yielded a significantly smaller log-likelihood value than models pertaining to a second class, where both open states were connected to different closed states as indicated in Figure 12B. Several examples models are given for both classes. Further analysis was based on the model marked by a dark box in Figure 12B, which resembles most closely the scheme proposed by Trapp et al. (1998).

A

kinetic model	log-likelihood	improvement(%)
	23468	0.2
	23504	7.9
 	25326	8.1
 	25362	8.7
	25507	8.7
	25511	

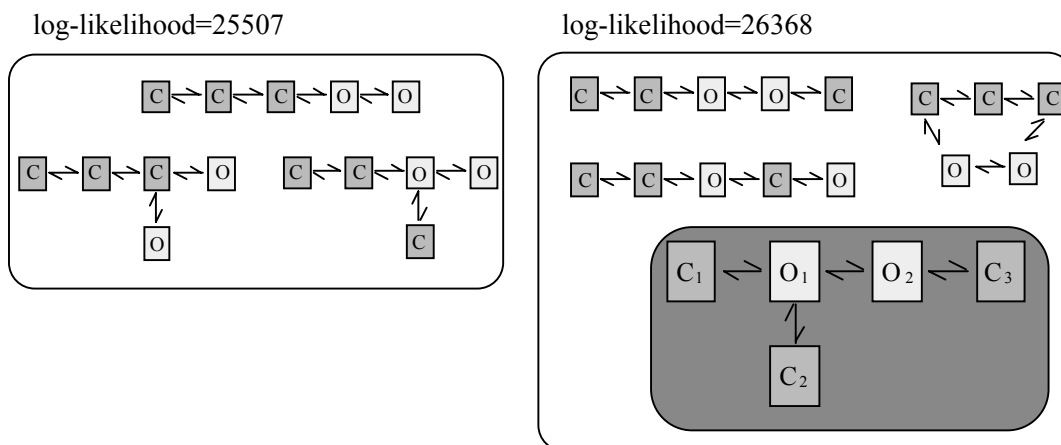
B

Figure 12: Kinetic models of K_{ATP} -channel gating. (A) The log-likelihood values for a number of distinct gating models as well as their improvement with respect to the first model are indicated. A maximal log-likelihood is typically reached for a model containing three closed and two open states. In two out of five cases a small further increase is observed upon addition of a fourth closed state. **(B)** Connectivity of model. Two different sets of connectivities yield two log-likelihood values as indicated. The larger value is reached when both open states are connected to at least one closed state and when at least two closed states are connected to open states.

To obtain valid log-likelihood estimates, only recordings containing a single K_{ATP} -channel were analyzed. This was assumed to be the case when no more than one channel was observed during prolonged single-channel recordings (> 5 minutes). The validity of this assumption was checked after the analysis by simulating single-channel currents for one and for two channels using the rate constants obtained through the log-likelihood method (Figure 13). The simulations showed that the presence of two channels should become apparent even in relatively short measurements of 8 sec duration, indicating that the initial assumption was correct and the recordings indeed only contained a single channel.

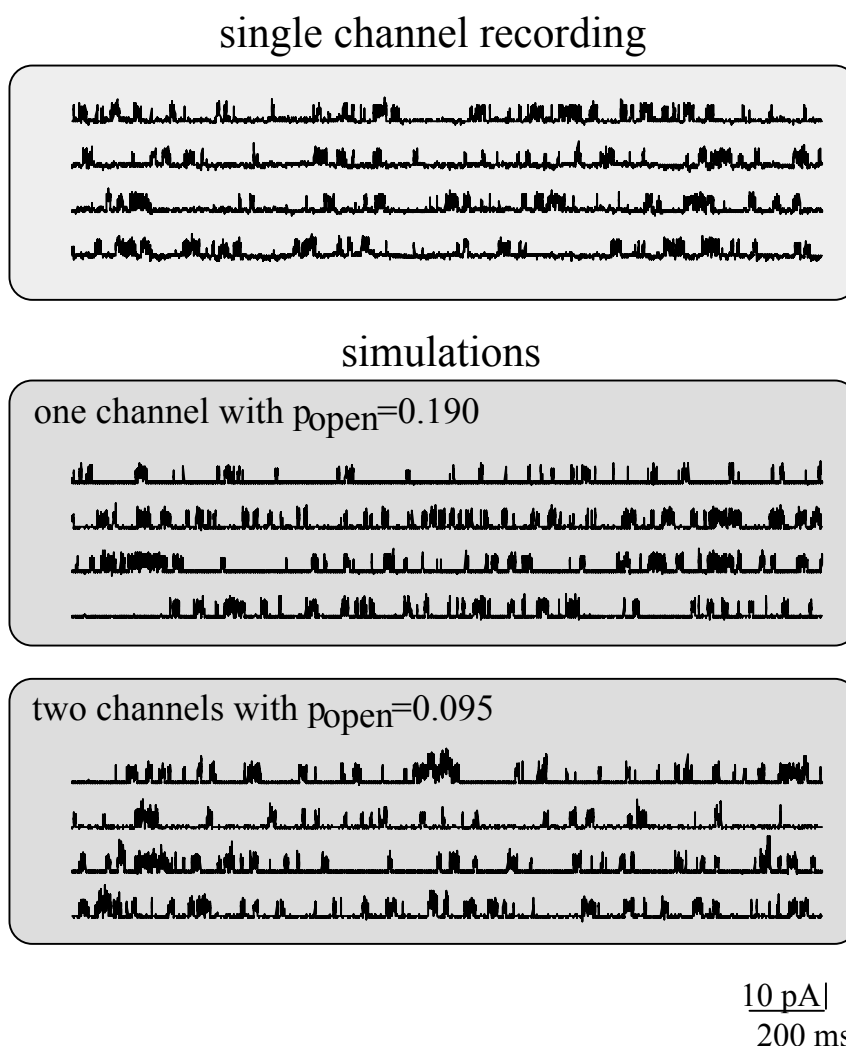


Figure 13: Check for multiple K_{ATP} -channels in patch. A single-channel recording of a K_{ATP} -channel (top) was simulated assuming either one channel of open probability 0.19 (middle) or two channels of open probability 0.095 (bottom). In the second simulation, a simultaneous opening of both channels occurred several times in the course of 8 sec, whereas no such concurrence was observed in the raw data (top), indicating that only one channel is present in the patch.

The estimation of rate constants was complicated by the finding that the open probability of K_{ATP} -channels underwent changes even during the course of one experiment. A mean open probability of these channels could therefore not be determined. The reasons for these changes remain unclear. It may be that cell metabolism is affected even during cell-attached experiments, when the cytosol remains undisturbed, or that the cytoskeleton attached to the patched membrane below the pipette is subjected to a certain tension, which might modulate the channel biophysics. Figure 14 shows an example of channel activity and the changes of rate constants within one experiment. It can be seen that rate constants changed quite dramatically, which makes it impossible to give a meaningful set of averaged rates for K_{ATP} -channels. There are, however, certain kinetic steps, which remain unaltered. For instance, in all patches analyzed ($n=5$), transitions $C_2 \rightarrow O_1$ and $O_2 \rightarrow C_3$ consistently displayed high rates, whereas the rates for the transition between open states $O_1 \rightarrow O_2$ were small. The transition that was most dramatically affected in the course of an experiment was $O_1 \rightarrow C_1$. In the example displayed in Figure 14 the corresponding rate constant decreased from 619 s^{-1} to 65 s^{-1} , indicating a pronounced increase in the dwell time in O_1 .

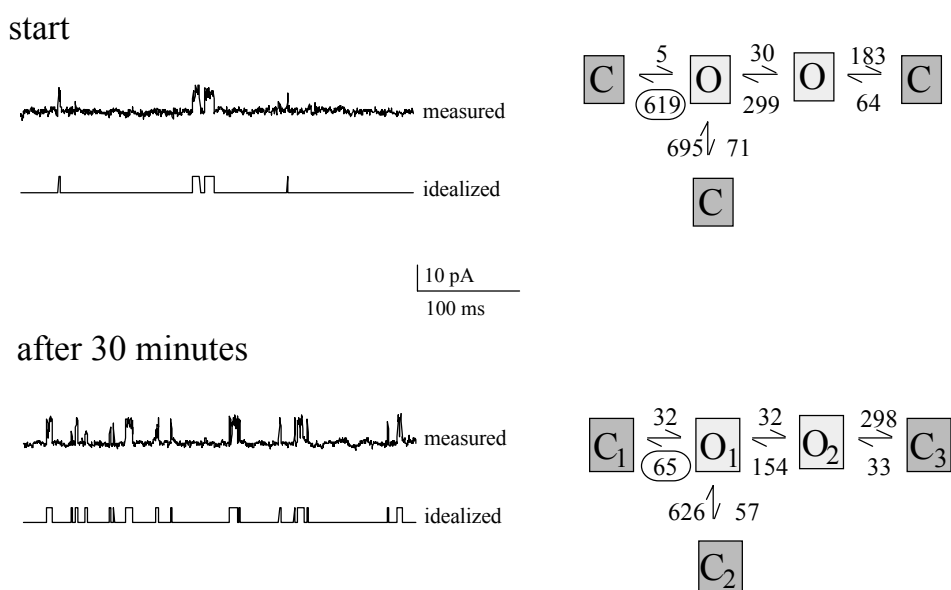


Figure 14: Changes of channel activity and rate constants within 30 minutes of a sample experiment. Raw cell-attached recording and idealized traces are presented on the left. Rate constants (in units of 1/sec) determined for data of 10 sec duration are indicated next to the corresponding transitions on the right. The rate constants of the transition $O_1 \rightarrow C_1$ are accentuated. Since the transitions $O_1 \leftrightarrow C_1$ and $O_1 \leftrightarrow C_2$ are equivalent, the model was arbitrarily arranged so that $C_1 \rightarrow O_1$ had the lower rate constant.

When the channel entered a mode of high activity nearly all transition rates were increased apart from the transition between open states and the transition $O_1 \rightarrow C_2$ (Figure 15). This latter transition fell significantly, again denoting a large increase in the dwell time in the state O_1 . Analog to Trapp et al. (1998), it might be speculated that the transitions $O_1 \leftrightarrow C_2$ or $O_1 \leftrightarrow C_1$ are ATP-dependent. The large change of rate constant might be a result of a decreasing ATP-sensitivity in the high activity gating mode.

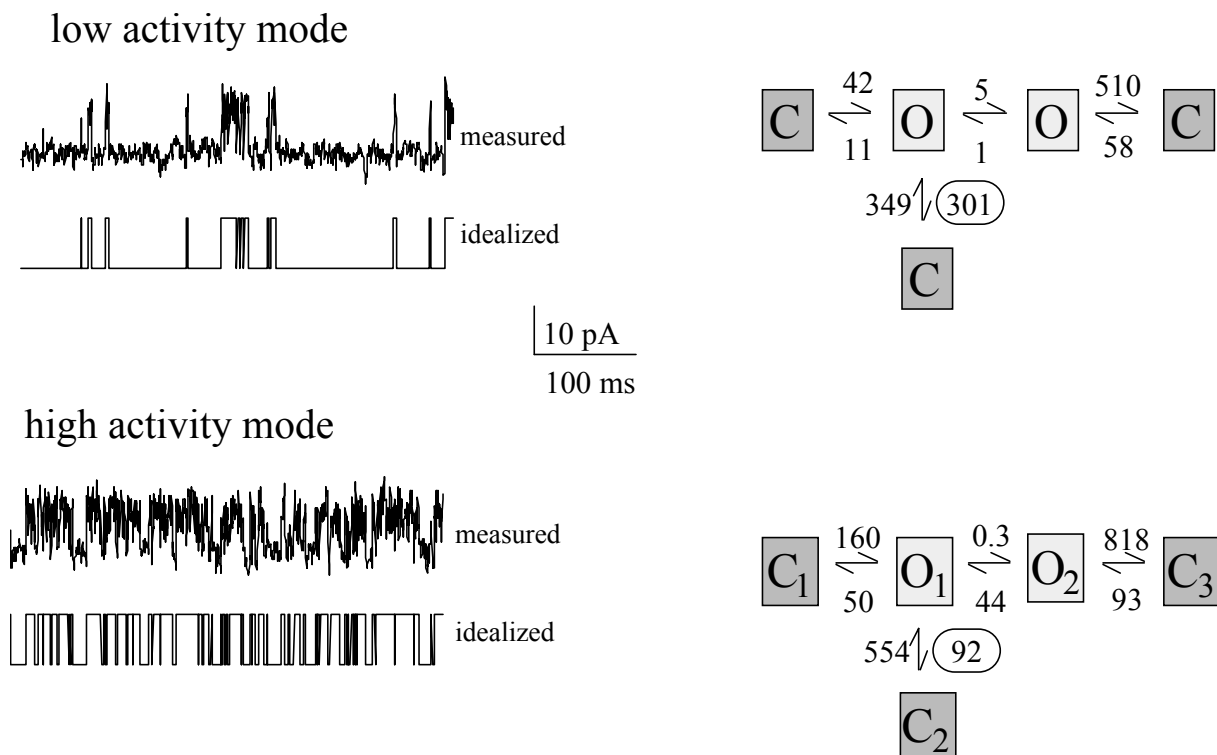


Figure 15: Two modes of channel gating. Note that rate constants vary greatly between the two gating modes of low and high activity.

4.3 *Effects of K_{ATP} -channel drugs on rhythmic activity*

The normoxic and hypoxic activities of respiratory neurons are effectively modulated by K_{ATP} -channels (Pierrefiche et al., 1996; Mironov et al., 1998). In order to test the contribution of K_{ATP} -channels to the respiratory rhythm specific drugs, such as glibenclamide, tolbutamide (blockers), diazoxide and pinacidil (openers), were applied. High concentrations of K_{ATP} -channel drugs affected the amplitude of integrated hypoglossal (XII) bursts as exemplified by Figure 16 (top). Application of diazoxide (300 - 500 μ M, n = 5) led to a decrease of integrated hypoglossal burst amplitude by 8.7 ± 9.0 % ($P < 0.01$), whereas tolbutamide (300 - 500 μ M, n = 6) and glibenclamide (30 - 50 μ M, n = 4) resulted in an increase of 9.6 ± 7.1 % ($P < 0.01$) within 10 minutes. The frequency of bursts was not significantly affected. More importantly, the respiratory neurons also reacted to such treatment in a similar manner. The amplitude of their synaptic drives decreased by 4.7 ± 9.0 % (n = 4) after application of activator drugs and increased by 4.9 ± 2.7 % (n = 4) when channel blockers were applied (Figure 16).

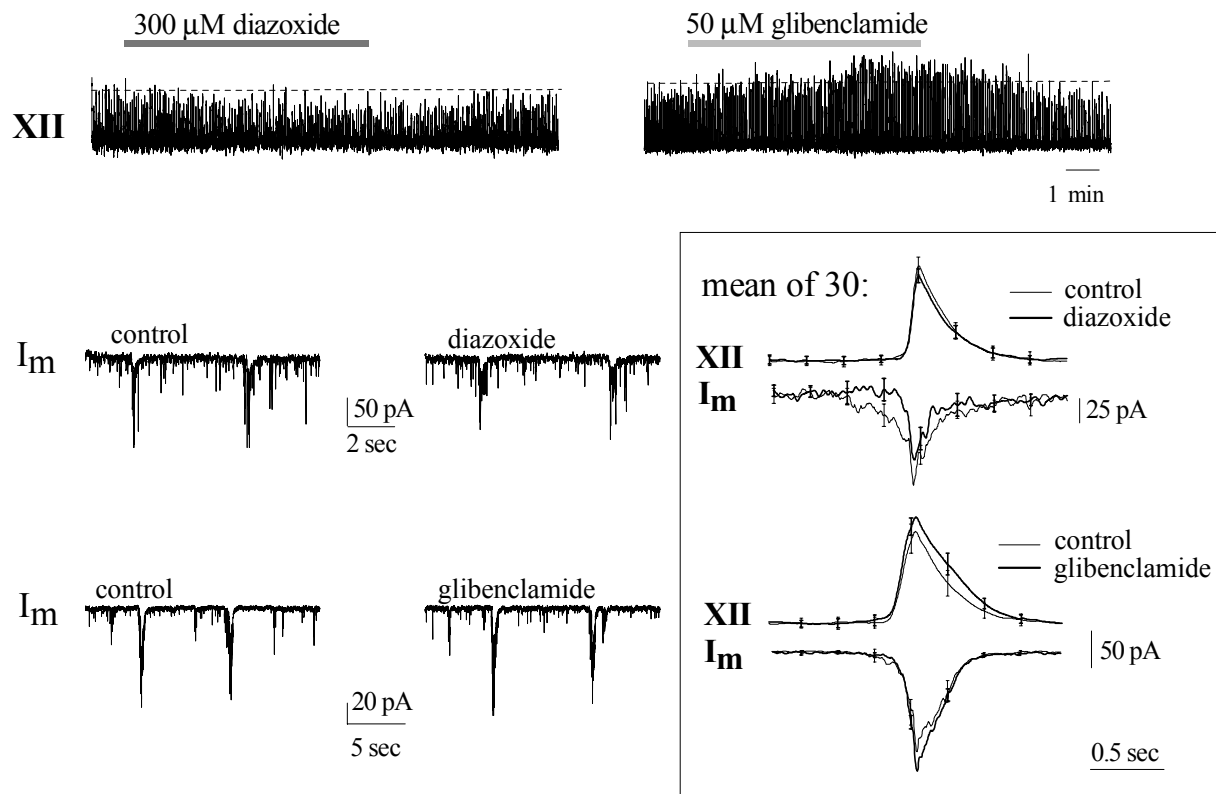


Figure 16: Respiratory rhythm and synaptic drive amplitude after K_{ATP} -channel drug application. The upper panel shows the response of the respiratory network to diazoxide/glibenclamide application. The amplitude of the integrated hypoglossal nerve (XII) activity decreases after diazoxide application and increases after glibenclamide application. (Below) Modulation of synaptic drives (membrane currents, I_m , recorded in whole-cell mode at holding potential -60 mV) could only be discerned when 30 traces were averaged and smoothed. As can be seen on the right-hand side, synaptic drive amplitude was affected in the same way as hypoglossal activity; i.e. it decreases with diazoxide and increased with glibenclamide.

4.4 Functional modulation of K_{ATP} -channel openings

The previous findings showed that K_{ATP} -channel activation modulates the respiratory rhythm. Next, the question was addressed whether this effect is mediated through a periodical fluctuation of channel activity during normal rhythmic (respiratory) bursting. A and B displays recordings from two different inspiratory cells (upper curves). The lower traces show time windows of 3 sec duration surrounding the inspiratory burst. The recordings from hypoglossal rootlets (XII) and the underlying gray areas indicate the timing of the inspiratory burst activity. The middle traces in grey color show sample traces of single cell-attached recordings. Action potentials and background were eliminated (see chapter 3.2) in order to isolate channel activities, as indicated by a superimposed trace in black. An accurate estimate of open probability was obtained by averaging 200 such traces and smoothing the resulting trace with a box smoothing algorithm.

A similar procedure was performed for time windows acquired *before* (Figure 17C) and *after* (Figure 17D) respiratory bursts. Due to the variation of cycle lengths, a second burst sometimes fell into this time interval as indicated by a second grey area on the left side of Figure 17C and the right side of Figure 17D. The same effect explains why the mean of hypoglossal activity does not show a single defined second peak, but rather a slight elevation where a second respiratory burst would occur.

The pattern of p_{open} -fluctuations was very consistent for all inspiratory neurons irrespective of whether small or large variations of cycle and burst durations were observed. All the data clearly revealed an increase of p_{open} following every respiratory burst. During constant respiratory burst discharges of neurons, p_{open} -values typically increased by 30 % - 60 %.

Neither rise nor decline in p_{open} could be reliably fitted with a simple exponential function. Therefore, the parameters $R_{\Delta T1/\Delta T2}$, $t_{1/2}(\text{rise})$ and $t_{1/2}(\text{fall})$ were defined (Figure 18), which describe p_{open} -fluctuations quantitatively. $R_{\Delta T1/\Delta T2}$ represents the position of the p_{open} -peak within the respiratory cycle, whereas $t_{1/2}(\text{rise})$ and $t_{1/2}(\text{fall})$ yield information about burst duration and burst kinetics. Mean values (\pm SD) for parameters obtained under control conditions, hypoxia and with low $[K^+]_e$ are listed in Table 2.

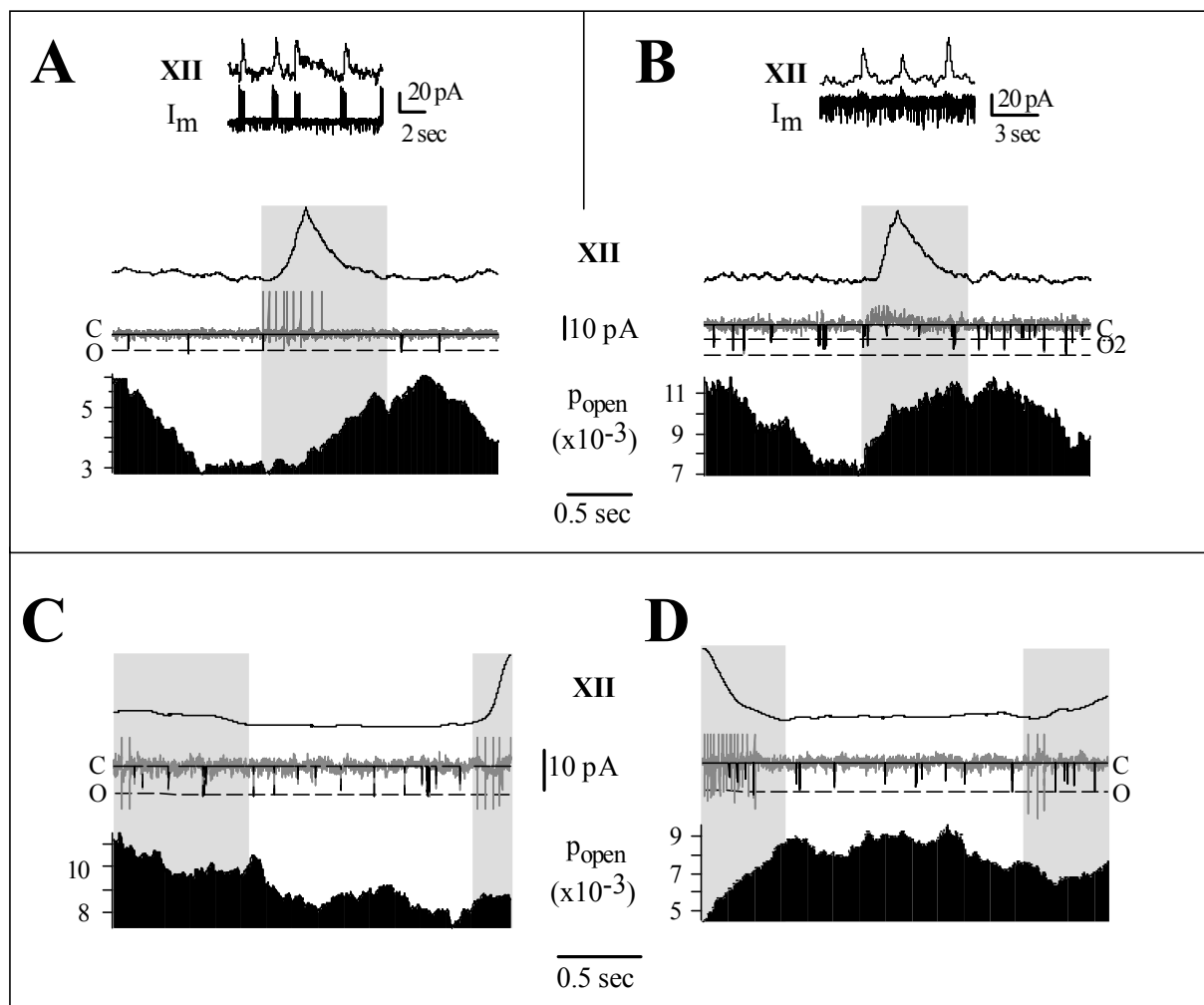


Figure 17: Modulation of K_{ATP} -channel activity during a respiratory cycle. Neurons were first identified as inspiratory by recording the bursting activity in the cell-attached mode with a pipette potential of +40 mV and by correlating the membrane current, I_m , with the integrated hypoglossal rootlet activity (XII) (upper panels of A and B). The lower panels show a time window selected around respiratory bursts. The respiratory burst is marked by a gray band. The peak in the upper curves is the inspiratory hypoglossal activity averaged over 200 traces. The traces below show a sample trace for the cell-attached recordings that were analyzed as described in the text. The open probability, p_{open} , was obtained by averaging over 200 traces. Curves were smoothed with a box smoothing procedure. Alternatively, time windows were selected to contain the time period before (C) and after (D) the respiratory burst.

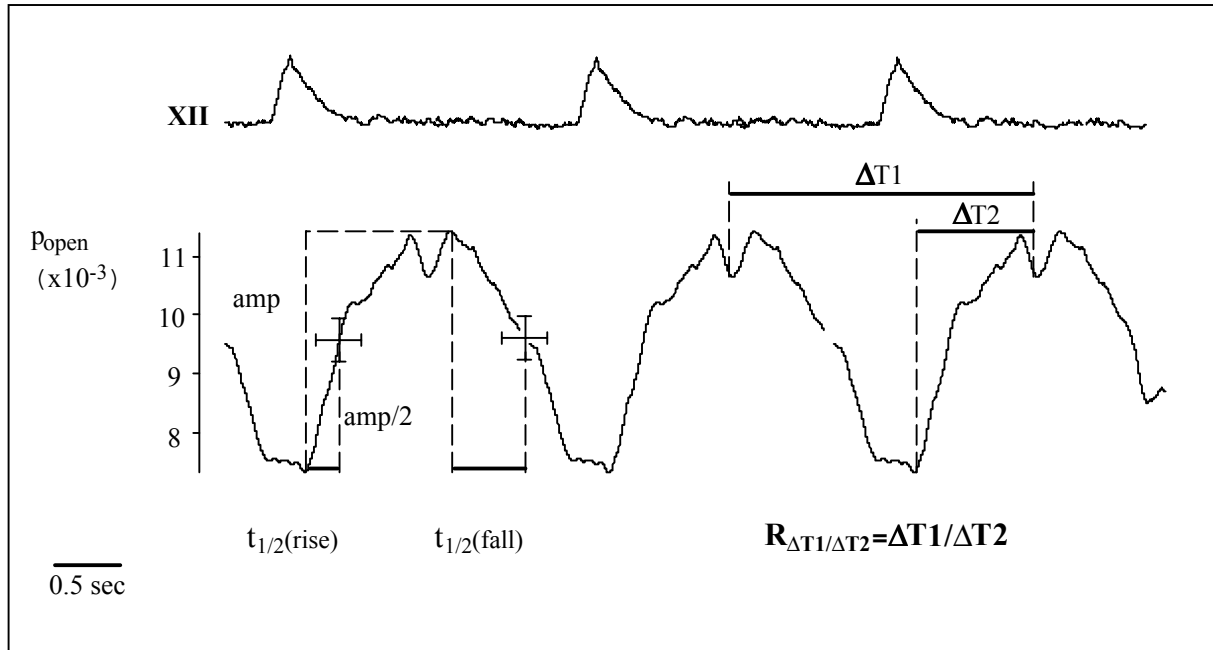


Figure 18: Parameters describing p_{open} -fluctuations. For a quantitative description of the changes in p_{open} -fluctuations the following parameters were analyzed: $R_{\Delta T1/\Delta T2}$ – the ratio of the peak-to-peak duration, $\Delta T1$, over the peak rise time $\Delta T2$; $t_{1/2}(\text{rise})$ – the rise time to half-maximal values ($\text{amp}/2$) and $t_{1/2}(\text{fall})$ – the time taken to fall from peak levels to half-maximal values.

	Control (10 cells)	Hypoxia (4 cells)	Low $[\text{K}^+]_e$ (8 cells)
Cycle length/sec	3.09 ± 0.45	2.19 ± 0.31	6.24 ± 1.32
$t_{1/2}(\text{rise})/\text{sec}$	0.35 ± 0.12	0.67 ± 0.22	0.31 ± 0.09
$t_{1/2}(\text{fall})/\text{sec}$	0.47 ± 0.11	0.37 ± 0.11	0.48 ± 0.08
$R_{\Delta T1/\Delta T2}$	2.81 ± 0.42	1.80 ± 0.21	5.70 ± 1.40

Table 2: Parameters describing the periodic modulation of p_{open} (for description see text and Figure 18)

4.4.1 Estimates of fluctuations in $[ATP]_i$

p_{open} -values can be used to estimate the free ATP concentration, $[ATP]_i$. According to Ashcroft and Gribble (1998) experimental data are best described by a model assuming four ATP-binding sites with equal affinities. Each of them may be located on one of the presumably four Kir6.2 subunits constituting a channel (Nichols et al., 1991). When one of these binding sites is occupied, the channel is blocked. For such a model, ATP concentrations can be estimated by the equation $[ATP]_i = K_d(1/p_{open}^{1/4} - 1)$. Therefore, $[ATP]_i$ was computed for p_{open} -values obtained experimentally for the four binding sites model using a K_d -value of 29 μM as given by Ashcroft and Gribble (1998).

Figure 19 illustrates the temporal fluctuations of the estimated $[ATP]_i$ -values for the p_{open} -fluctuations depicted in Figure 17A and B. For all cells analyzed, baseline levels of $[ATP]_i$ were in the range 10 - 200 μM and peak-to-peak variations occurring during the respiratory cycle ranged between 5 and 40 μM . Higher baseline levels of $[ATP]_i$ gave rise to larger amplitudes of $[ATP]_i$ -variations.

The estimated levels of free $[ATP]_i$ were about 10 times smaller than the generally assumed total cytosolic ATP level. This discrepancy can be attributed to ATP-binding of Mg^{2+} . Assuming that the total ATP concentration is 1 mM (Kargacin and Kargacin, 1997), the free ATP level was computed using K_d -values as given in Figure 27 for Ca^{2+} and Mg^{2+} complexes with ATP, ADP. The total concentration of an endogenous cytoplasmic Ca^{2+} -buffer with the dissociation constant, $K_{d,\text{Ca}} = 10 \mu\text{M}$ (Klingauf and Neher, 1997; Palecek et al., 1999), was assumed to be 500 μM analog to motoneurons in the spinal cord (Palecek et al., 1999). For Mg^{2+} binding to the endogenous buffer a dissociation constant $K_{d,\text{Mg}} = 10 \text{ mM}$ was implemented as suggested by Kargacin and Kargacin (1997).

Total concentrations of these species were adjusted in order to obtain the desired free concentrations of Ca^{2+} , Mg^{2+} , ADP and Ca^{2+} -buffer (free $[\text{Ca}^{2+}]_i = 106 \text{ nM}$, free $[\text{Mg}^{2+}]_i = 843 \mu\text{M}$, free ADP = 54 μM and free buffer concentration = 232 μM). The procedure gave an estimation of 107 μM for the free ATP concentration, which is well within the range of the $[ATP]_i$ -values obtained by the above described estimation based on p_{open} .

The periodic fall of free $[ATP]_i$ could be caused by ATP binding to Ca^{2+} as intracellular $[\text{Ca}^{2+}]_i$ fluctuates with rhythmic activity (Frermann et al., 1999), the amplitude being of the order of 200 nM. Even allowing for much larger Ca^{2+} -fluctuations of 5 μM in

submembrane compartments (Klingauf and Neher, 1997), the model predicts a Ca^{2+} -dependent $[\text{ATP}]_i$ -decrease of less than $5 \mu\text{M}$ (free $[\text{ATP}]_i = 103 \mu\text{M}$, free $[\text{Ca}^{2+}]_i = 5.2 \mu\text{M}$, free $[\text{Mg}^{2+}]_i = 883 \mu\text{M}$, free ADP = $26 \mu\text{M}$ and free buffer concentration = $9.45 \mu\text{M}$). Thus, changes in Ca^{2+} concentrations could account only for a minor portion of the observed fluctuations of $[\text{ATP}]_i$. Therefore, the more likely reason for $[\text{ATP}]_i$ -fluctuations seems to be ATP-consumption during the respiratory burst due to the operation of the Na^+/K^+ -pump.

Assuming a 1:1 stoichiometry for ATP-consumption by the Na^+/K^+ -ATPase and a transport of 2K^+ against 3Na^+ , the local $[\text{ATP}]_i$ -changes could be directly obtained from the total Na^+ -influx during a burst. Rose et al. (1999) measured AP-induced $[\text{Na}^+]_i$ -transients, reaching values of 4mM during a train of 20 APs in dendritic spines. In inspiratory neurons, a burst typically consisted of 5 APs, which would correspond to a $[\text{Na}^+]_i$ -transient of 1mM and to a decrease of total $[\text{ATP}]_i$ by $333 \mu\text{M}$. Assuming a decrease in total $[\text{ATP}]_i$ from 1mM to 0.66mM , a corresponding decrease of free $[\text{ATP}]_i$ from $107 \mu\text{M}$ to $55 \mu\text{M}$ was computed. Such a decrease of approximately $50 \mu\text{M}$ only slightly exceeds the fluctuations in free $[\text{ATP}]_i$ as calculated from p_{open} during respiratory bursts.

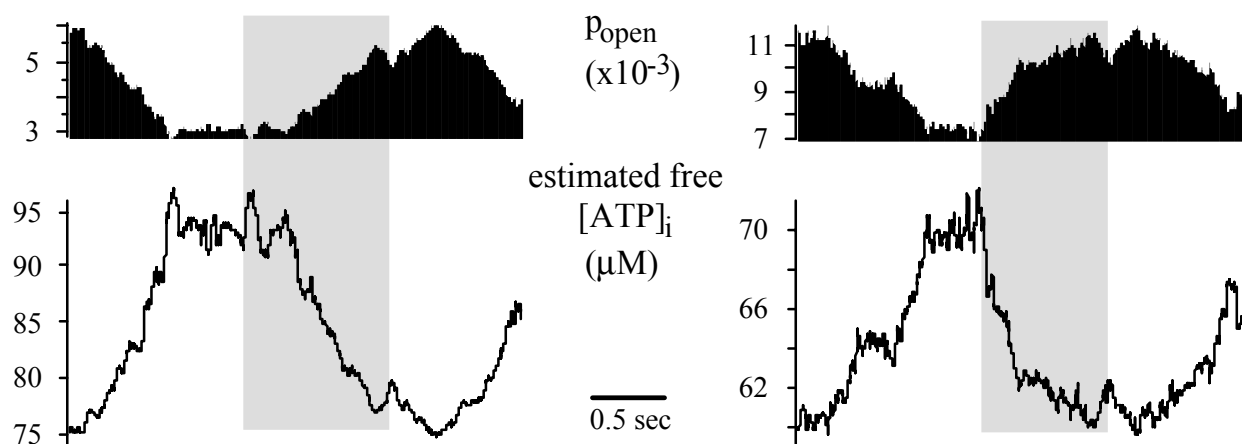


Figure 19: Estimate of $[\text{ATP}]_i$. $[\text{ATP}]_i$ -values (lower panel) were estimated from p_{open} ($[\text{ATP}]_i = K_d(1/p_{\text{open}}^{1/4} - 1)$) with $K_d = 29 \mu\text{M}$ (Ashcroft and Gribble, 1998) for the two p_{open} -traces previously displayed in Figure 17A and B.

4.4.2 Exceptions from p_{open} modulation

Next, it was tested, whether the p_{open} -fluctuations can also be observed in the high activity gating mode. In Figure 20 respiratory bursts correlated with peak hypoglossal activity (XII) are indicated by gray bands. The open probability corresponding to the ‘normal’ low activity mode is given in the following two traces – one in terms of p_{open} , the other in terms of the percentage change of p_{open} ($n = 49$). p_{open} -fluctuations follow the pattern described above. The corresponding traces are depicted below for time periods when the channel is in the mode of high activity ($n = 21$). It can be seen that the respiratory fluctuations usually observed are absent. This became obvious when the relative changes in p_{open} were compared. In the low activity mode, p_{open} increased by up to 60 % during the periodic fluctuations, whereas fluctuations never exceeded 15 % in the high activity mode. The effect could be observed in 4/5 cells analyzed, with only one cell also indicating p_{open} -fluctuations in the high activity mode.

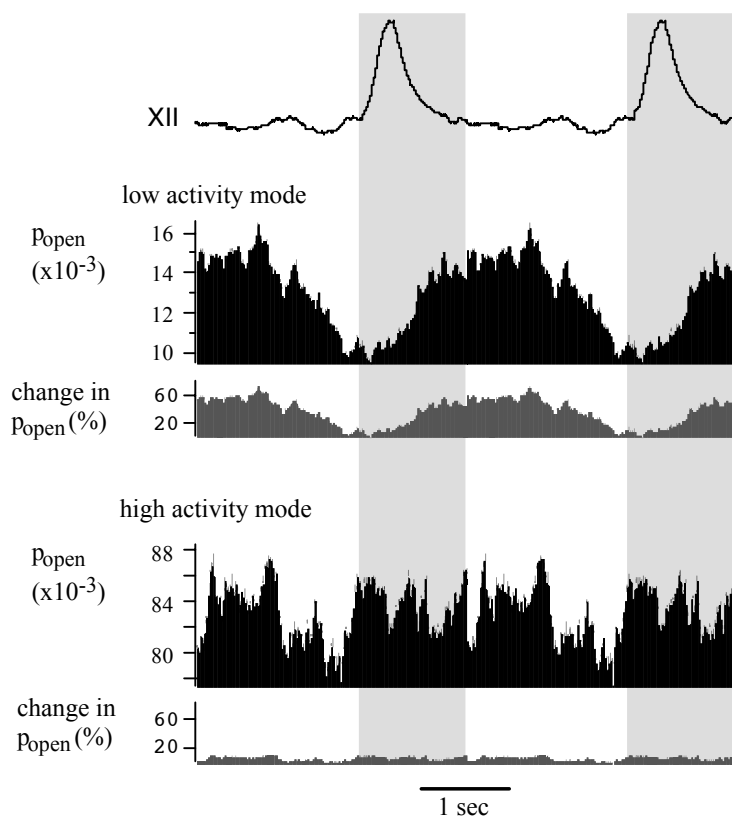


Figure 20: Modulation of p_{open} in different channel gating modes. Respiratory bursts are indicated by the transient peaks in integrated hypoglossal activity (XII) as indicated by the gray lanes. p_{open} and the corresponding change in p_{open} are displayed below for time periods when the channel is in the mode of low activity ($n = 49$) or high activity ($n = 21$). The periodic fluctuations typical for ‘normal’ channel gating cannot be observed during periods of the high activity mode.

In order to test whether the K_{ATP} -fluctuations described above were unique to inspiratory neurons several controls were performed. Membrane depolarization of neurons underlying rhythmic bursts sometimes led to a transient deflection of the baseline in cell-attached recordings. In order to exclude the possibility that the p_{open} -fluctuations observed were an artifact due to such baseline fluctuations, the same procedure was employed to analyze traces from respiratory neurons that did not exhibit K_{ATP} -channel activity (Figure 21B). The noise subtraction criterion was lowered (see chapter 3.2). The mean fluctuations of 100 traces were then displayed as a percentage change in fluctuations. It can be seen that the amplitudes of fluctuations were much smaller than in the case of a respiratory neuron with channel activity (Figure 21A). When spontaneously active K_{ATP} -channels as seen in tonic or silent cells in the pre-Bötzinger complex were analyzed (Figure 21C and D, respectively), the fluctuations exhibited only very small amplitudes or were absent.

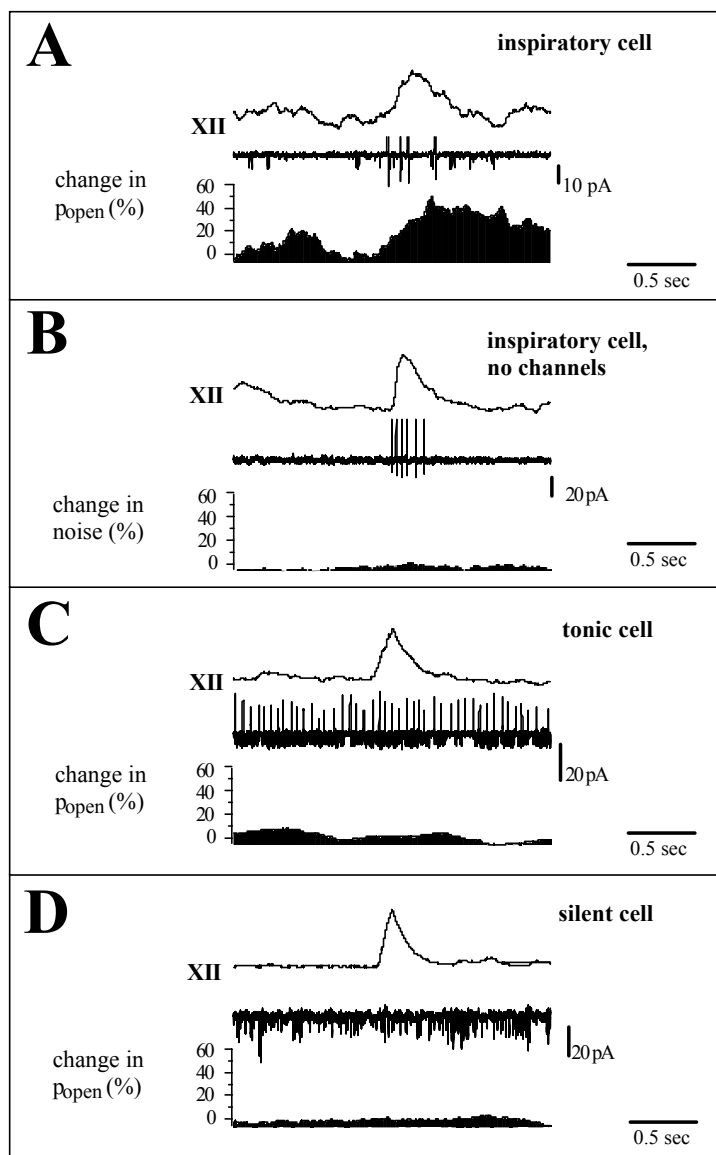


Figure 21: p_{open} modulation in different cell types. Cell-attached recordings from inspiratory cells without channel activity (2 cells), tonic cells and cells without action potential discharge (2 cells) were used for controls (B, C and D, respectively). The analysis was performed as described for Figure 17. The analysis in (B) was performed in order to exclude the possibility that baseline fluctuations were responsible for apparent channel modulations. For this reason an inspiratory neuron without channel activity was analyzed with a low-level noise subtraction criterion – noise was subtracted only in a range of ± 1 pA from the baseline. A direct comparison of p_{open} -fluctuations is difficult because of the low open probabilities. Thus, the open probabilities were not compared directly, but rather in terms of the degree of change of p_{open} expressed in percent. It can be seen that neither the cell in (B) nor (C) nor (D) displayed the same pattern of channel modulation as an inspiratory neuron with channel openings (A). In addition, amplitudes of fluctuations of p_{open} were much lower than those observed under (A).

4.4.3 Variation of cycle length

An effective tool that can be used to modulate periodic p_{open} -fluctuations is the modification of $[\text{K}^+]_e$. An increase/decrease of $[\text{K}^+]_e$ leads to a decrease/increase of the mean cycle length. Figure 22A shows traces of hypoglossal rootlet recordings (XII), p_{open} -values for a $[\text{K}^+]_e$ of 8 mM or 11 mM and estimated $[\text{ATP}]_i$. At low $[\text{K}^+]_e$, the cycle length increased and the averaged open probability decreased (3 cells). The only parameter that differed significantly when traces of long cycle lengths (5 sec and above) were compared with control cycles (length approximately 3 sec) was $R_{\Delta T1/\Delta T2}$, which increased from 2.81 ± 0.42 (10 cells) at elevated $[\text{K}^+]_e$ to values of 5.70 ± 1.40 (8 cells) at low $[\text{K}^+]_e$ (Table 2). Presumably, this reflects a longer persistence of the channel in a low p_{open} state before the onset of the next burst when neuronal activity was low. The $t_{1/2}$ -values, however, were hardly affected, as burst dynamics did not change considerably with variation of interburst intervals. A plot of mean p_{open} -values against cycle length is shown in Figure 22B. Linear regression gives a slope of -0.0011 ($r = -0.31$; $P < 0.01$) for this particular experiment and an average slope of -0.0012 ± 0.0011 for 10 cells. A possible explanation for this correlation would be that as cycle length decreases, less time is available for ATP-replenishment between bursts, resulting in a lower mean $[\text{ATP}]_i$ level and a higher mean p_{open} .

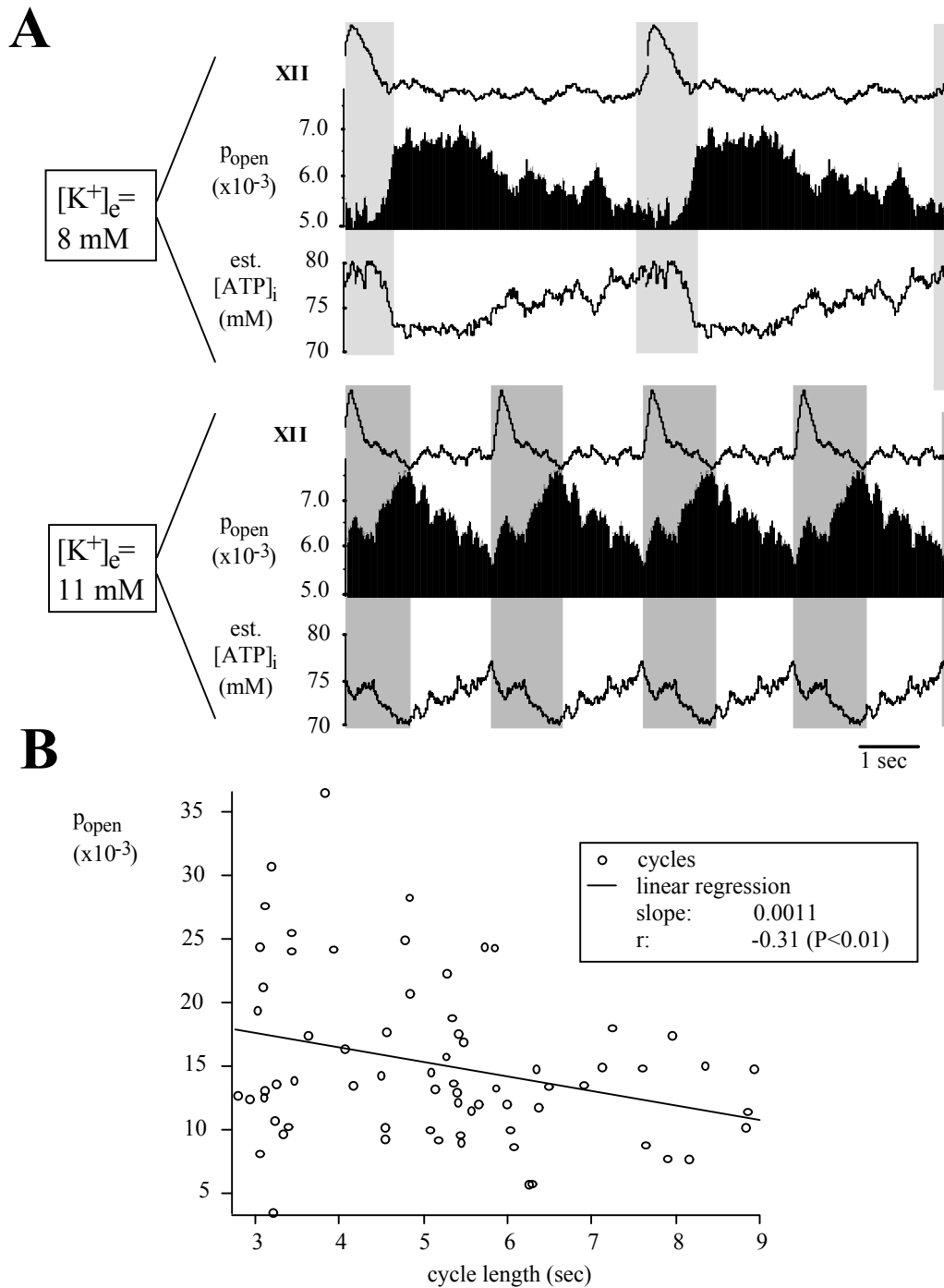


Figure 22: Modulation of K_{ATP} -channel activity for different cycle lengths. Fluctuations of p_{open} and $[ATP]_i$ with 8 mM (upper panel) or 11 mM $[K^+]_e$ (lower panel). 100 traces of duration 5 sec and 2.5 sec were selected for a $[K^+]_e$ of 8 mM and 11 mM, respectively, and analyzed as described in the text. Hypoglossal rootlet activity (XII), p_{open} and $[ATP]_i$ were reproduced and repeated twice (above) or four times (below). It can be seen that the cycle length decreases and the mean open probability increases as $[K^+]_e$ is elevated. However, the basic pattern of fluctuation remains the same: p_{open} rises during the inspiratory bursts and falls after the inspiratory burst. (B) Plot of mean p_{open} against cycle length for 71 consecutive traces. The individual values are represented by empty circles, the linear regression by a straight line (slope = -0.0011, $P < 0.01$). The mean slope obtained by linear regression from $n = 10$ experiments was -0.0012 ± 0.0011 .

4.4.4 Effect of hypoxia on K_{ATP} -channel modulation

Another manipulation, which affects cycle length dramatically, is hypoxia. Figure 23A shows the response of hypoglossal activity to hypoxia. An initial hypoxic augmentation exhibiting an increase in respiratory burst frequency is followed by a secondary hypoxic depression revealing a decrease in burst frequency. The effect of hypoxia on p_{open} -fluctuations was analyzed by comparing the channel activities in control (indicated by a dark gray area) with those measured during a period of enhanced neuronal activity (indicated by a light gray area) shortly before the onset of hypoxic depression. During hypoxic depression of respiratory activity, analyses could not be performed due to the low number of bursts in this time period and the high variations in burst durations. The left panel of Figure 23B shows the mean hypoglossal activity, a sample trace displaying a burst of action potentials and the mean p_{open} as well as $[ATP]_i$ for traces obtained under control conditions ($n = 34$). The right panel displays the corresponding traces during the initial phase of hypoxia ($n = 21$). Traces were reproduced twice during control and three times during hypoxia for better visualization of periodic activities. The duration of respiratory bursts was marked by gray areas. It is noteworthy that the channel activity is enhanced during hypoxia, presumably due to an overall fall in $[ATP]_i$ levels.

During early hypoxia, $t_{1/2}(\text{rise})$ and $t_{1/2}(\text{fall})$ increased to $0.67 \text{ sec} \pm 0.22 \text{ sec}$ (control: $0.35 \text{ sec} \pm 0.12 \text{ sec}$) and decreased to $0.38 \text{ sec} \pm 0.11 \text{ sec}$ (control: $0.46 \text{ sec} \pm 0.11 \text{ sec}$), respectively (see Table 2). Thus, p_{open} continued to rise for a considerably longer time during a hypoxic burst even when the total cycle length was decreased. A possible explanation of this effect could be the increase of AP burst duration during hypoxia, an example of which can be seen in the cell-attached traces displayed in Figure 23B. All four cells analyzed displayed prolonged burst durations and increased numbers of APs, the burst duration increasing from 0.22 s to maximally 0.84 s and the number of APs increasing from 3.9 to 12.8 (data not shown). The hypoxic rise of $R_{\Delta T1/\Delta T2}$ observed most likely results from burst prolongation leading to a prolonged period of ATP-depletion, $\Delta T1$, accompanied by a shortening of cycle duration, i.e. a decrease in $\Delta T2$.

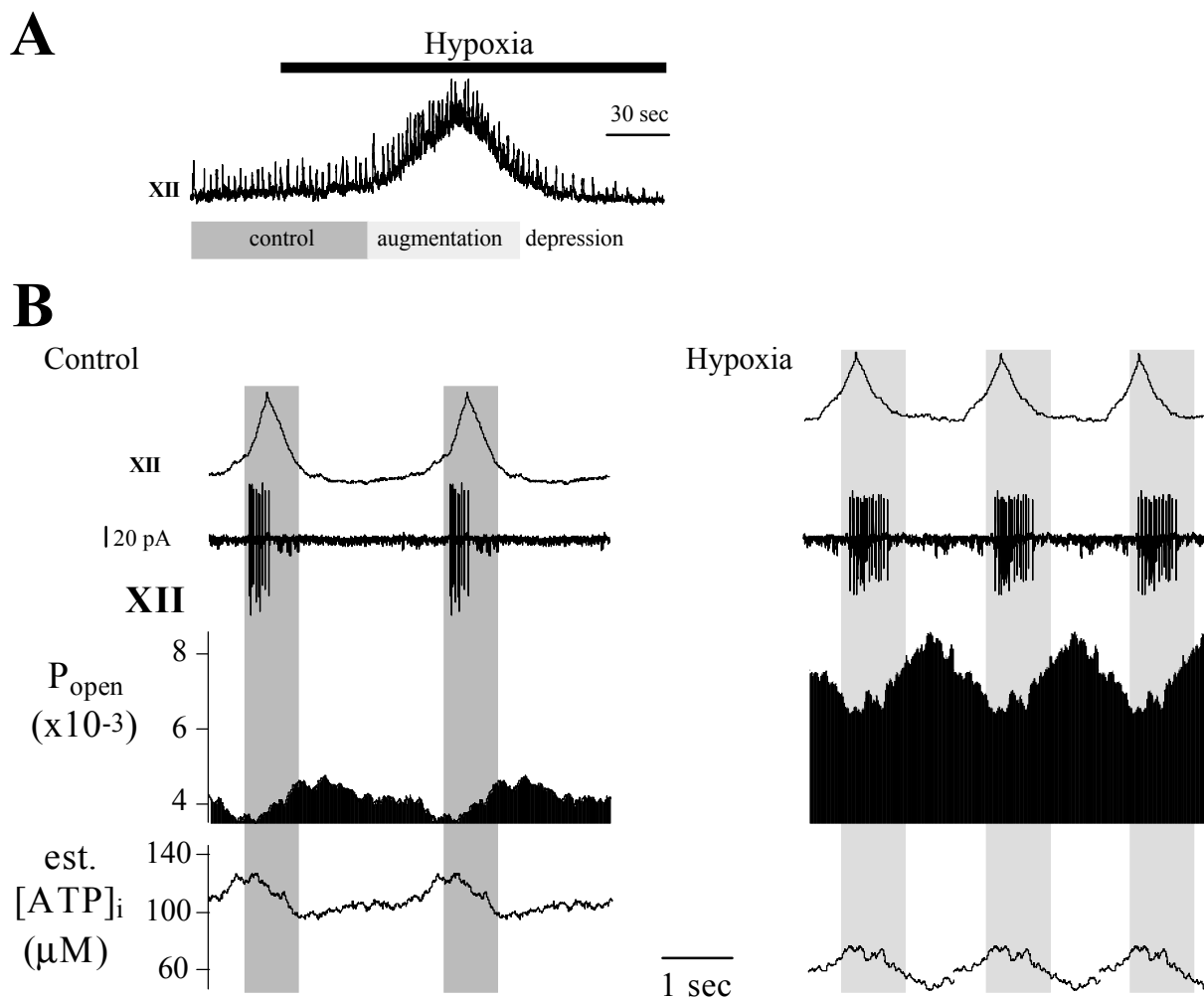


Figure 23: Modulation of K_{ATP} -channel activity during hypoxia. (A) displays the response of hypoglossal activity to hypoxia. An increase in respiratory burst frequency and amplitude (hypoxic augmentation) is followed by a decrease in both parameters (hypoxic depression). p_{open} -values for control sweeps (dark gray area) and those for the augmentation phase of hypoxia (light gray area) were analyzed separately. The mean open probability of K_{ATP} -channels and calculated $[ATP]_i$ -values were then computed as described in the text. For control conditions (B, upper panel, $n = 34$) traces were reproduced and duplicated, for hypoxic conditions (B, lower panel, $n = 21$) traces were consecutively depicted three times. The durations of respiratory burst activity were marked by gray areas. The open probability shows a marked increase during hypoxia. $R_{\Delta T1/\Delta T2}$, $t_{1/2}(\text{rise})$ and $t_{1/2}(\text{fall})$ were modulated during hypoxia in 4/4 cells (see text).

4.5 Estimation of $[ATP]_i$ based on fluorometric measurements

It has been mentioned before that K_{ATP} -channels are strongly activated by hypoxia. Figure 24 shows the time course of this activation. It can be seen that channel activity reaches a plateau during the phase of hypoxic depression, suggesting that K_{ATP} -channels might be involved in a series of inhibitory mechanisms that are activated by hypoxia. A number of factors might lead to hypoxic K_{ATP} -channel activation, ranging from decrease in $[ATP]_i$ and pH, and activation of PKC and PKA, to disruption of the cytoskeleton during cell swelling.

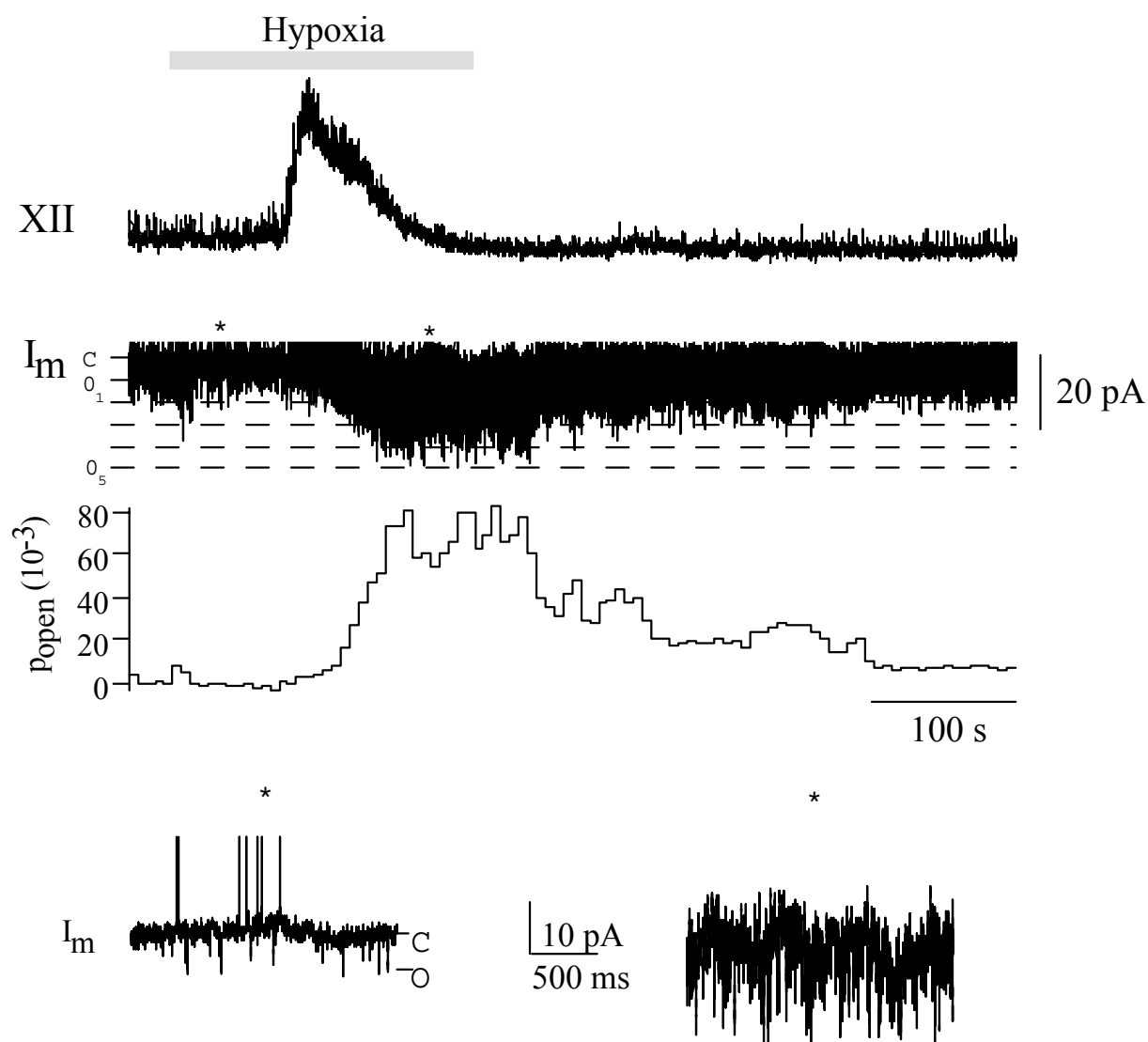


Figure 24: K_{ATP} -channels are activated by hypoxia. The upper traces show hypoglossal (XII) activity, single-channel currents (I_m) recorded in the cell-attached mode and the open probability, p_{open} . The small inserts below show data taken from the cell-attached recording above (as indicated by *) and extended on a larger scale.

In order to determine the contribution of $[ATP]_i$ the amplitude of the hypoxia-induced $[ATP]_i$ -decrease was investigated: Intracellular ATP concentrations have been monitored previously either directly using the chemiluminescent couple, luciferin-luciferase (Bowers et al., 1993), or indirectly using the Mg^{2+} fluorescent indicator Magnesium Green (Leysens et al., 1996). Being single-wavelength methods it is not feasible to apply either in respiratory neurons due to the strong cell swelling during hypoxia. Thus, only a ratiometric dye such as mag-fura-2 allows reliable measurements. Use of a Mg^{2+} -sensitive dye to provide an index of changing ATP concentrations follows the rationale that bound Mg^{2+} is partially released as ATP is hydrolyzed to ADP during hypoxia, due to the lower affinity of ADP for Mg^{2+} . The increase in free Mg^{2+} , which can be estimated by a Mg^{2+} -sensitive dye, thus reflects the hypoxic fall of $[ATP]_i$ (Figure 25).

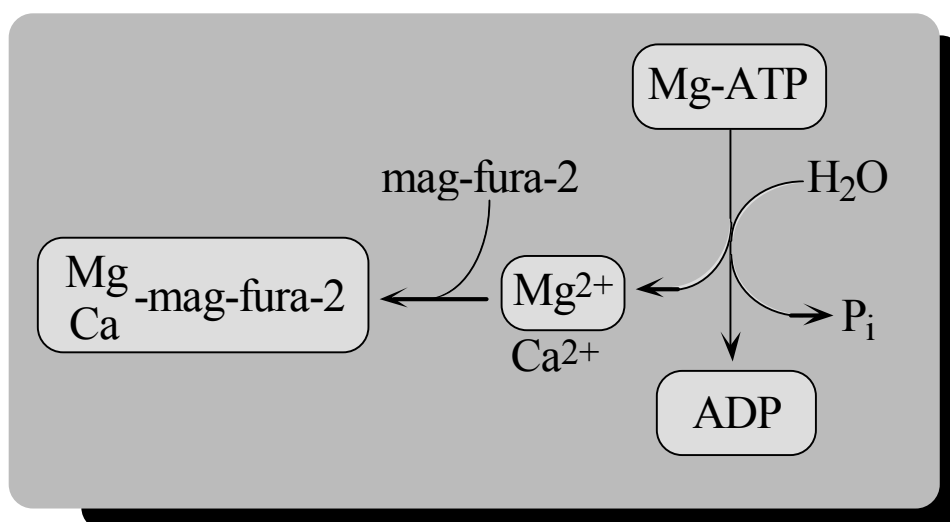


Figure 25: Indirect measurement of $[ATP]_i$ -changes based on mag-fura-2.

However, intracellular Ca^{2+} levels also increase during hypoxia (Ballanyi and Kulik, 1998). This may be due to a Ca^{2+} -influx through L-type Ca^{2+} channels or Ca^{2+} release from internal stores, including mitochondria (Mironov, unpublished data). The mag-fura-2 signal is therefore expected to depend on rises in both hypoxic Mg^{2+} and Ca^{2+} . For this reason the hypoxic Ca^{2+} -increase was measured using the Ca^{2+} -sensitive dye fura-2 ($n = 3$) as well as the mag-fura-2 signal ($n = 5$) (Figure 26).

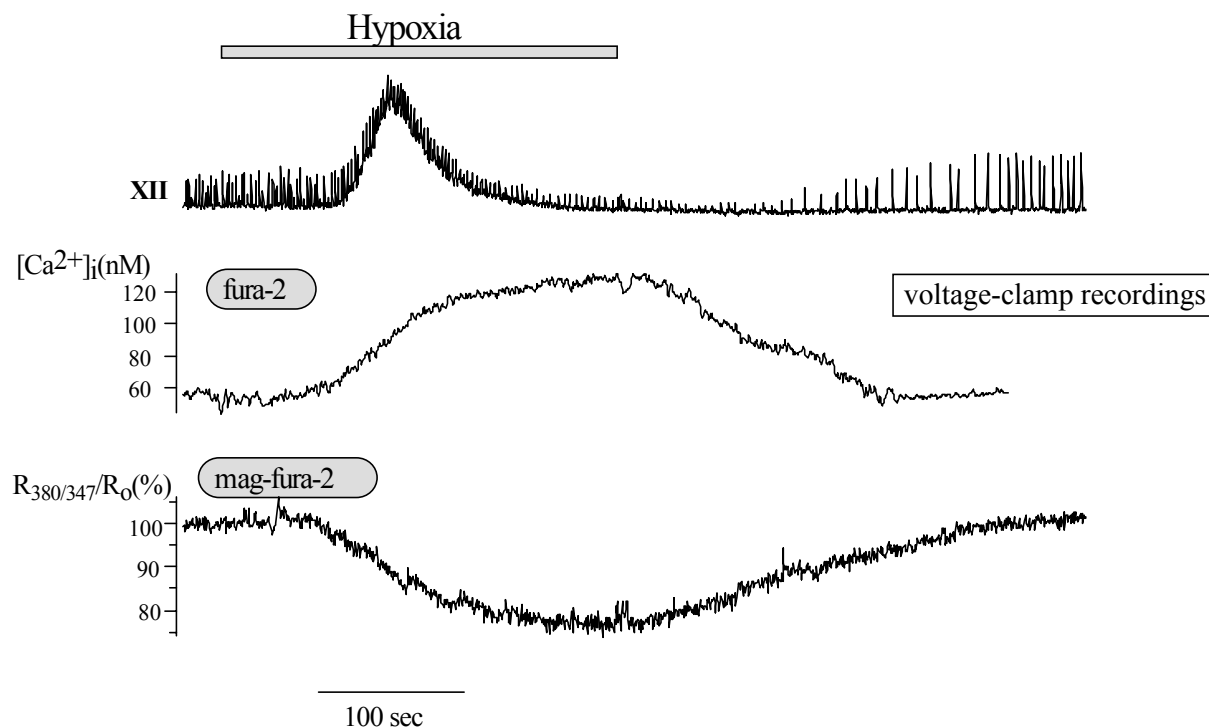


Figure 26: Fluorometric measurements during hypoxia. The upper panel represents the response of the hypoglossal nerve (XII) activity to hypoxia. The middle trace shows the Ca^{2+} signal as measured by fura-2. The lower trace displays the fall of free mag-fura-2 presented as the ratio of the fluorescence signals measured at excitation wavelengths of 380 nm and 347 nm, which reflects the concentration of free and total mag-fura-2, respectively. Fura-2 and mag-fura-2 signals were measured in different cells filled with solutions containing either fura-2 or mag-fura-2.

Levels of intracellular Ca^{2+} concentration measured during hypoxia did not exceed levels of 200 - 300 nM, which is in agreement with values obtained by Ballanyi and Kulik (1998) in dorsal vagus neurons of the brainstem. The mag-fura-2 signal is displayed as the relative decrease (in percent) of the ratio of the signal measured at 380 nm and 347 nm. Thus, by dividing the concentration of free mag-fura-2 (measured at 380 nm) by the concentration of total mag-fura-2 (measured at 347 nm), an index is obtained for the decrease of free mag-fura-2 corresponding to a decrease in $[\text{ATP}]_i$. The average decrease in the mag-fura-2 signal at a time point three minutes after the onset of hypoxia was found to be $21.7 \pm 4.8\%$ ($n = 5$). It can be seen that the greatest rate of mag-fura-2 decrease is reached during the augmentation phase of hypoxia and that the mag-fura-2 signal levels off toward the depression phase. This is in good agreement with the time course observed for p_{open} as seen in Figure 24.

Knowledge of the hypoxic levels of intracellular Ca^{2+} allows an evaluation of the possible contribution of Ca^{2+} to the mag-fura-2 signal. Calculation of the free concentrations was based

on the total concentrations of Mg^{2+} , Ca^{2+} , ATP, ADP, EGTA and mag-fura-2 used for the intracellular pipette solution (see chapter 2.2) and on the pK_d values of the equilibrium indicated in Figure 27 below. The equilibrium concentrations were calculated using a Newton-Raphson iterative algorithm.

H_4ATP	$\leftarrow -1^a \rightarrow$	$H_3ATP^- + H^+$	$\leftarrow -1^a \rightarrow$	$H_2ATP^{2-} + 2H^+$	$\leftarrow -4.05^a \rightarrow$	$HATP^{3-} + 3H^+$	$\leftarrow -6.95^b \rightarrow$	$ATP^{4-} + 4H^+$
H_4ADP	$\leftarrow -1^c \rightarrow$	$H_3ADP^- + H^+$	$\leftarrow -1^c \rightarrow$	$H_2ADP^{2-} + 2H^+$	$\leftarrow -3.96^c \rightarrow$	$HADP^{3-} + 3H^+$	$\leftarrow -6.40^c \rightarrow$	$ADP^{4-} + 4H^+$
H_4EGTA	$\leftarrow -2^d \rightarrow$	$H_3EGTA^- + H^+$	$\leftarrow -2.66^d \rightarrow$	$H_2EGTA^{2-} + 2H^+$	$\leftarrow -8.85^d \rightarrow$	$HEGTA^{3-} + 3H^+$	$\leftarrow -9.47^d \rightarrow$	$EGTA^{4-} + 4H^+$
$CaHATP^-$	$\leftarrow -4.69^c \rightarrow$	$CaATP^{2-} + H^+$	$\leftarrow -3.77^c \rightarrow$	$ATP^{4-} + 2H^+ + Ca^{2+}$				
$MgHATP^-$	$\leftarrow -4.55^c \rightarrow$	$MgATP^{2-} + H^+$	$\leftarrow -4.06^c \rightarrow$	$ATP^{4-} + 2H^+ + Mg^{2+}$				
$CaHADP^-$	$\leftarrow -5.16 \rightarrow$	$CaADP^{2-} + H^+$	$\leftarrow -2.81 \rightarrow$	$ADP^{4-} + 2H^+ + Ca^{2+}$				
$MgHADP^-$	$\leftarrow -4.91^c \rightarrow$	$MgADP^{2-} + H^+$	$\leftarrow -3.17^c \rightarrow$	$ADP^{4-} + H^+ + Mg^{2+}$				
$CaHEGTA^-$	$\leftarrow -3.79^d \rightarrow$	$CaEGTA^{2-} + H^+$	$\leftarrow -10.97^d \rightarrow$	$EGTA^{4-} + H^+ + Ca^{2+}$				
$MgHEGTA^-$	$\leftarrow -7.62^d \rightarrow$	$MgEGTA^{2-} + H^+$	$\leftarrow -5.21^d \rightarrow$	$EGTA^{4-} + H^+ + Mg^{2+}$				
$Ca\text{-magfura}$	$\leftarrow -5.40^c \rightarrow$	$\text{magfura}^{2-} + Ca^{2+}$						
$Mg\text{-magfura}$	$\leftarrow -2.70^c \rightarrow$	$\text{magfura}^{2-} + Mg^{2+}$						

Figure 27: pK_d values used for simulation. ^a from (Martell and Smith, 1982). ^b from (Fabiato, 1981). ^c from (Smith and Martell, 1975a). ^d from (Smith and Martell, 1975b). ^e from (Konishi et al., 1991).

Hypoxic conditions were simulated (Figure 28) by assuming an exponential fall of total ATP concentrations from 2 mM to 22 μ M and a concomitant rise of ADP concentrations from 0 to 1.98 mM. Free concentrations were computed twice – once with a constant total Ca^{2+} concentration of 1 mM and once with an assumed rise in total Ca^{2+} from 1 to 7 mM, corresponding to a rise in free Ca^{2+} from 31 nM to 311 nM. The simulation did not account for any diffusion of fresh solution from the patch pipette (see chapter 5). During hypoxia, mag-fura-2 levels decreased by 14 % at resting Ca^{2+} and by 17 % when Ca^{2+} was assumed to increase. This simulation thus indicates that intracellular Ca^{2+} will contribute no more than approximately 18 % to the mag-fura-2 signal.

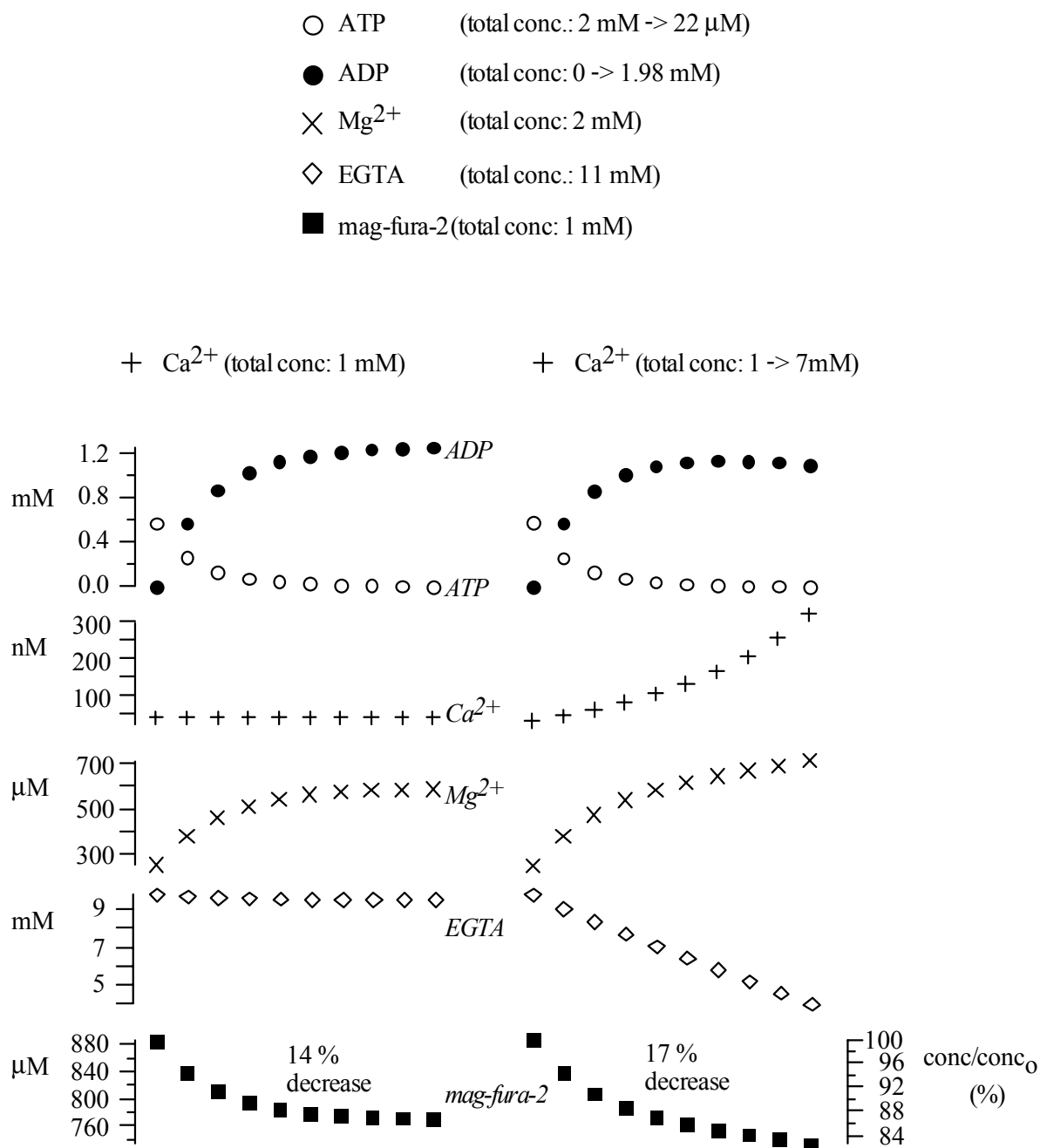


Figure 28: Simulation of hypoxic effects: changes in the Ca^{2+} concentration contribute approximately 20 % to the mag-fura-2 signal. The left side shows simulated changes in intracellular Mg^{2+} , Ca^{2+} , EGTA and mag-fura-2 due to a presumed decrease in total intracellular ATP concentration from 2 mM to 22 μ M, which is accompanied by a simultaneous rise in ADP from 0 mM to 1.98 mM. The right column includes a simultaneous rise in free Ca^{2+} from 31 nM to 311 nM.

Assuming consequently that 80 % of the mag-fura-2 is actually due to an $[ATP]_i$ -decrease it became possible to estimate the hypoxia-induced decrease in $[ATP]_i$ based on mag-fura-2 measurements as show in Figure 26. The resulting $[ATP]_i$ -trace is displayed in Figure 29.

[ATP]_i was computed for each point by slowly decreasing the total ATP concentration (initial value 2 mM) until the estimated equilibrium concentration of free mag-fura-2 matched the value observed in the experiment ($\pm 5\%$). Total [ADP]_i was set to be $2\text{ mM} - \text{ATP}$ and [Ca²⁺]_i was set to a constant value of 1 mM. A decrease in [ATP]_i of approximately 500 μM was observed during hypoxia.

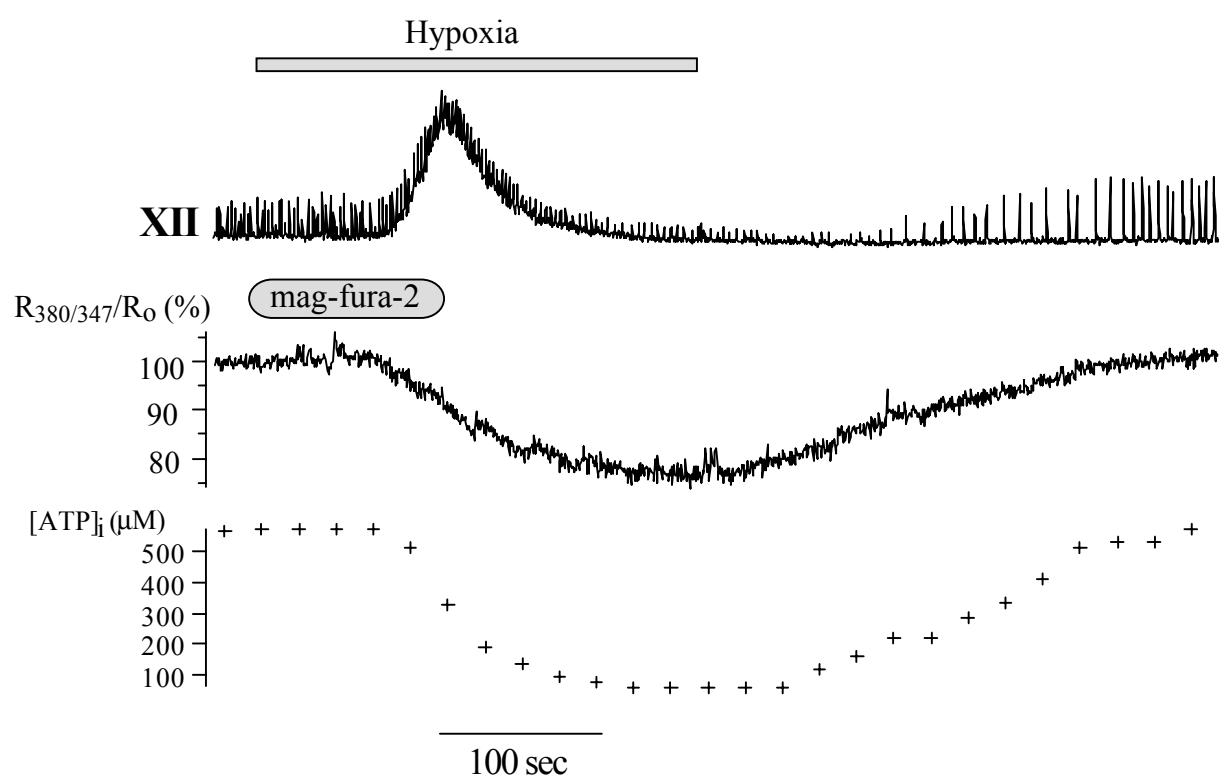


Figure 29: Estimate of intracellular decrease in [ATP]_i during hypoxia. The lowest trace gives the computed ATP concentrations reflecting the measured mag-fura-2 fluorescence signal (middle trace).

4.6 Effect of purinoceptor activation

As described in chapter 1.6, ATP is also known to act on neurons extracellularly, functioning as a neurotransmitter. Previously, P₂ purinoceptors have been reported to be involved in a whole variety of ATP-induced responses of neurons ranging from total inhibition to excitation of synaptic activity (for detailed descriptions see Illes and Norenberg (1993) and Harden et al. (1995)).

Studies of the purine effects are complicated by the fact that apart from activating P_{2X}- and P_{2Y}-purinoceptors, ATP will also degrade to adenosine, which in turn is effective via adenosine receptors. In preliminary single cell PCR experiments the presence of P_{2X}- and P_{2Y}-purinoceptors in respiratory neurons was revealed.

However, the effect of bath application of extracellular NaATP (500 µM - 1 mM) on the respiratory rhythm was found to be quite variable. In 17 experiments respiratory bursts were depressed in 7 cases and augmented in 10, but in 6 cases the augmentation was only transient, lasting no longer than approximately 1 - 2 minutes, and was followed by a secondary depression as exemplified by Figure 30. In most cases hypoglossal activity also exhibited a transient rise in baseline similar to the response typically observed during hypoxia. In all cases, the frequency decreased after ATP application. Amplitude and frequency of synaptic drives typically changed in correlation with rhythmic activity. When the P₂-antagonist PPADS (pyridoxal-phosphate-6-azophenyl-2', 4'-disulphonic-acid) was added, the transient augmentation was removed, but both depression and decrease in frequency persisted, indicating that these two might be adenosine-mediated (and not purinoceptor-mediated) responses. This would be in agreement with the adenosine responses described in Mironov et al. (1999).

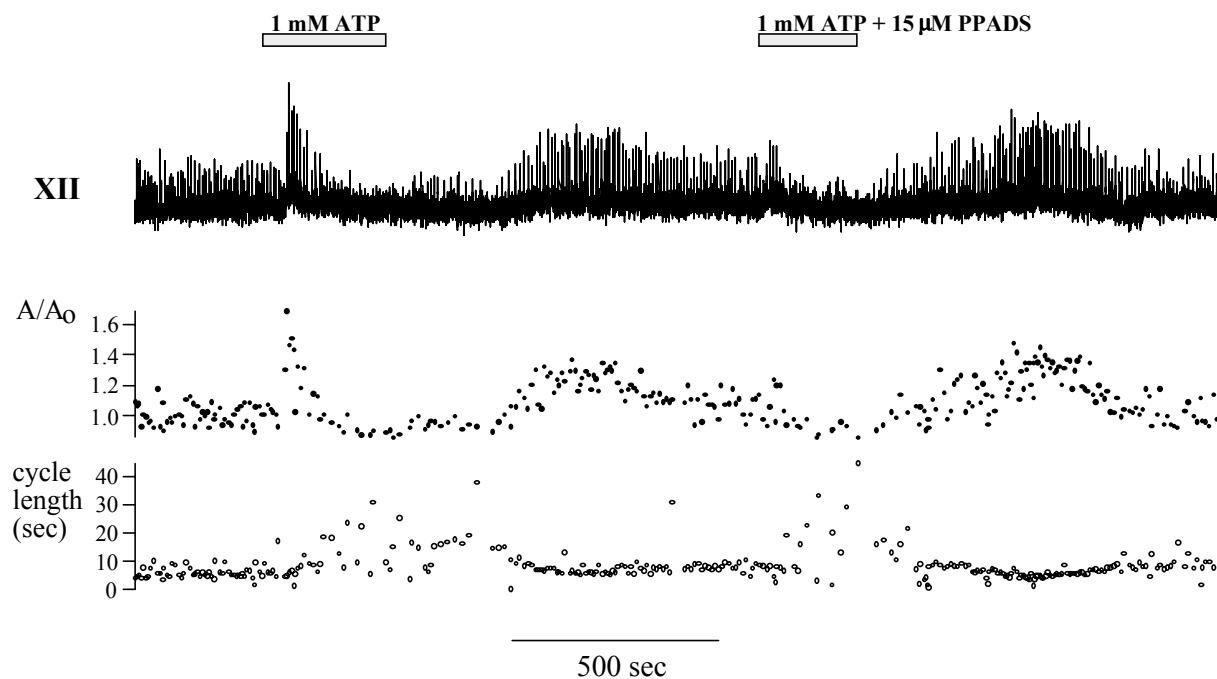


Figure 30: Effect of extracellular ATP on rhythmic activity. Bath application of ATP sometimes lead to a transient augmentation of rhythmic activity (XII) which is blocked by the P_{2X} receptor antagonist PPADS (pyridoxal-phosphate-6-azophenyl-2', 4'-disulphonic acid). The upper trace shows the hypoglossal activity (XII) and the lower two traces the relative change in amplitude, A/A_0 and the cycle lengths. Burst amplitudes exhibited a PPADS-sensitive transient augmentation followed by a PPADS-insensitive depression. The cycle lengths were observed to increase after ATP application even in the presence of PPADS.

The assumption that purinoceptors contribute to the augmentation of respiratory activity is further corroborated by the finding that a transient augmentation but no depression in amplitude or frequency was observed following the application of the non-hydrolysable ATP analog and P_2 purinoceptor agonist alpha,beta-methyleneadenosine 5'-triphosphate (α,β -MeATP) (Figure 31).

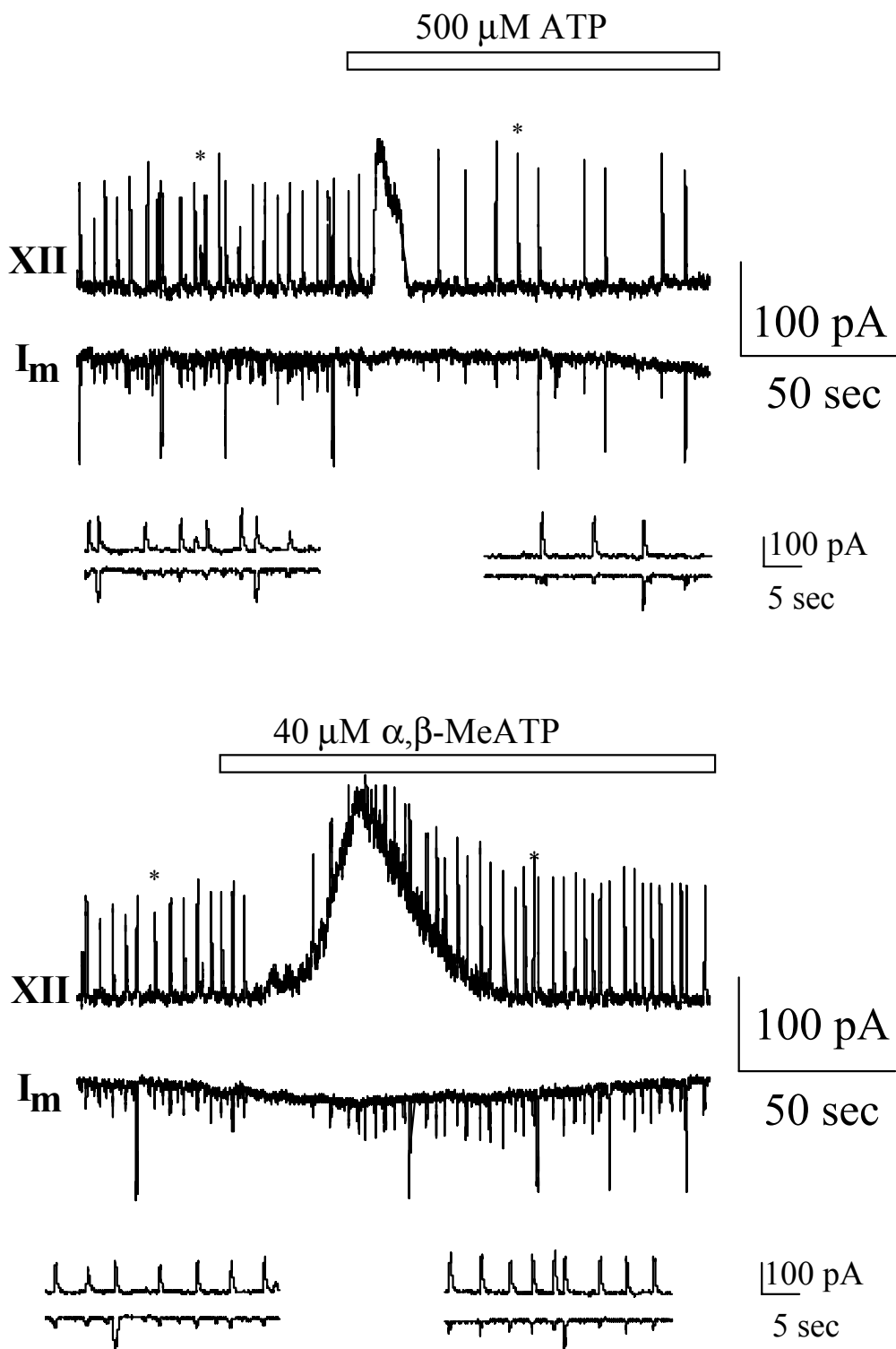


Figure 31: Response of the respiratory center to purinoceptor activation. Integrated hypoglossal nerve activity (XII) and membrane current (I_m) were recorded after application of ATP (top) and $\alpha,\beta\text{-MeATP}$ (bottom). Sections marked by * are displayed on an extended scale underneath. $\alpha,\beta\text{-MeATP}$ induced an augmentation similar to the one observed after ATP application, but did not elicit a secondary depression.

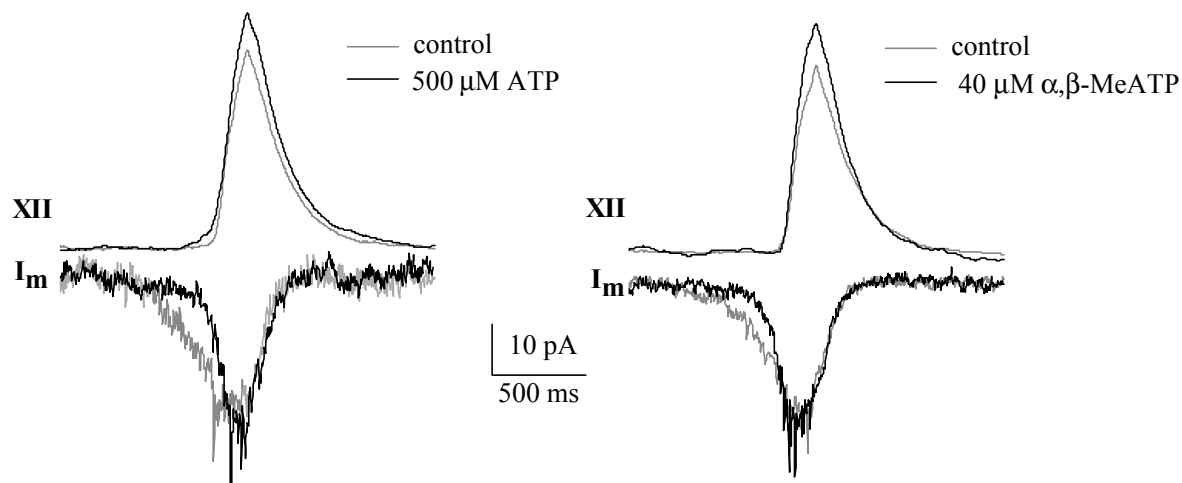


Figure 32: Synaptic drives are modulated by ATP and α,β -MeATP. Averages of 10 are given for hypoglossal bursts (XII) and the corresponding synaptic drives before and after application of ATP (left) and α,β -MeATP (right). Drug application lead to an augmentation of the respiratory burst as described before and a “narrowing” of the synaptic drive.

Interestingly, the shape of the synaptic drives is modulated following ATP or α,β -MeATP application resulting in a “slimmer” synaptic drive (Figure 32) in all experiments analyzed ($n=5$). Such findings suggest that purinoceptors contribute to the process involved in rhythmogenesis. P_{2Y} purinoceptors are known to activate phospholipase C (PLC) through a GTP-liganded G-protein (Boyer et al., 1989; Berrie et al., 1989; Boyer et al., 1990; Boyer et al., 1994) and PLC, in turn, has been reported to modulate K_{ATP} -channel activity (Hilgemann, 1997). For this reason P_{2Y} purinoceptor activation would also be expected to affect K_{ATP} -channel activity. In order to test whether K_{ATP} -channels in inspiratory neurons might be modulated via this pathway, α,β -MeATP was applied in the cell-attached mode (Figure 33). Channels were observed to be reversibly potentiated by α,β -MeATP, which corroborates a participation of purinoceptors in K_{ATP} -channel modulation. The slow time course of the bath application of agonists has made it impossible to examine the role of P_2 receptor subtypes in more detail.

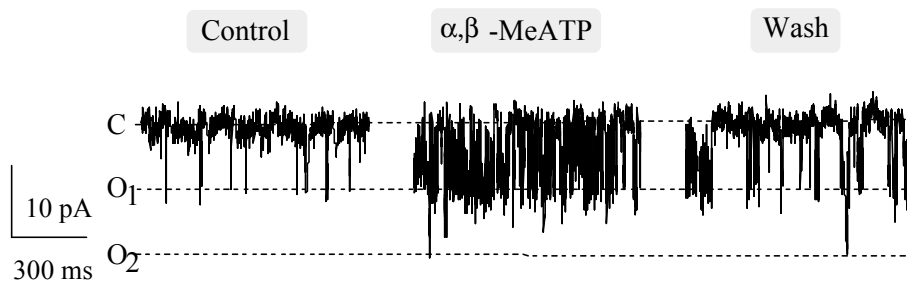


Figure 33: K_{ATP} -channels are potentiated by α,β -MeATP.

4.7 Flash photolysis of caged- Ca^{2+} and caged-ATP

A flash photolysis unit was integrated into the experimental setup with the aim of studying the response of K_{ATP} -channels to fast elevations of $[\text{ATP}]_i$ using a caged-ATP probe.

As a first test of the flash photolysis unit, cells were loaded with a solution containing caged- Ca^{2+} (see chapter 2.2). A medium flash of 250 μs duration with electrical parameters 3000 μF and 350 V was then applied. The light was additionally attenuated by a 50 % neutral density filter. A flash induced a $[\text{Ca}^{2+}]_i$ -transient of several seconds duration as monitored with the Ca^{2+} -sensitive dye fura-2 (Figure 34A). When flashes were given every 4 minutes the resulting Ca^{2+} -transients remained constant. However, during hypoxia the time course of $[\text{Ca}^{2+}]_i$ recovery changed. Generally, $[\text{Ca}^{2+}]_i$ recovery is biexponential (Mironov, 1995), with a fast component, which is determined by diffusion (and partially by Ca^{2+} -pumps), and a slow component, which is thought to result exclusively from Ca^{2+} -pumps. Only the slow component of Ca^{2+} -transients could be measured accurately due to the slow sampling rate of the camera. The corresponding time constants increased during hypoxia (Figure 34A). Furthermore, $[\text{Ca}^{2+}]_i$ did not recover or only very slowly recovered to baseline levels during hypoxia. Both effects were reversible and Ca^{2+} -transients restored their initial form after 10 minutes of reoxygenation. These observations indicate that $[\text{Ca}^{2+}]_i$ -homeostasis is affected during hypoxia.

Actually, $[\text{Ca}^{2+}]_i$ -homeostasis depends strongly on $[\text{ATP}]_i$ because Ca^{2+} -pumps in the plasma membrane, intracellular Ca^{2+} stores, the endoplasmatic reticulum and mitochondria directly or indirectly need the energy of ATP-hydrolysis/ Ca -ATPase to transport Ca^{2+} out of the cell or into internal stores. Thus, hypoxic disturbance of $[\text{Ca}^{2+}]_i$ -homeostasis again indicates decreases in $[\text{ATP}]_i$. After flash photolysis of caged Ca^{2+} an outward current was activated, which was presumably mediated by Ca^{2+} -activated K^+ -channels (Figure 34B).

In contrast to the flash photolysis of caged Ca^{2+} , there were no effects when UV-flashes of even maximal intensity were applied to cells that had been filled with either of the caged-ATP solutions described in chapter 2.2. A variety of pulse protocols were tried to elicit a current or voltage response following flash photolysis. Two examples are given in Figure 34C and D – one for current-clamp (C) and one for voltage-clamp (D) experiments. Neither membrane potentials nor currents were affected by flash photolysis of caged-ATP in either of the protocols. Possible reasons for this lack of response are discussed in chapter 5.

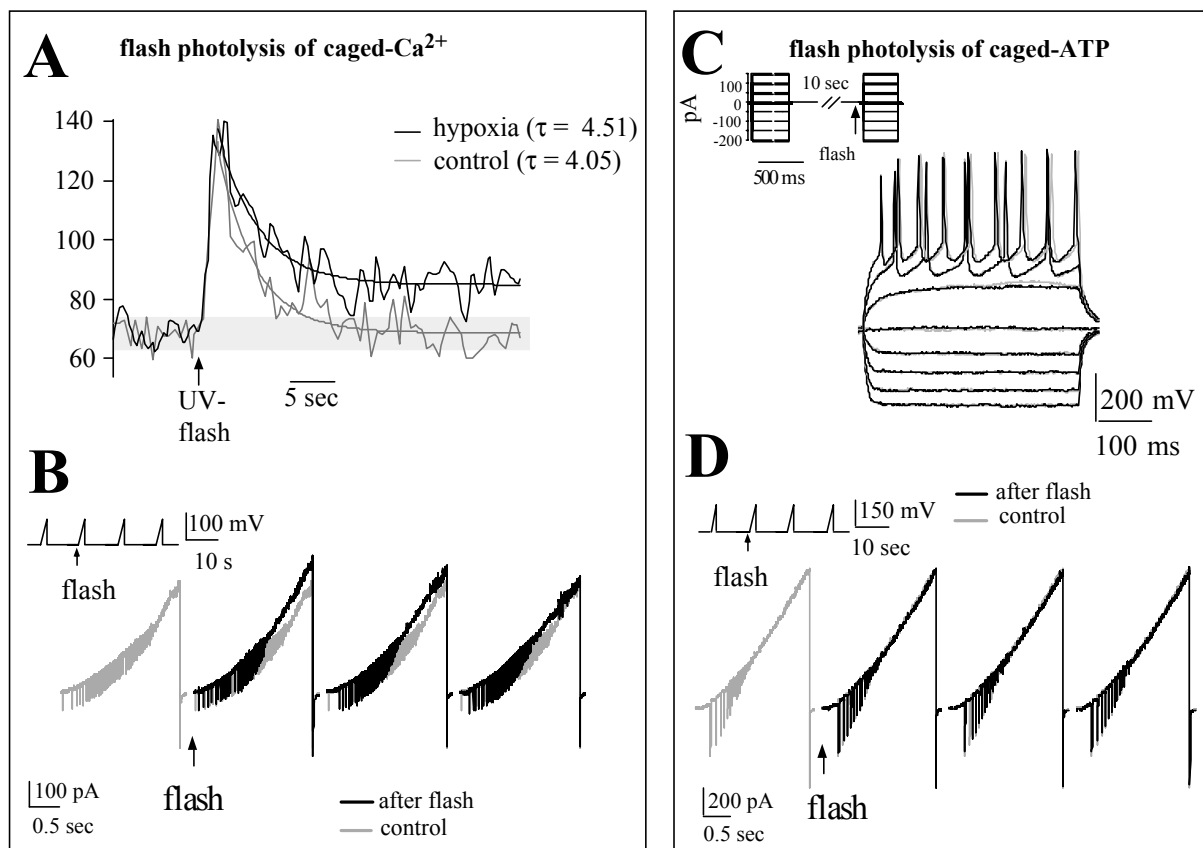


Figure 34: Flash photolysis of caged substances. (A) shows Ca^{2+} -transient following the flash photolysis of caged Ca^{2+} as measured by fura-2. The Ca^{2+} -transient measured at normoxia/hypoxia (average of 5 traces) is represented by a gray/black trace. Time constants of exponential fits are indicated above. (B) A flash given during the pulse protocol indicated in the insert resulted in the activation of an outward current. (C+D) Cell currents and potentials remained unaffected by flash photolysis of caged-ATP. Neither in the current-clamp mode (stimulus protocol as given in (C)) nor in the voltage-clamp mode (stimulus protocol as given in (D)) were any effects observed following the photo-release of ATP.

4.8 Measurements of the intrinsic optical signal (IOS)

4.8.1 IOS during cell swelling and hypoxia

In another set of experiments the intrinsic optical signal (IOS) of the rhythmic slice preparation was monitored as a probe for neuronal activity. Research concentrated especially on hypoxia-induced changes to the IOS.

Figure 35A shows the IR image of the preparation at low magnification. IOS measurements focused on two regions that are functionally important in rhythm generation, the nucleus ambiguus (n.a.) and the nucleus hypoglossus (XII) as defined by rectangles in Figure 35A. The relative IOS changes in these regions during hypoxia are displayed in Figure 35B using a pseudocolor scale. It was seen that the IOS showed a pronounced increase within 4 minutes after oxygen depletion and recovered completely after 15 minutes of reoxygenation.

Individual cells were observed to swell during hypoxia (Figure 35C). Cell volume changes of identified inspiratory neurons were monitored in cells loaded with mag-fura-2. The dye was excited at its isosbestic point for Ca^{2+} binding (346 nm) in order to eliminate the contribution of the hypoxic rise in Ca^{2+} to the fluorescence signal. The cell contours were defined from corresponding cell masks obtained by setting a threshold light intensity (right-hand side of Figure 35C). The lowermost images represent the difference between the mask obtained after 4 minutes of hypoxia and the control one. The areas of volume increase of the cell are highlighted by red (positive) regions.

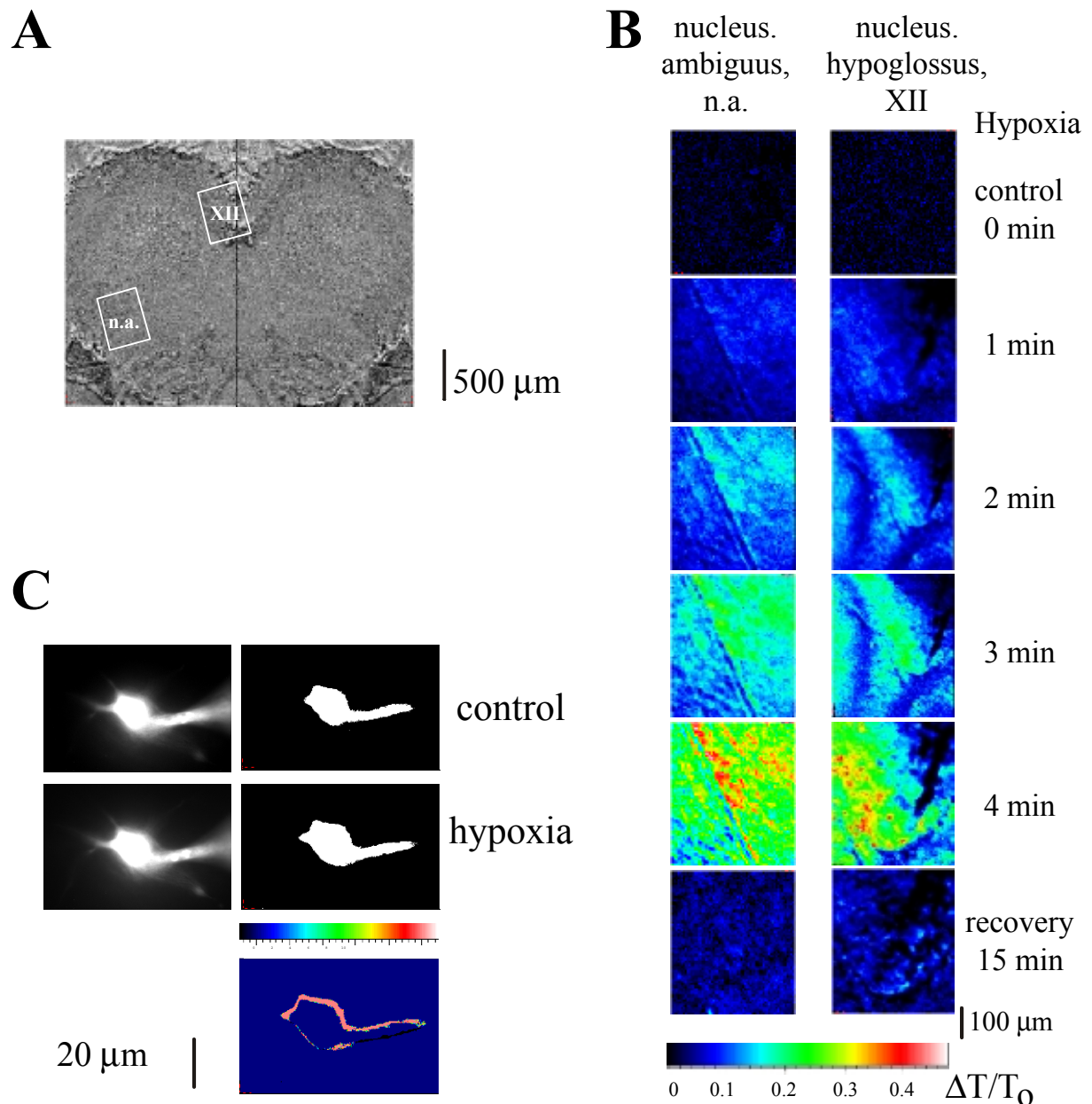


Figure 35: Intrinsic optical signal and cell volume changes during hypoxia. (A) Subtraction image of slice. Use of the subtraction algorithm eliminates the nylon mesh and the stabilizing ‘horse-shoe’ from the image. The boxes mark the regions of the nucleus hypoglossus and nucleus ambiguus displayed in pseudocolors in B ($n = 11$). (B) The IOS displayed a reversible hypoxic increase of up to 40 %. (C) During hypoxia an identified inspiratory neuron filled with mag-fura-2 was observed to swell ($n = 3$). The images on the left-hand side display pictures take before (top) and during hypoxia (bottom) which were then subjected to a threshold procedure (right-hand side). Finally, the control picture is subtracted from the hypoxia picture. The resulting image, which clearly demonstrates a volume increase, is displayed in pseudocolors below.

The IOS changed during various maneuvers that induced modification of the respiratory activity. Figure 36 shows simultaneous measurements of the respiratory output as indicated in hypoglossal nerve activity (XII) and the corresponding IOS obtained from the nucleus hypoglossus (gray trace) and the nucleus ambiguus (black trace). Increase of K^+ concentration within the external bath solution from 3 mM to 9 mM (Figure 36A) resulted in the appearance of the rhythmic activity, which was accompanied by a significant rise in IOS. The IOS was also reversibly changed during variations in the osmolarity of the perfusion solution (Figure 36B). In slices exposed to a hyperosmotic solution (+15 mosm) obtained by addition of mannitol, the IOS declined, whereas there was a rise in IOS in hyposmotic medium (-15 mosm). In both cases the IOS returned to control levels within 15 minutes after restoration of isosmotic conditions. Thus, as expected, cell swelling caused an increase in light transmittance whereas shrinkage resulted in a decrease.

As was mentioned before, hypoxia leads to an initial augmentation of respiratory activity followed by a secondary depression (Cherniack et al., 1970; Richter et al., 1991) (Figure 36C). Correspondingly, the IOS rose steeply throughout the initial phase of hypoxic augmentation. During the secondary depressive phase, IOS continued to rise, but the rate of IOS rise (displayed below) decreased and in some cases the IOS leveled off.

Metabolic poisoning with KCN elicited responses similar to hypoxia (Figure 36D) and occluded the subsequent hypoxic reactions. Respiratory activity and IOS recovered fully after wash-out of KCN.

IOS signals obtained from the two nuclei differed. During the initial phase of hypoxia and after changing extracellular K^+ , both the amplitude and the rate of IOS rise were larger in the nucleus hypoglossus than in the nucleus ambiguus (Figure 36A, C, D). However, there were no such regional differences after changing the osmolarity of the perfusion solution (Figure 36B).

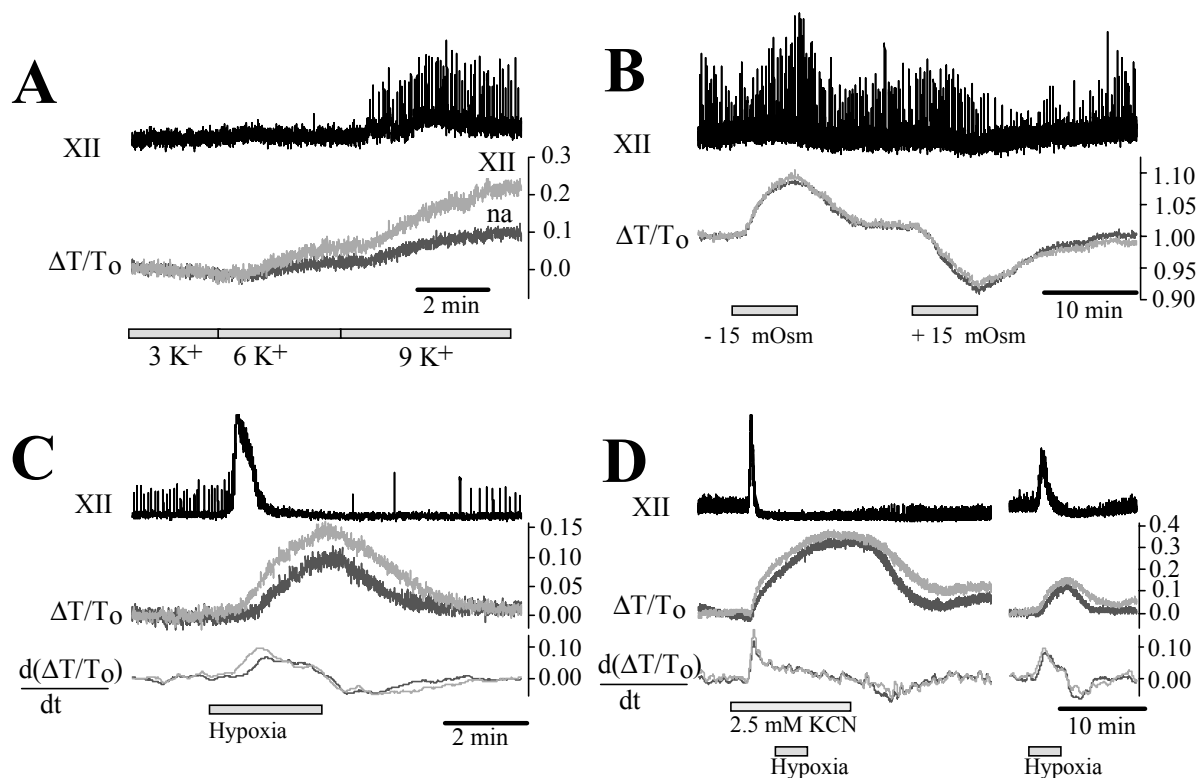


Figure 36: Hypoglossal nerve activity and IOS recorded from nucleus hypoglossus (XII) and nucleus ambiguus (na). (A) When extracellular K⁺ was elevated the respiratory rhythm appeared (upper trace) and the IOS (lower trace) increased both in the nucl. amb. (na) and the nucl. hypogl. (XII) (n = 3). (B) The IOS rose during hyposmotic conditions and fell during hyperosmotic conditions (n = 4). (C) During hypoxia, the IOS increased and returned to control levels upon reoxygenation (n = 18). The same profile was displayed during chemical hypoxia (n = 2) (D). The respiratory rhythm (XII) exhibits a biphasic response to hypoxia consisting of an initial augmentation and a subsequent depression (C and D, upper traces). The derivative of $\Delta T/T_0$ (Fig.2C and D, lowest traces) shows that the fastest change in IOS occurs approximately toward the end of the augmentation phase of hypoxia and that rate of increase in IOS is greater for nucl. amb. (na) than for nucl. hypogl. (XII).

4.8.2 The hypoxic IOS response

Hypoxia induces the release of many neurotransmitters and neuromodulators (Richter et al., 1999), which might contribute to the observed hypoxic IOS response. Therefore, the effect of activation of specific ligand-controlled receptors was tested. Application of NMDA and kainate led to a marked increase in the IOS, which was blocked by the specific antagonists AP-5 and CNQX, respectively (Figure 37A and B). In contrast, addition of adenosine (200 μ M) induced only a slight and transient decrease in IOS (Figure 37C).

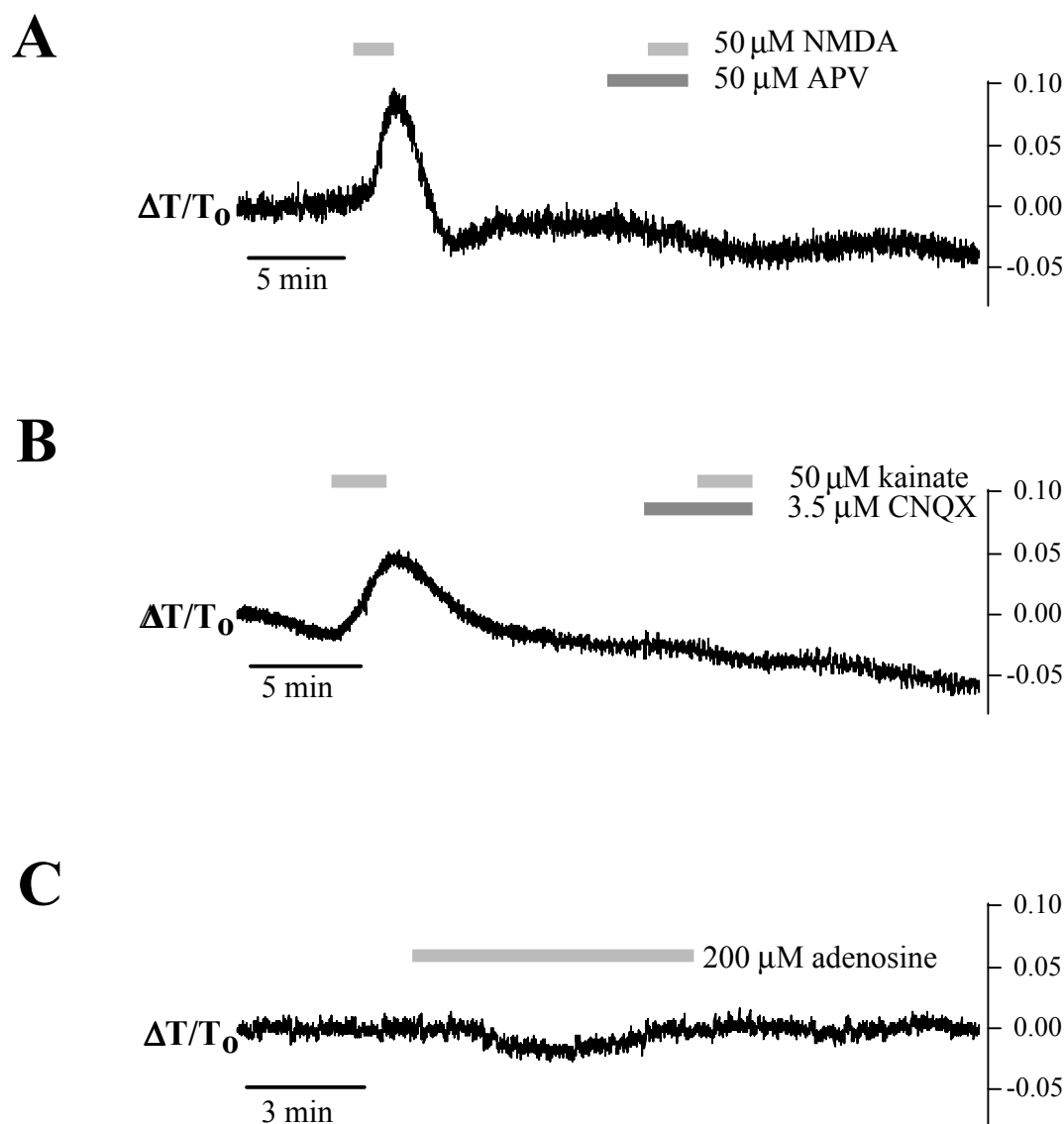


Figure 37: Effect of application of neurotransmitters on IOS. Application of N-methyl-D-aspartate (NMDA) (A) and kainate (B) led to an increase in IOS which could be blocked by 2-amino-5-phosphonovalerate (AP-5) and 6-cyano-7-nitroquinoxaline-2,3-dione (CNQX), respectively (n = 2). (C) Adenosine resulted in a small transient decrease in IOS (n = 3).

All the data described so far indicate that those agents enhancing neuronal activity, such as ($[K^+]_e$, Glutamate receptor activation and early hypoxia, produce an increase in IOS, whereas agents depressing spontaneous neuronal activity, such as adenosine, decrease IOS. It can be assumed that both mechanisms contribute to the hypoxic IOS response. The decrease in slope of the IOS during the depression phase of hypoxia (as seen in Figure 36C) could be explained by the release of adenosine at the onset of hypoxic depression (Richter et al., 1999).

Another mechanism of the hypoxic IOS response might be cell swelling due to ATP-depletion and depression of Na^+/K^+ -ATPase activity in the plasma membrane which will be accompanied by accumulation of intracellular Na^+ and loss of intracellular K^+ . To test this possibility the Na^+/K^+ -ATPase blocker ouabain was applied. The respiratory activity showed a hypoxia-like increase upon ouabain application, but the IOS baseline decreased (Figure 38A). In the presence of ouabain, hypoxic stimuli elicited only 1-2 further IOS responses until the reaction of both the respiratory output and IOS were completely suppressed and did not recover even after 1h of wash-out.

The fact that the hypoxic IOS response was not blocked immediately might be due to a delay in the ouabain action at cells within deeper layers of the tissue. The decrease of IOS observed in the presence of ouabain could be caused by cell shrinkage (see chapter 5) due to Ca^{2+} entry and subsequent activation of K^+ -efflux through Ca^{2+} -activated K^+ -channels (Smith et al., 1993; Alvarez-Leefmans et al., 1994). To test this hypothesis, blocked Ca^{2+} -channels were blocked with Cd^{2+} . Ouabain application then resulted in a pronounced rise in IOS, which was transient and followed by a prolonged IOS decrease (Figure 38D).

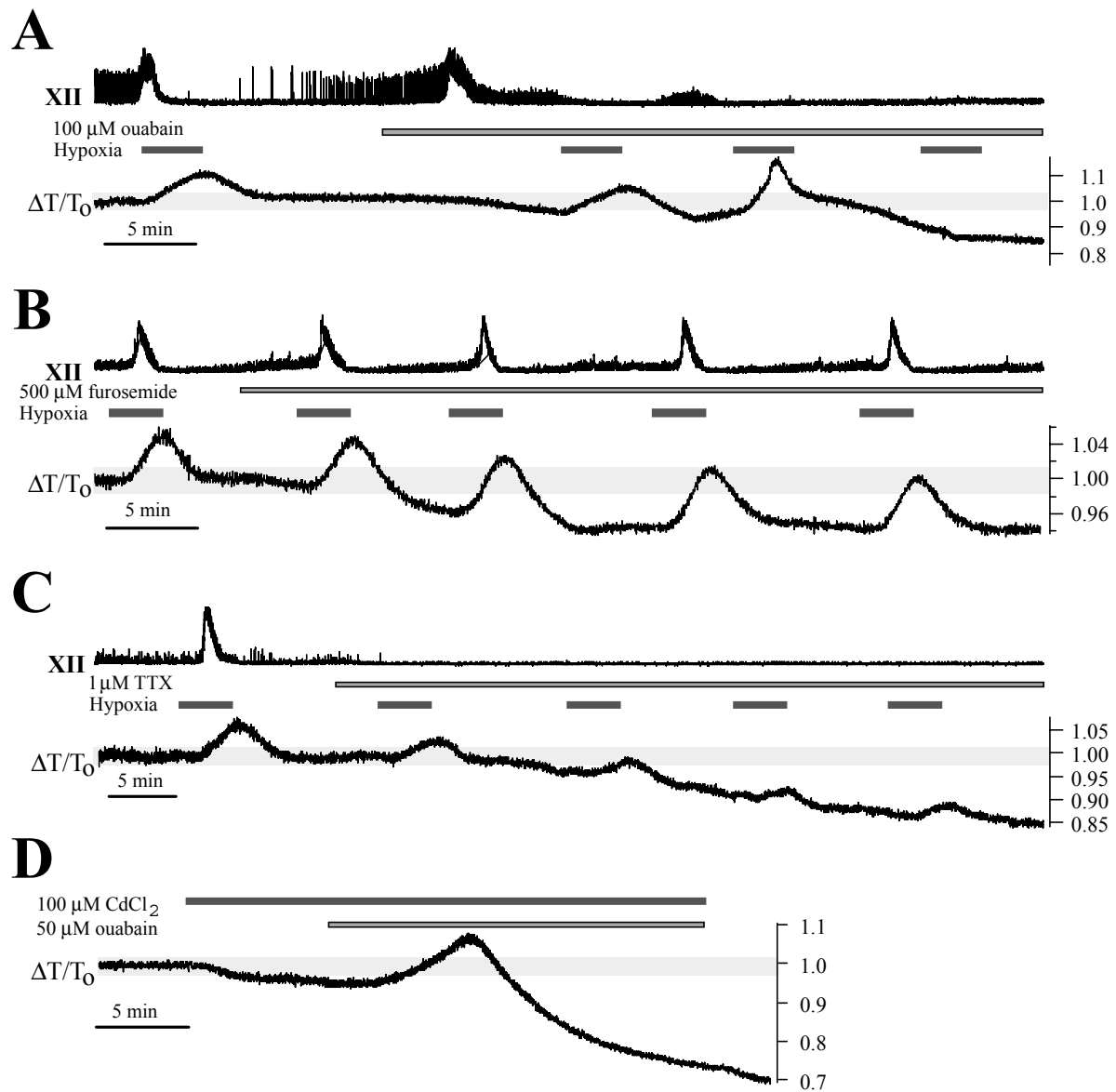


Figure 38: Effect of ouabain, furosemide and TTX (tetrodotoxin) on IOS. (A) Changes to the respiratory rhythm and the IOS after application of 100 μ M ouabain. The IOS exhibited a slow decrease and the hypoxic IOS response was blocked within 1 - 2 hypoxic stimuli ($n = 5$). The respiratory rhythm displayed a hypoxia-like response to ouabain application and was subsequently blocked. **(B)** After furosemide application ($n = 3$) the IOS exhibited a slow decrease. The hypoxic IOS response was not affected by furosemide. **(C)** Following application of 1 μ M TTX the IOS decreased slowly. Hypoxic responses were partially blocked ($n = 3$). **(D)** When Ca^{2+} channels were blocked with Cd^{2+} , ouabain elicited a transient IOS increase.

An important mechanism of volume regulation in glial cells is the $\text{Na}^+/\text{K}^+/\text{2Cl}^-$ -cotransporter, which mediates the electroneutral uptake of ions (Kimmelberg et al., 1986; Haas, 1994) and plays an important role in volume regulation (Baba, 1992; Chen et al., 1992; Hoffmann, 1992; Walz, 1992). Activation of the cotransporter would be expected to lead to cell swelling as uptake of Na^+ , K^+ and Cl^- -ions is followed by water influx. Consequently, blockade of the $\text{Na}^+/\text{K}^+/\text{2Cl}^-$ -cotransporter should lead to shrinkage of glial cells. Inhibition of the $\text{Na}^+/\text{K}^+/\text{2Cl}^-$ -cotransporter by furosemide indeed induced a similar decrease in the IOS signal. These changes were reversible after wash-out for 60 - 80 minutes. In the presence of furosemide, the hypoxic responses of IOS and respiratory activity remained unmodified (Figure 38B), indicating that the $\text{Na}^+/\text{K}^+/\text{2Cl}^-$ -cotransporter does not play a substantial role in generating or maintaining the hypoxic IOS response.

Blocking neuronal activity with tetrodotoxin (TTX) caused the respiratory activity to be completely suppressed and IOS to slowly decrease (Figure 38C). The hypoxic IOS responses became progressively smaller but were not completely suppressed even after cessation of neuronal activity.

4.8.3 IOS response following application of K_{ATP} -channel drugs

It has been shown before that rhythmic activity is modulated by K_{ATP} -channel drugs (see Figure 39). Correspondingly, the expected IOS response upon application of K_{ATP} -channel blockers would be a rise in IOS due to enhancement of neuronal activity and cell swelling and a decrease in IOS upon application of K_{ATP} -channel activators. The results, however, were variable. Applications of diazoxide ($n = 28$) and glibenclamide ($n = 23$) resulted in an increase in IOS in approximately half of the tests but in a decrease in the other trials. Responses were specific for a given slice and could be reproduced over a time-span of several hours. These findings indicate that the mechanisms underlying IOS involve processes other than neuronal or glial swelling. One of these processes might be mitochondrial swelling as K_{ATP} -channels are highly expressed in mitochondrial membranes (Hu et al., 1999; Wang and Ashraf, 1999). In order to test this possibility reproducible metabolic conditions were established by applying K_{ATP} -channel-directed drugs after approximately 10 minutes of hypoxia (Figure 39A). Now the IOS rose further after application of the channel opener diazoxide and decreased after application of the channel blocker glibenclamide in all tests performed ($n = 8$). The involvement of mitochondria was also verified by applying a mitochondrial uncoupler, carbonylcyanide *m*-chlorophenylhydrazone, CCCP.

Figure 39B shows that CCCP application led to an initial increase in the IOS, which then decreased to levels well below control levels. The latter effect manifested severe damage to cells, as the respiratory output was irreversibly lost.

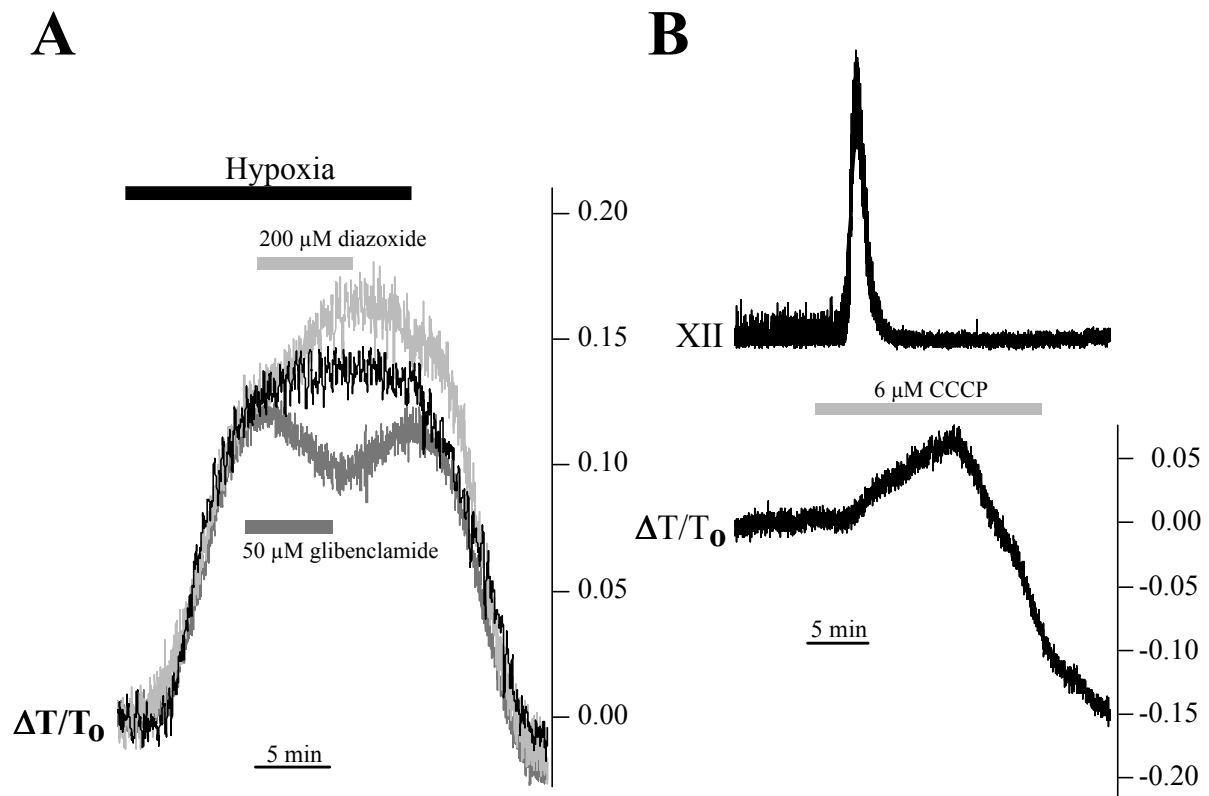


Figure 39: K_{ATP} -channel drugs and IOS. (A) Following 10 minutes of hypoxia the application of K_{ATP} -channel drugs led to an increase in IOS after diazoxide and a decrease after glibenclamide ($n = 4$, different preparations). (B) Application of the mitochondrial uncoupler CCCP resulted in a transient increase in IOS ($n = 3$).

5 Discussion

This work investigated the structure and function of K_{ATP} -channels in inspiratory neurons of the pre-Bötzinger complex. Specifically, the question was addressed as to how these channels modulate the respiratory rhythm and how, in turn, they themselves are modulated by factors released during normal and hypoxic conditions. A variety of different techniques were employed, such as PCR analysis, single-channel recordings and their theoretical analysis, microfluorometry and measurements of the intrinsic optical signal.

5.1 K_{ATP} -channel structure and gating kinetics

It was shown that K_{ATP} -channels in these neurons are composed of Kir6.2 and SUR1 subunits. This corresponds to the channel population typically found in pancreatic β -cells and in neurons of the dorsal nucleus of the vagus nerve in rat brainstem (Karschin et al., 1998).

With regard to its gating kinetics, however, the channel behavior deviated from that observed in pancreatic β -cells. While the latter were reported to display one open state and three closed states (Gillis et al., 1989; Trapp et al., 1998) channels in respiratory neurons are functioning in two open states and at least three closed states, which resembles more closely the cardiac (Nichols et al., 1991; Benz and Kohlhardt, 1994) and skeletal muscle cells (Davies et al., 1989; Davies et al., 1992; Spruce et al., 1987). The gating kinetics of neuronal K_{ATP} -channels have so far not been investigated in detail. Most of the studies used inside-out measurements of K_{ATP} -channels, which are inherently complicated by the problem of run-down of channel activity.

Another problem arises in cell-attached analysis: channel activity progressively increased during the recording period, which presumably is due to the tension exerted by the pipette. For this reason estimates of the mean open probability and rate constants of channels were rendered meaningless. Nevertheless, specific transition steps were observed, which consistently revealed higher or lower rate constants as compared to the rest. This feature becomes evident in the examples presented in Figure 14 and Figure 15. The ATP-dependence of specific steps needs to be investigated in the future.

K_{ATP} -channels also exhibited a bimodal gating behavior, which has as yet not been reported for K_{ATP} -channels. However, different gating modes have been described for a variety of

other ion channels. Typical examples are N-type Ca^{2+} -channels, which reveal a balance between modal behavior that is regulated through G-proteins (Lipscombe et al., 1989; Delcour and Tsien, 1993), Na^+ -channels, which show transitions between gating modes depending on membrane voltage (Palmer and Frindt, 1996; Bohle and Benndorf, 1995) and also on stretch-activation (Tabarean et al., 1999). Furthermore, 4-aminopyridine (4-AP)- and tetraethylammonium (TEA)-sensitive voltage-gated K^+ -channels in pyramidal cells reveal two activity modes alternating randomly (Bossu and Gahwiler, 1996).

The two different channel gating modes displayed by K_{ATP} -channels of inspiratory neurons are a low open probability that appeared to be the common mode and a much higher open probability that appeared to occur more frequently during episodes of reduced energy supply to neurons. So far, the mechanisms, which regulate these transitions between channel gating modes, remain unclear. However, the fact that transitions into the high open probability mode were more likely to occur during hypoxia points to a regulatory role of $[\text{ATP}]_i$ levels and possibly changes in the ATP-sensitivity of the channels. Such a process may involve G-proteins that are activated by the hypoxia-induced release and accumulation of neuromodulators such as serotonin and adenosine (Richter et al., 1999), or osmo-mechanical stress, which affects K_{ATP} -channel activity (Mironov and Richter, 2000). Another mechanism to be considered is an increase of $[\text{H}^+]$ during hypoxia (Ballanyi et al., 1996), which also modulates the ATP-sensitivity of channels (Forestier et al., 1996; Davies et al., 1992). In the high-activity mode, the channel does not display periodic modulation, which again indicates a diminished ATP-sensitivity under these conditions.

5.2 K_{ATP} -channel drugs and rhythmic activity

It was found (Figure 16) that application of K_{ATP} -channel affecting drugs modulated ongoing rhythmic neural activity. Blockers of the K_{ATP} -channel had an excitatory effect increasing the amplitude of both hypoglossal (XII) nerve activity and synaptic drives of respiratory neurons, whereas activators of channels were inhibitory. The findings were consistent with the drug effects on individual respiratory cells as described previously (Pierrefiche et al., 1996), namely that blockers depolarize and activators hyperpolarize neurons.

5.3 Periodic modulation of K_{ATP} -channel activity

Analysis of the open probability of K_{ATP} -channels revealed that in the low activity mode p_{open} is periodically modulated in synchronization with bursting of respiratory neurons. The

functional significance appears to be a contribution to periodic membrane repolarization of inspiratory neurons after each burst discharge and thus stabilization of the rhythmic network activity.

It should be mentioned that the calculation of p_{open} -fluctuations was subject to some unavoidable systematic errors.

First, the open probability could not be accurately computed during a burst of action potentials (APs). APs had to be subtracted from the trace and therefore some channel openings occurring during APs and their afterpotentials may have been missed. Consequently the open probability was underestimated during this period. Secondly, it should be noted that the number and frequency of APs varied between bursts. Respiratory bursts displaying prolonged trains of APs would be expected to lead to a longer risetime of p_{open} than short respiratory bursts (see Figure 23). Finally, the durations of spontaneous respiratory cycles varied significantly. For the computation of p_{open} , however, up to 200 sweeps pertaining to different cycle lengths had to be averaged. Consequently, the estimates of p_{open} become progressively less accurate further apart from the onset of the respiratory bursts. This can be seen in Figure 17C and D, where the selected time window preceded and followed a respiratory burst, respectively. For this reason, time windows were chosen to surround the respiratory burst in all the other analysis.

First, the open probability could not be accurately computed during a burst of action potentials (APs). APs had to be subtracted from the trace and therefore some channel openings occurring during APs and their afterpotentials may have been missed. Consequently the open probability was underestimated during this period. Secondly, it should be noted that the number and frequency of APs varied between bursts. Respiratory bursts displaying prolonged trains of APs would be expected to lead to a longer risetime of p_{open} than short respiratory bursts (see). Finally, the durations of spontaneous respiratory cycles varied significantly. For the computation of p_{open} , however, up to 200 sweeps pertaining to different cycle lengths had to be averaged. Consequently, the estimates of p_{open} become progressively less accurate further apart from the onset of the respiratory bursts. This can be seen in Figure 17C and D, where the selected time window preceded and followed a respiratory burst, respectively. For this reason, time windows were chosen to surround the respiratory burst in all the other analysis.

Nevertheless, the findings clearly revealed rhythmic fluctuations in K_{ATP} -channel open probability, most probably indicating an interaction between energy consuming

Na^+/K^+ -pumping and K_{ATP} -channel activity. This assumption follows the rationale that periodically enhanced Na^+/K^+ -pump activity leads to variations in submembraneous $[\text{ATP}]_i$, directly inducing an increase in K_{ATP} -channel open probability. Such an interpretation is in line with the evidence that blockage of Na^+/K^+ -pumping often results in declined K_{ATP} -channel activity (Abe et al., 1999; Mauerer et al., 1998; Kabakov, 1998; Urbach et al., 1996).

Estimates of the variations in free $[\text{ATP}]_i$ were obtained from p_{open} using a model described in chapter 4.5. Periodic changes in free $[\text{ATP}]_i$ ranged between 5 and 40 μM . Arguments were given as to why periodic decreases in free $[\text{ATP}]_i$ cannot be caused by ATP binding to Ca^{2+} that is accumulating during burst of neuronal activity (Frermann et al., 1999). It should be pointed out, however, that estimates of the contribution of Ca^{2+} -fluctuations strongly depend on the value used for the dissociation constant $K_{\text{d,Mg}}$ of the endogenous buffer, which is not known exactly. For instance, using a $K_{\text{d,Mg}}$ of 1 mM (as opposed to the value of 10 mM used before) a $[\text{Ca}^{2+}]_i$ -rise from 100 nM to 5 μM was found to contribute an $[\text{ATP}]_i$ decrease of amplitude 13 μM (as opposed to the previously estimated 5 μM). Nevertheless, it seems unlikely that Ca^{2+} concentrations as high as 5 μM are on average actually encountered close to the channels.

Quantitatively, $[\text{ATP}]_i$ -fluctuations could therefore be much better explained by ATP-consumption by the Na^+/K^+ -pump. The calculations suggested that its activity-dependent activation can account for a decrease in free $[\text{ATP}]_i$ level of about 50 μM . There is only a slight difference to experimental data, which may be due to the fact that neither ATP-synthesis nor the effects of surface potential were considered. One has to bear in mind, of course, that there are other mechanisms than $[\text{ATP}]_i$ -fluctuations that might explain modulation of K_{ATP} -channel activity. For instance, the channel might be affected by periodic neurotransmitter release, such as cyclic release of adenosine affecting the cAMP pathway and activation of channels via the PKC-pathway (Mironov et al., 1999; Richter et al., 1997).

For a quantitative description of p_{open} -fluctuations, the parameters $t_{1/2}(\text{rise})$, $t_{1/2}(\text{fall})$ and $R_{\Delta T1/\Delta T2}$ were used, which reflect the relationship between cycle and burst durations as well as burst kinetics. In terms of $[\text{ATP}]_i$ -homeostasis, $t_{1/2}(\text{rise})$ and $t_{1/2}(\text{fall})$ would correspond to the rate of ATP-consumption and ATP-replenishment, respectively. When the frequency of respiratory bursts declined during lowering of $[\text{K}^+]_e$, only $R_{\Delta T1/\Delta T2}$ was significantly enhanced. This increase in $R_{\Delta T1/\Delta T2}$ can reasonably be explained by the longer periods of low p_{open}

following replenishment of ATP during burst intervals. However, when the burst duration and burst frequency increased during hypoxia, all three parameters changed. $R_{\Delta T1/\Delta T2}$ decreased with a prolongation of burst durations and a concomitant decrease in cycle length. $t_{1/2}(\text{rise})$ increased and $t_{1/2}(\text{fall})$ decreased, indicating a prolonged duration of ATP-depletion followed by a shortened period of ATP-replenishment.

It should be emphasized that whilst the hypoxia-induced increase in $t_{1/2}(\text{rise})$ might be explained in terms of the prolongation of burst duration and the decrease in $t_{1/2}(\text{fall})$ by the simultaneous decrease in total cycle length, other explanations might also be possible. Assuming again that the channel modulation might not be caused by ATP-depletion but rather by periodic neurotransmitter release, one might speculate that the time course and composition of neurotransmitter release might be changed during hypoxia (Richter et al., 1999). This might also lead to the observed delay in K_{ATP} -channel activation.

5.4 Estimation of $[ATP]_i$ during hypoxia

Intracellular ATP concentrations were not amenable to *direct* measurements. Using the Mg^{2+} -sensitive dye mag-fura-2, changes in neuronal $[Mg^{2+}]_i$ were therefore monitored during hypoxia in order to *indirectly* estimate changes in $[ATP]_i$. Since mag-fura-2 also binds Ca^{2+} with a K_d of 44 μM as compared to the K_d of 5.3 mM for Mg^{2+} (Konishi et al., 1991), fluorescence changes represent the result of both $[Mg^{2+}]_i$ and $[Ca^{2+}]_i$ variations. For this reason the contribution of $[Ca^{2+}]_i$ to the overall change in mag-fura-2 fluorescence was modeled. Hypoxic changes in $[Ca^{2+}]_i$ typically range between 200 - 300 nM as measured by fura-2. This would contribute maximally 20 % to the hypoxic mag-fura-2 signal. Assuming that 80 % of the mag-fura-2 signal is due to Mg^{2+} that is released during ATP-hydrolysis, hypoxia-induced $[ATP]_i$ -changes can be estimated as approximately 500 μM .

This value has to be considered as the lower limit of the total decrease in ATP concentration during hypoxia since – given the slow time course of hypoxia of approximately 20 minutes – diffusion from the patch pipette will lead to the constant exchange between ‘hydrolyzed’ and ‘fresh’ solution. In the case of cell-attached recordings of K_{ATP} -channel activity there will be no ‘fresh’ solution available and intracellular ATP rather has to be assumed to decrease by even more than the amount observed in whole-cell experiments.

It is important to note that the time course of p_{open} -increase is in good agreement with the time course of the decrease of the mag-fura-2-fluorescence – displaying its highest rate of change during the augmentation phase of hypoxia and leveling off during the depressive phase. Thus,

the present data are in full accordance with the hypothesis that the hypoxic channel activation is due to ATP-depletion and that mag-fura-2 is a valid probe to monitor ATP.

It was reported previously that cytosolic Mg^{2+} affects K_{ATP} -channel activity directly. In isolated patches (Findlay, 1987) and in cell-attached patches recorded from the internally permeabilized cardiac myocytes (Horie et al., 1987), Mg^{2+} applied at the cytosolic side of the membrane reduced both the amplitude and the activity of outwardly directed currents through K_{ATP} -channels. However, as the cell-attached recordings presented here always portray inwardly directed currents, this effect should not contribute to the observed channel activity changes.

5.5 Purinoceptor activation modulates the respiratory rhythm

In preliminary experiments, ATP was found to also act on K_{ATP} -channels from the extracellular side. Its neurotransmitter action modulated the respiratory rhythm and synaptic drives leading to a transient augmentation of the amplitudes of both values which was followed by a secondary depression. Recently, a similar excitatory action of ATP was reported in inspiratory neurons (Thomas and Spyer, 2000; Thomas et al., 1999), where extracellular recordings displayed an increase in the number of action potentials per burst after ATP application. This is in agreement with the increase in the amplitude of integrated hypoglossal (XII) nerve activity and synaptic drives observed in some neurons here. In this work, the ATP-mediated augmentation could be reproduced by application of α,β -MeATP, which is a much more potent agonist of P_{2X} -purinoceptors than of P_{2Y} purinoceptors. This indicates that ATP is acting via P_{2X} purinoceptors. On the other hand, K_{ATP} -channel activity was potentiated by α,β -MeATP, which rather points to the activation of phospholipase C by P_{2Y} purinoceptors. Further experiments will be necessary to distinguish between the various purinoceptor subtypes that are involved and to determine in more detail their regulatory role in K_{ATP} -channel activation as well as in the modulation of the respiratory rhythm.

5.6 Flash photolysis

One of the aims of this work was to investigate the kinetics of K_{ATP} -channel behavior by the flash photolysis of caged-ATP. Previously, flash photolysis of caged-ATP (DMNPE-caged) was found to cause rapid depolarization and inhibition of ongoing K^+ -channel activity in smooth muscle cells (Clapp and Gurney, 1992). In inspiratory neurons, however, neither

whole-cell currents nor membrane potential were affected by photorelease of ATP. Previously, similar problems with respect to studying K_{ATP} -channel kinetics with caged-ATP (DMNPE-caged) have been reported in cardiac (Nichols et al., 1990) and in pancreatic β -cells (Ammala et al., 1991). In inside-out patches, the blocking capacities of the caged precursor and ATP itself were found to be similar (Ammala et al., 1991). A possible explanation of such problems is that caged-ATP might not be fully caged with respect to its allosteric action on the K_{ATP} -channel. In this case, ‘uncaging’ of ATP would have no effect, as the apparent ATP concentration blocking the channel remains the same.

It can be assumed that in the case of K_{ATP} -channels of respiratory neurons the portion of the ATP-molecule that binds to the channels is not sufficiently protected in caged-ATP and these compounds are therefore not suitable for studying the kinetics of K_{ATP} -channel inhibition (Nichols et al., 1990; Ammala et al., 1991).

5.7 *Intrinsic optical signal*

In the previous chapters, properties of K_{ATP} -channels in respiratory neurons were discussed with regard to their molecular structure, gating kinetics, periodic activation and modulation by various factors. As a next step it was intended to use the intrinsic optical signal (IOS) to map changes in neuronal activity following the application of K_{ATP} -channel blockers and openers. However, this was complicated by the fact that processes other than cell volume changes appeared to contribute significantly to IOS, necessitating a more detailed investigation into the origin of the IOS in the rhythmic slice preparation.

5.7.1 *Changes in cell volume*

It is commonly accepted that any changes in intracellular and/or extracellular osmolarity induce changes in cell volume (Andrew and MacVicar, 1994; Lipton, 1973). In this work, changes in osmolarity were observed to modulate the IOS in the rhythmic brainstem slice preparation, indicating that *at least part of the IOS reflects cell volume changes*. This finding was further substantiated by measurements of identified inspiratory neurons, which exhibited a pronounced and reversible increase in both volume and IOS during hypoxia. The effect was similar to that described for hippocampal neurons in slices (Turner et al., 1995; Kreisman and LaManna, 1999).

5.7.2 *Regional differences in IOS*

It has been observed in previous studies (Haddad and Donnelly, 1990; O'Reilly et al., 1995; Pierrefiche et al., 1996) that hypoglossal motoneurons have a low tolerance to hypoxia. In contrast to hippocampal neurons and other brainstem neurons, such as respiratory or dorsal vagal neurons, hypoglossal neurons exhibited a much larger and faster anoxic depolarization in response to O₂ deprivation (Richter et al., 1991; Richter et al., 1992; Donnelly et al., 1992; O'Reilly et al., 1995). A larger anoxic depolarization in hypoglossal neurons would be expected to lead to a higher degree of cell swelling due to a larger influx of ions. Indeed, comparison of respiratory neurons and hypoglossal motoneurons revealed pertinent differences in the hypoxic IOS responses. The initial hypoxic rise in IOS was consistently higher and faster in the region of the nucleus hypoglossus than in nucleus ambiguus. Similar regional differences were observed when the resting membrane potential was depolarized by elevation of extracellular K⁺. After changes in bath osmolarity (± 15 mosm), however, the IOS displayed no regional diversity, which indicates that passive water movement imposed by osmolarity changes affects the volume of all cell populations in a similar manner.

5.7.3 *Mechanisms underlying the hypoxic IOS response*

As mentioned above, hypoxia has been observed to elicit a pronounced IOS response that is in part due to cell swelling. In turn, the most likely mechanism underlying hypoxic cell swelling is Ca²⁺ and Na⁺ influx (Haddad and Donnelly, 1990; Mercuri et al., 1994). This *anoxic depolarization* is also partially mediated by failure of the Na⁺/K⁺-pump following ATP-depletion (Calabresi et al., 1995; Le Corrone et al., 1999). In the following, the portion of the hypoxic IOS response that is caused by cell swelling was further investigated by mimicking hypoxic conditions (i.e. release of neurotransmitters, blocking of Na⁺/K⁺-pump) and monitoring the corresponding IOS signal.

5.7.3.1 *Effect of neurotransmitters on IOS*

The principal excitatory neurotransmitter involved in the early phase of hypoxia is glutamate (Richter et al., 1999). Glutamate receptors can be divided into the NMDA and kainate/AMPA receptor subtypes and both kinds appear to be involved in the neuronal response to hypoxia (Choi, 1993; Schurr et al., 1995). Thus, in order to elicit a hypoxia-like IOS response, NMDA and kainate were applied to the respiratory slice preparation. As expected, agonist application resulted in a marked reversible increase in IOS similar to the hypoxic IOS response. The

effects were blocked by application of the specific antagonists AP-5 and CNQX, indicating the involvement of NMDA and AMPA/kainate receptors respectively. This is in agreement with previous studies on hippocampal slices (Andrew et al., 1996; Andrew and MacVicar, 1994). Adenosine, which is effective in the modulation of the respiratory rhythm (Schmidt et al., 1995; Mironov et al., 1999) and is released during the later phase of hypoxia (Richter et al., 1999), led to a slight decrease in IOS. Consequently, it might be speculated that this adenosine-mediated fall in IOS is partly responsible for the decreasing slope of the hypoxic IOS signal that is observed during the depression phase of hypoxia.

The findings are in agreement with the assumption that *hypoxic neurotransmitter release modulates the IOS through cell volume regulation*.

5.7.3.2 Na^+/K^+ -pump and neuronal activity

It is generally thought that the inhibition of Na^+/K^+ -pump activity leads to cell swelling due to accumulation of intracellular Na^+ (Shimizu and Nakamura, 1992; Buckley et al., 1999), thereby causing an increase in IOS similar to that observed during hypoxia. Surprisingly, blocking of Na^+/K^+ -pump activity with ouabain did *not* mimic the hypoxic IOS response but the rather the IOS baseline decreased markedly. This is consistent with the observations in a number of studies (Alvarez-Leefmans et al., 1994; Smith et al., 1993) that ouabain induced cell shrinkage rather than swelling. The authors suggested that ouabain induced transient elevation of $[\text{Ca}^{2+}]_i$, which in turn activates a K^+ efflux through Ca^{2+} -activated K^+ -channels, leading to water loss and thus cell shrinkage. Indeed, the effect could be transiently reversed when Ca^{2+} -entry was blocked with CdCl_2 (Figure 38D), suggesting that ouabain induced cell shrinkage plays a role in the IOS signal. An alternative explanation for the ouabain-induced fall in IOS baseline relies on the fact that not all IOS signals can be attributed to changes in total cell volume alone (Buchheim et al., 1999; Muller and Somjen, 1999). For instance, ouabain-induced excitotoxicity as described by Zeevalk and Nicklas (1996) might lead to irreversible changes in dendritic morphology, denominated *dendritic beading* (Andrew et al., 1999; Polischuk et al., 1998), which have previously been suggested to reflect damage to the dendritic areas, e.g. following a prolonged exposure to hypoxia and/or high levels of NMDA (Park et al., 1996; Hori and Carpenter, 1994). Dendritic beading is expected to result in a decrease in IOS (Andrew et al., 1999; Polischuk et al., 1998), such as was observed after ouabain application, and would also account for the irreversibility of the ouabain action.

It can be concluded that blocking of the Na^+/K^+ -pump alone is not sufficient to mimic the hypoxic IOS response. Nevertheless, IOS responses elicited during repetitive hypoxic

episodes were blocked in the presence of the ouabain, which suggests that the normal operation of the pump is a vital prerequisite for the maintenance of the IOS response.

Further investigations were carried out to ascertain whether Na^+ influx through TTX-sensitive Na^+ -currents contributes to the hypoxic cell swelling. Application of TTX led to a steady decrease in the IOS baseline. This can be attributed to its blocking action on neuronal activity, which would lead to a decrease in both neuronal and glial cell volumes. Similar results were reported in the region of the nucleus tractus solitarius in brainstem slices when neuronal activity was blocked (Torres et al., 1997). The hypoxic IOS response was partially blocked by TTX, indicating that *anoxic depolarization is a combination of TTX-sensitive and TTX-insensitive ion influx.*

In conclusion, the hypoxic IOS response can be interpreted as a result of several distinct underlying mechanisms as illustrated in Figure 40. First, it might be subdivided into a component due to cell swelling and another one due to ‘other’ mechanisms such as dendritic beading or mitochondrial swelling. Cell swelling, in turn, can be attributed to anoxic depolarization due to hypoxic release and accumulation of neurotransmitters and neuromodulators, and to the inhibition of Na^+/K^+ -pump activity. Alternatively, anoxic depolarization might be separated into a component mediated through TTX-sensitive Na^+ -channels and another one that is TTX-insensitive.

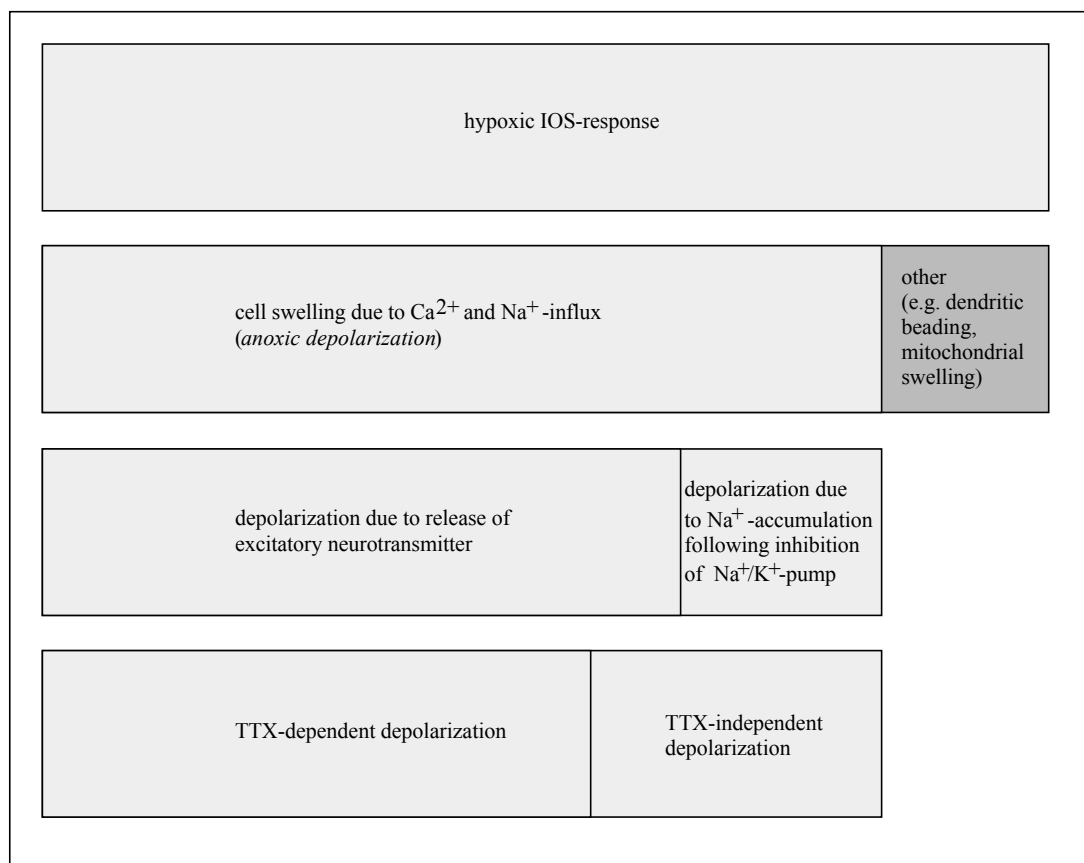


Figure 40: Possible components of the hypoxic IOS response. Boxes depict the qualitative contribution of each mechanism. Note that the IOS component that was *not* due to cell swelling (denoted ‘other’) was arbitrarily assumed to represent an increase in IOS (as a result of mitochondrial swelling, for instance), whereas it might equally well reflect a decrease (as might occur during dendritic beading).

5.7.4 Involvement of mitochondrial K_{ATP} -channels in IOS generation

Another mechanism associated with the IOS signal is the swelling of cytoplasmic organelles, such as mitochondrial swelling (Aitken et al., 1999), which has long been known to be a result of hypoxia and/or ischemia (Vladimirov Iu and Kogan, 1981; Allen et al., 1989; Lazriev et al., 1980; Aitken et al., 1999). Swelling of mitochondria is accompanied by a decrease in light scattering (Mar, 1981) or light absorbance (Stoner and Sirak, 1969). Flow cytometry analysis also showed that swelling of individual mitochondria leads to a decrease in light absorbance (Macouillard-Poulletier de et al., 1998; Beavis et al., 1985), indicating that mitochondria behave as light-scattering objects that affect the IOS in the same way as the whole cell (i.e. swelling leads to an increase in IOS, shrinkage to a decrease).

Interestingly, an indication of the contribution of mitochondrial swelling to IOS generation was observed when K_{ATP} -channel drugs were applied:

As K_{ATP} -channels regulate the excitability of respiratory neurons (Pierrefiche et al., 1997), the application of K_{ATP} -channel blockers/activators would also be expected to lead to a rise/fall in the IOS as the neurons are depolarized/hyperpolarized. In the experiments presented, however, the effects of K_{ATP} -directed drugs were highly variable during normoxia. One possible explanation is that the drugs targeted other structures, e.g. mitochondrial K_{ATP} (mito K_{ATP}) channels. Activation of these channels with diazoxide was previously observed to induce depolarization of the mitochondrial membrane potential (Grimmsmann and Rustenbeck, 1998; Holmuhamedov et al., 1998; Gross and Fryer, 1999), which normally induces mitochondrial swelling. K_{ATP} -antagonists reversed this effect (Garlid et al., 1997). Based on these data, one may speculate that activation of mito K_{ATP} -channels is capable of inducing IOS changes that are opposite to the contribution of plasmalemmal K_{ATP} -channels. To test this hypothesis the slice was exposed to a prolonged period of hypoxia prior to drug application in order to induce maximal activation of plasmalemmal K_{ATP} -channels. Under these conditions application of K_{ATP} -directed drugs induced IOS responses which could be attributed to changes in the activity of mito K_{ATP} -channels (fall after glibenclamide, rise after diazoxide). The results were remarkably reproducible, indicating that the effects of the two types of K_{ATP} -channels are different and can be distinguished.

From these findings it can be concluded that during prolonged hypoxia, K_{ATP} -channel blockers and openers act on mitochondrial K_{ATP} -channels rather than plasmalemmal K_{ATP} -channels. This hypothesis is supported by the observation (data not shown) that glibenclamide and tolbutamide, applied after hypoxic activation of K_{ATP} -channels in cell-attached patches of respiratory neurons, have a much weaker effect on channel activity. A similar finding, i.e. that glibenclamide is much less potent in inhibiting K_{ATP} -channels after metabolic poisoning, was previously observed in pancreatic β -cells (Mukai et al., 1998).

The mitochondrial contribution to the IOS signal was verified through applying the uncoupler of mitochondrial oxidative phosphorylation, CCCP, which has been reported to depolarize mitochondria and produce mitochondrial swelling (Minamikawa et al., 1999). CCCP indeed induced a rapid increase in IOS, indicating that swelling of mitochondria might play a significant role in IOS generation.

5.8 Conclusion and perspectives

The results show that K_{ATP} -channels in inspiratory neurons are composed of the Kir6.2/SUR1 subunits and display gating kinetics similar to the ones observed in smooth muscle cells. The channels are periodically modulated in synchronization with the respiratory rhythm,

indicating that they serve as accurate “receptors” of the metabolic demands, sensing even minor changes in ATP-consumption by ion pumping. The functional task of K_{ATP} -channels is to support membrane repolarization after each inspiratory burst, thus lowering metabolic demands and enabling adequate ATP-replenishment. During hypoxia the channel open probability increases severalfold, which can be attributed to a decrease in submembraneous $[ATP]_i$ levels. Evidence was presented that mitochondrial K_{ATP} -channels are also involved in the hypoxic response of the cell.

It was mentioned in chapter 1.4 that during the analysis of K_{ATP} -channel contribution to the bursting behavior of the pancreatic β -cells, two opposing views have crystallized: K_{ATP} -channels were assumed to either underlie oscillations in electrical activity (Larsson et al., 1996) or to modulate them (Kinard et al., 1999). Based on the findings that in the rhythmic slice preparation respiratory activity was found to be neither disrupted nor profoundly disturbed by application of K_{ATP} -channel drugs and that periodic channel modulation and channel activation during metabolic stress could be comprehensively explained by ATP-depletion due to Na^+/K^+ -pumping, the second mechanism of modulation seems more likely to be involved in respiratory neurons. It can be concluded that K_{ATP} -channels represent an important component modulating the excitability of rhythmically active neuronal networks in general.

In the future it will be an interesting task to identify the mechanisms, which underlie the periodic modulation of K_{ATP} -channel activity. Is the oscillation of K_{ATP} -channel activities caused by fluctuations of cytosolic factors such as $[ATP]_i$, $[Mg^{2+}]_i$, $[Ca^{2+}]_i$, $[Na^+]_i$ and $[H_2O]_i$, or rather by periodic neuromodulatory activation of intracellular pathways, or possible by a combination of both? In particular, the functions of neurotransmitters, G-proteins and phosphorylation by protein kinases should be investigated in more detail.

Another interesting question concerns the contribution of purinoceptor activation to the periodic modulation of K_{ATP} -channels. The use of a fast application system would allow a more detailed analysis of the participation of distinct P_{2X} receptor subtypes with electrophysiological and pharmacological tools.

It was found in this work that intracellular ATP concentration changes can be monitored indirectly via fluorometric measurements of $[Mg^{2+}]_i$. This method could be employed in future studies. For instance, K_{ATP} -channel activity could be directly correlated with $[ATP]_i$ by using the cell-permeant AM ester dyes of mag-fura-2 in combination with cell-attached recordings.

Recently, studies have focused more precisely on the function of mitochondrial K_{ATP} -channels and specifically on their contribution to neuroprotection (see Garlid et al. (1997), Gross and Fryer (1999) and Liu et al. (1999)). In the future it would be interesting to investigate these channels in inspiratory neurons and to find out whether they might constitute a protective mechanism against hypoxia, which might be of clinical relevance.

6 Summary

K_{ATP} -channels couple cell metabolism with the electrical excitability of the cell. Their hallmark is inhibition by intracellular ATP but they are also modulated by various intracellular and extracellular factors, which involve complicated signal pathways. These factors include ADP concentration, pH, G-protein-coupled processes and adenosine to mention just the most obvious ones.

The functional relevance of K_{ATP} -channels is well understood in pancreatic β -cells, where they regulate insulin secretion, and in cardiac cells, where they play a part in cardioprotection. Less is known, however, about their significance in neurons. For this reason, K_{ATP} -channels were investigated in respiratory neurons in vitro using the *rhythmic brainstem slice preparation*. This preparation allows simultaneous recordings of respiratory output activity from hypoglossal nerve rootlets and patch-clamp data from single respiratory neurons. By temporal correlation of their activity with the hypoglossal nerve activity, respiratory neurons can be identified and attributed to distinct populations. One subgroup is ideally suited to the study of K_{ATP} -channels: the inspiratory neurons, which fire bursts of action potentials every 3 - 4 sec that are synchronized with inspiration. This ongoing activity is expected to cause high metabolic demands leading to activity-dependent fluctuations of intracellular ATP concentrations. Indeed, K_{ATP} -channels were observed to be persistently active in inspiratory neurons. One of the main objectives of this work was the investigation of whether K_{ATP} -channels in inspiratory neurons were periodically modulated, i.e. whether their open probability changed in the course of a single respiratory cycle. It was found that the channel open probability rose to a maximum during or slightly after the inspiratory burst and then fell back to baseline levels. Parameters that quantitatively describe this behavior were defined and used as criteria to test the channels under conditions affecting the respiratory output (hypoxia, elevation of $[K^+]_e$). The data strongly indicate that the periodic modulation of K_{ATP} -channels is due to $[ATP]_i$ -fluctuations following Na^+/K^+ -pump activity during rhythmic respiratory bursting. Using this data, periodic changes in the ATP concentration underlying K_{ATP} -channel modulation were computed from the open probabilities.

As revealed by single cell PCR analysis of amplified aRNA, K_{ATP} -channels of inspiratory neurons are composed of Kir6.2 and SUR1 subunits and thus correspond to the pancreatic β -cell type. Their gating behavior, however, more closely resembles the channel kinetics

described for the smooth muscle cell type as it displayed at least three closed states and two open states.

In addition, K_{ATP} -channels of inspiratory neurons exhibited two distinct gating modes, corresponding to the low and high channel activity. This feature has not previously been described for K_{ATP} -channels in any other tissue.

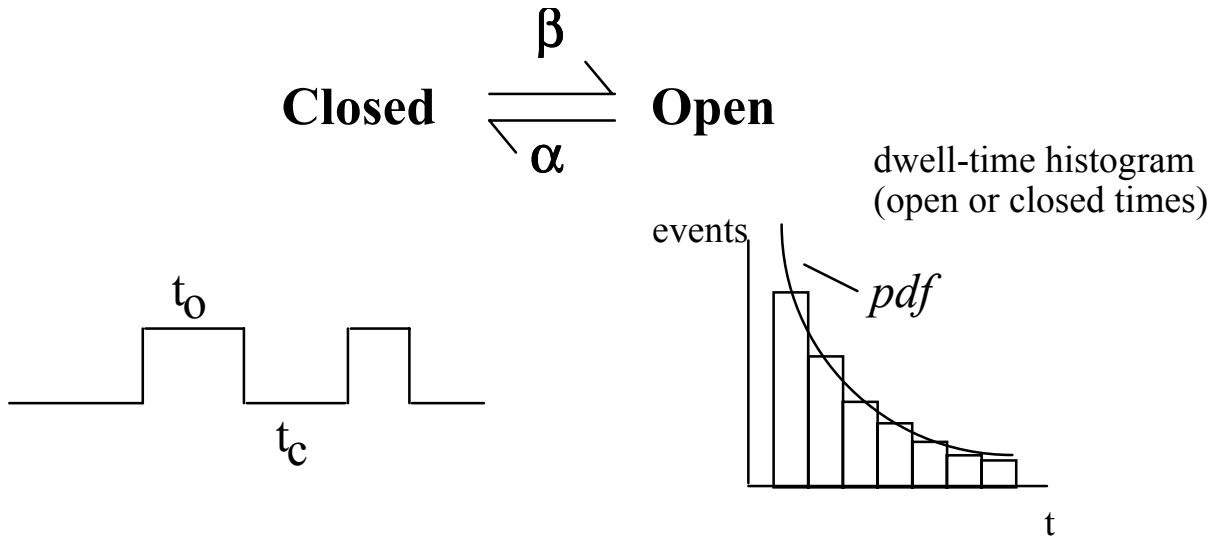
K_{ATP} -channels were activated during hypoxia, which was attributed to significant intracellular ATP-depletion. The intracellular ATP concentration was estimated through microfluorometric measurements according to the following rationale: as ATP is hydrolyzed to ADP, the lower affinity of ADP for Mg^{2+} will lead to a partial release of Mg^{2+} . Signals of the Mg^{2+} -sensitive ratiometric dye mag-fura-2 can thus be used to estimate the changes in $[ATP]_i$. The amplitude of ATP-depletion was revealed to be approximately 500 μM by model simulations of the hypoxic effects that were based on the measured mag-fura-2 signal. The calculations also accounted for ‘contamination’ of the signal by Ca^{2+} changes.

K_{ATP} -channels were potentiated by extracellular application of ATP, indicating the presence of P_2 purinoceptors, which was verified through single cell PCR experiments. The activation of P_2 purinoceptors exerted specific effects on the respiratory rhythm.

When flash photolysis was employed to study changes in Ca^{2+} -homeostasis during hypoxia, it revealed a slowing of Ca^{2+} recovery following photolytic release of Ca^{2+} . In contrast, no effect on membrane potential or membrane currents was observed after flash photolysis of ‘caged-ATP’ compounds, indicating that the caged-ATP-molecule might not be sufficiently protected and participates in blocking the channels even prior to photorelease of ATP. Another set of experiments focused on the measurement of changes of the infrared light transmittance, denoted as the *intrinsic optical signal (IOS)*, which is believed to derive primarily from changes in cell volume. Neuronal cell volume, in turn, is governed by neuronal activity. For this reason, the IOS has previously been utilized as an indirect sensor for neuronal activity changes. In this work the IOS response to hypoxic stimuli was investigated in detail. Regional differences in IOS were observed for distinct cell populations, which presumably reflect differences in sensitivities of these neurons to metabolic stress. Evidence was presented that mechanisms other than cell volume changes, e.g. mitochondrial volume changes, are also involved and contribute to the IOS. IOS responses obtained upon application of K_{ATP} -channel drugs could be explained only by implicating mitochondrial volume changes mediated by mitochondrial K_{ATP} -channels.

7 Appendix

Information about the transition rates between the various states of a channel can be obtained from the distribution of open and closed times. The simplest reaction mechanism of channel gating is represented by a single closed state and a single open state whose lifetimes are determined by the rate constants α and β (3). The corresponding dwell-time histograms can be fitted with a simple exponential probability density function (pdf).



For open (closed) time distributions the probability density function can then be expressed in terms of the time constant $\tau = 1/\alpha$ ($\tau = 1/\beta$):

$$f(t) = \tau^{-1} e^{-t/\tau} \quad (3)$$

For more than one open or closed state the distribution becomes a mixture of exponential functions:

$$f(t) = \sum_{i=1}^N a_i \tau_i^{-1} e^{-t/\tau_i} \quad (4)$$

with

$$\sum_{i=1}^N a_i = 1, \quad (5)$$

where a_i represents the weight of the i th component, τ_i its time constant and N the number of open or closed states.

The time constants, τ_i , can be obtained from the dwell time histograms using *the method of maximum likelihood*. This method can be explained most easily for the case of a two-state channel distribution as described above. Let the data – for instance the closed-time distribution of the channel – consist of M time intervals: $t_1, t_2, t_3, \dots, t_M$.

According to (3) the probability of making the first observation t_1 is given by

$$f(t_1) = \tau^{-1} e^{-t_1/\tau} \quad (6)$$

If the observations are independent, then the probability of making all the observations $(t_1, t_2, t_3, \dots, t_M)$ is proportional to the product of the separate probability densities. This is called the likelihood of τ :

$$Lik(\tau) = f(t_1) \cdot f(t_2) \cdots f(t_M). \quad (7)$$

As this function is a product, it is more convenient to use the logarithm of the likelihood, termed the *log-likelihood*, which is given by:

$$L(\tau) = \sum_{i=1}^M \ln f(t_i) = M \cdot \ln(\tau^{-1}) - \tau^{-1} \sum_{i=1}^M t_i \quad (8)$$

When $L(\tau)$ is plotted against various values of τ the curve passes through a maximum and the value of τ at the maximum is called the maximum likelihood value of τ , and reliably converges to the true time constant if the number of events M is sufficiently large.

The expression for $L(\tau)$ for a single exponential distribution can be generalized for the case of multiple exponential components. When the values of the parameters to be estimated $(\theta_1, \theta_2, \theta_3, \dots)$ are denoted by θ , the j th observation as y_j and the probability of a particular observation y_i by $f(y_i|\theta)$, then the log-likelihood of θ is given by

$$L(\theta) = \sum_{i=1}^M \ln f(y_i|\theta). \quad (9)$$

For a detailed description see chapter 19 in Sakmann and Neher (1995).

8 Abbreviations

ABC	ATP-binding cassette
α,β -MeATP	alpha,beta-methyleneadenosine 5'-triphosphate
ATP	adenosine 5'-triphosphate
ADP	adenosine 5'-diphosphate
AP-5	2-amino-5-phosphonovalerate
CCCP	carbonylcyanide m-chlorophenylhydrazine
CNQX	6-cyano-7-nitroquinoxaline-2,3-dione
DMNPE-caged-ATP	3-O-(1-(4,5-dimethoxy-2-nitrophenyl)ethyl) adenosine-5'-triphosphate
EGTA	glycol-bis(beta-aminoethyl ether)-N,N,N',N'-tetraacetic acid
HEPES	N-2-hydroxyethylpiperazine-N'-2-ethane sulfonic acid
IOS	intrinsic optical signal
K_{ATP} -channels	ATP-sensitive K^+ -channels
KCO	K^+ -channel openers
Kir	inwardly rectifying K^+ -channel subunit
NBF	nucleotide binding folds
NA	nucleus ambiguus
NH	nucleus hypoglossus
NMDA	N-methyl-D-aspartate
NPE-caged-ATP	3-O-(1-(2-nitrophenyl)ethyl)adenosine-5'-triphosphate
PBC	pre-Bötzinger complex
PKA, PKC, PKG	protein kinase A, protein kinase C, protein kinase G
PLC	phospholipase C
PLA ₂	phospholipase A ₂
PPADS	pyridoxal-phosphate-6-azophenyl-2', 4'-disulphonic acid
ROI	region of interest
SUR	sulphonylurea receptor subunit
TTX	tetrodotoxin

9 References

- Abbracchio, M. P., and G. Burnstock. 1994. Purinoceptors: are there families of P2X and P2Y purinoceptors? *Pharmacol Ther.* 64:445-475.
- Abbracchio, M. P., and G. Burnstock. 1998. Purinergic signalling: pathophysiological roles. *Jpn J Pharmacol.* 78:113-145.
- Abe, T., T. Sato, T. Kiyosue, T. Saikawa, T. Sakata, and M. Arita. 1999. Inhibition of Na(+)-K+ pump alleviates the shortening of action potential duration caused by metabolic inhibition via blockade of K_{ATP} channels in coronary perfused ventricular muscles of guinea-pigs. *J Mol Cell Cardiol.* 31:533-542.
- Aguilar-Bryan, L., C. G. Nichols, S. W. Wechsler, J. P. t. Clement, A. E. Boyd, 3rd, G. Gonzalez, H. Herrera-Sosa, K. Nguy, J. Bryan, and D. A. Nelson. 1995. Cloning of the beta cell high-affinity sulfonylurea receptor: a regulator of insulin secretion [see comments]. *Science.* 268:423-426.
- Aitken, P. G., D. Fayuk, G. G. Somjen, and D. A. Turner. 1999. Use of intrinsic optical signals to monitor physiological changes in brain tissue slices [In Process Citation]. *Methods.* 18:91-103.
- Alekseev, A. E., M. E. Kennedy, B. Navarro, and A. Terzic. 1997. Burst kinetics of co-expressed Kir6.2/SUR1 clones: comparison of recombinant with native ATP-sensitive K⁺ channel behavior. *J Membr Biol.* 159:161-168.
- Allen, A., J. Yanushka, J. H. Fitzpatrick, L. W. Jenkins, and D. D. Gilboe. 1989. Acute ultrastructural response of hypoxic hypoxia with relative ischemia in the isolated brain. *Acta Neuropathol.* 78:637-648.
- Alvarez-Leefmans, F. J., H. Cruzblanca, S. M. Gamino, J. Altamirano, A. Nani, and L. Reuss. 1994. Transmembrane ion movements elicited by sodium pump inhibition in *Helix aspersa* neurons. *J Neurophysiol.* 71:1787-1796.
- Ammala, C., K. Bokvist, S. Galt, and P. Rorsman. 1991. Inhibition of ATP-regulated K(+) channels by a photoactivatable ATP- analogue in mouse pancreatic beta-cells. *Biochim Biophys Acta.* 1092:347-349.
- Andrew, R. D., J. R. Adams, and T. M. Polischuk. 1996. Imaging NMDA- and kainate-induced intrinsic optical signals from the hippocampal slice. *J Neurophysiol.* 76:2707-2717.
- Andrew, R. D., C. R. Jarvis, and A. S. Obeidat. 1999. Potential sources of intrinsic optical signals imaged in live brain slices [In Process Citation]. *Methods.* 18:185-196.
- Andrew, R. D., and B. A. MacVicar. 1994. Imaging cell volume changes and neuronal excitation in the hippocampal slice. *Neuroscience.* 62:371-383.
- Ashcroft, F. M. 1988. Adenosine 5'-triphosphate-sensitive potassium channels. *Annu Rev Neurosci.* 11:97-118.
- Ashcroft, F. M., and F. M. Gribble. 1998. Correlating structure and function in ATP-sensitive K⁺ channels. *Trends Neurosci.* 21:288-294.
- Ashcroft, F. M., D. E. Harrison, and S. J. Ashcroft. 1984. Glucose induces closure of single potassium channels in isolated rat pancreatic beta-cells. *Nature.* 312:446-448.
- Ashcroft, F. M., and M. Takei. 1989. ATP-sensitive K⁺ channels in rat pancreatic beta-cells: modulation by ATP and Mg²⁺ ions. *J Physiol (Lond).* 416:349-367.
- Ashcroft, S. J., and F. M. Ashcroft. 1990. Properties and functions of ATP-sensitive K-channels. *Cell Signal.* 2:197-214.
- Baba, A. 1992. [Regulation by chloride ion of astroglial cell functions and morphological transformation]. *Nippon Yakurigaku Zasshi.* 99:297-305.
- Baines, C. P., G. S. Liu, M. Birincioglu, S. D. Critz, M. V. Cohen, and J. M. Downey. 1999. Ischemic preconditioning depends on interaction between mitochondrial K_{ATP} channels and actin cytoskeleton. *Am J Physiol.* 276:H1361-1368.
- Ballanyi, K., J. Doutheil, and J. Brockhaus. 1996. Membrane potentials and microenvironment of rat dorsal vagal cells in vitro during energy depletion. *J Physiol (Lond).* 495:769-784.
- Ballanyi, K., and A. Kulik. 1998. Intracellular Ca²⁺ during metabolic activation of K_{ATP} channels in spontaneously active dorsal vagal neurons in medullary slices. *Eur J Neurosci.* 10:2574-2585.

- Ballanyi, K., K. Muckenhoff, M. C. Bellingham, Y. Okada, P. Scheid, and D. W. Richter. 1994. Activity-related pH changes in respiratory neurones and glial cells of cats. *Neuroreport*. 6:33-36.
- Beavis, A. D., R. D. Brannan, and K. D. Garlid. 1985. Swelling and contraction of the mitochondrial matrix. I. A structural interpretation of the relationship between light scattering and matrix volume. *J Biol Chem*. 260:13424-13433.
- Beech, D. J., H. Zhang, K. Nakao, and T. B. Bolton. 1993a. K channel activation by nucleotide diphosphates and its inhibition by glibenclamide in vascular smooth muscle cells. *Br J Pharmacol*. 110:573-582.
- Beech, D. J., H. Zhang, K. Nakao, and T. B. Bolton. 1993b. Single channel and whole-cell K-currents evoked by levcromakalim in smooth muscle cells from the rabbit portal vein. *Br J Pharmacol*. 110:583-590.
- Berrie, C. P., P. T. Hawkins, L. R. Stephens, T. K. Harden, and C. P. Downes. 1989. Phosphatidylinositol 4,5-bisphosphate hydrolysis in turkey erythrocytes is regulated by P2y purinoceptors. *Mol Pharmacol*. 35:526-532.
- Bianchi, A. L., M. Denavit-Saubie, and J. Champagnat. 1995. Central control of breathing in mammals: neuronal circuitry, membrane properties, and neurotransmitters. *Physiol Rev*. 75:1-45.
- Blazynski, C., and M. T. Perez. 1991. Adenosine in vertebrate retina: localization, receptor characterization, and function. *Cell Mol Neurobiol*. 11:463-484.
- Bohle, T., and K. Benndorf. 1995. Voltage-dependent properties of three different gating modes in single cardiac Na⁺ channels. *Biophys J*. 69:873-882.
- Bossu, J. L., and B. H. Gahwiler. 1996. Distinct modes of channel gating underlie inactivation of somatic K⁺ current in rat hippocampal pyramidal cells in vitro. *J Physiol (Lond)*. 495:383-397.
- Bowers, K. C., A. P. Allshire, and P. H. Cobbold. 1993. Continuous measurements of cytoplasmic ATP in single cardiomyocytes during simulation of the "oxygen paradox". *Cardiovasc Res*. 27:1836-1839.
- Boyer, J. L., C. L. Cooper, and T. K. Harden. 1990. [32P]3'-O-(4-benzoyl)benzoyl ATP as a photoaffinity label for a phospholipase C-coupled P2Y-purinergic receptor. *J Biol Chem*. 265:13515-13520.
- Boyer, J. L., C. P. Downes, and T. K. Harden. 1989. Kinetics of activation of phospholipase C by P2Y purinergic receptor agonists and guanine nucleotides. *J Biol Chem*. 264:884-890.
- Boyer, J. L., I. E. Zohn, K. A. Jacobson, and T. K. Harden. 1994. Differential effects of P2 purinoceptor antagonists on phospholipase C- and adenylyl cyclase-coupled P2Y purinoceptors. *Br J Pharmacol*. 113:614-620.
- Brady, P. A., A. E. Alekseev, L. A. Aleksandrova, L. A. Gomez, and A. Terzic. 1996. A disrupter of actin microfilaments impairs sulfonylurea-inhibitory gating of cardiac K_{ATP} channels. *Am J Physiol*. 271:H2710-2716.
- Buchheim, K., S. Schuchmann, H. Siegmund, H. J. Gabriel, U. Heinemann, and H. Meierkord. 1999. Intrinsic optical signal measurements reveal characteristic features during different forms of spontaneous neuronal hyperactivity associated with ECS shrinkage in vitro. *Eur J Neurosci*. 11:1877-1882.
- Buckley, D. L., J. D. Bui, M. I. Phillips, T. Zelles, B. A. Inglis, H. D. Plant, and S. J. Blackband. 1999. The effect of ouabain on water diffusion in the rat hippocampal slice measured by high resolution NMR imaging. *Magn Reson Med*. 41:137-142.
- Calabresi, P., A. Pisani, N. B. Mercuri, and G. Bernardi. 1995. On the mechanisms underlying hypoxia-induced membrane depolarization in striatal neurons. *Brain*. 118:1027-1038.
- Champagnat, J., M. Denavit-Saubie, S. Moyanova, and G. Rondouin. 1982. Involvement of amino acids in periodic inhibitions of bulbar respiratory neurones. *Brain Res*. 237:351-365.
- Chen, Y., J. R. McNeill, I. Hajek, and L. Hertz. 1992. Effect of vasopressin on brain swelling at the cellular level: do astrocytes exhibit a furosemide--vasopressin-sensitive mechanism for volume regulation? *Can J Physiol Pharmacol*. 70:S367-373.
- Cherniack, N. S., N. H. Edelman, and S. Lahiri. 1970. Hypoxia and hypercapnia as respiratory stimulants and depressants. *Respir Physiol*. 11:113-126.
- Choi, D. W. 1993. NMDA receptors and AMPA/kainate receptors mediate parallel injury in cerebral cortical cultures subjected to oxygen-glucose deprivation. *Prog Brain Res*. 96:137-143.

- Chutkow, W. A., M. C. Simon, M. M. Le Beau, and C. F. Burant. 1996. Cloning, tissue expression, and chromosomal localization of SUR2, the putative drug-binding subunit of cardiac, skeletal muscle, and vascular K_{ATP} channels. *Diabetes*. 45:1439-1445.
- Clapp, L. H., and A. M. Gurney. 1992. ATP-sensitive K⁺ channels regulate resting potential of pulmonary arterial smooth muscle cells. *Am J Physiol*. 262:H916-920.
- Clement, J. P. t., K. Kunjilwar, G. Gonzalez, M. Schwanstecher, U. Panten, L. Aguilar-Bryan, and J. Bryan. 1997. Association and stoichiometry of K(ATP) channel subunits. *Neuron*. 18:827-838.
- Cook, D. L., and C. N. Hales. 1984. Intracellular ATP directly blocks K⁺ channels in pancreatic B-cells. *Nature*. 311:271-273.
- Cook, D. L., L. S. Satin, M. L. Ashford, and C. N. Hales. 1988. ATP-sensitive K⁺ channels in pancreatic beta-cells. Spare-channel hypothesis. *Diabetes*. 37:495-498.
- Cuevas, J., A. L. Bassett, J. S. Cameron, T. Furukawa, R. J. Myerburg, and S. Kimura. 1991. Effect of H⁺ on ATP-regulated K⁺ channels in feline ventricular myocytes. *Am J Physiol*. 261:H755-761.
- Davies, N. W. 1990. Modulation of ATP-sensitive K⁺ channels in skeletal muscle by intracellular protons. *Nature*. 343:375-377.
- Davies, N. W., A. E. Spruce, N. B. Standen, and P. R. Stanfield. 1989. Multiple blocking mechanisms of ATP-sensitive potassium channels of frog skeletal muscle by tetraethylammonium ions. *J Physiol (Lond)*. 413:31-48.
- Davies, N. W., N. B. Standen, and P. R. Stanfield. 1991. ATP-dependent potassium channels of muscle cells: their properties, regulation, and possible functions. *J Bioenerg Biomembr*. 23:509-535.
- Davies, N. W., N. B. Standen, and P. R. Stanfield. 1992. The effect of intracellular pH on ATP-dependent potassium channels of frog skeletal muscle. *J Physiol (Lond)*. 445:549-568.
- Delcour, A. H., and R. W. Tsien. 1993. Altered prevalence of gating modes in neurotransmitter inhibition of N-type calcium channels. *Science*. 259:980-984.
- Donnelly, D. F., C. Jiang, and G. G. Haddad. 1992. Comparative responses of brain stem and hippocampal neurons to O₂ deprivation: in vitro intracellular studies. *Am J Physiol*. 262:L549-554.
- Dunne, M. J., and O. H. Petersen. 1986. GTP and GDP activation of K⁺ channels that can be inhibited by ATP. *Pflugers Arch*. 407:564-565.
- Eberwine, J., H. Yeh, K. Miyashiro, Y. Cao, S. Nair, R. Finnell, M. Zettel, and P. Coleman. 1992. Analysis of gene expression in single live neurons. *Proc Natl Acad Sci U S A*. 89:3010-3014.
- Edwards, F. A. 1994. ATP receptors. *Curr Opin Neurobiol*. 4:347-352.
- Edwards, G., and A. H. Weston. 1993. The pharmacology of ATP-sensitive potassium channels. *Annu Rev Pharmacol Toxicol*. 33:597-637.
- Ezure, K. 1990. Synaptic connections between medullary respiratory neurons and considerations on the genesis of respiratory rhythm. *Prog Neurobiol*. 35:429-450.
- Fabiato, A. 1981. Myoplasmic free calcium concentration reached during the twitch of an intact isolated cardiac cell and during calcium-induced release of calcium from the sarcoplasmic reticulum of a skinned cardiac cell from the adult rat or rabbit ventricle. *J Gen Physiol*. 78:457-497.
- Faehling, M., and F. M. Ashcroft. 1997. Heterogeneity of beta-cell secretion. Possible involvement of K-ATP channels. *Adv Exp Med Biol*. 426:247-252.
- Federico, P., S. G. Borg, A. G. Salkauskus, and B. A. MacVicar. 1994. Mapping patterns of neuronal activity and seizure propagation by imaging intrinsic optical signals in the isolated whole brain of the guinea-pig. *Neuroscience*. 58:461-480.
- Fernandes de Lima, V. M., M. Wiedemann, H. Klottig, H. Rahmann, and W. Hanke. 1997. Exogenous application of gangliosides changes the state of excitability of retinal tissue as demonstrated by retinal spreading depression experiments. *Naunyn Schmiedebergs Arch Pharmacol*. 355:507-514.
- Findlay, I. 1987. The effects of magnesium upon adenosine triphosphate-sensitive potassium channels in a rat insulin-secreting cell line. *J Physiol (Lond)*. 391:611-629.
- Findlay, I. 1992. Effects of pH upon the inhibition by sulphonylurea drugs of ATP-sensitive K⁺ channels in cardiac muscle. *J Pharmacol Exp Ther*. 262:71-79.
- Forestier, C., J. Pierrard, and M. Vivaudou. 1996. Mechanism of action of K channel openers on skeletal muscle K_{ATP} channels. Interactions with nucleotides and protons. *J Gen Physiol*. 107:489-502.
- Fremann, D., B. U. Keller, and D. W. Richter. 1999. Calcium oscillations in rhythmically active respiratory neurones in the brainstem of the mouse. *J Physiol (Lond)*. 515:119-131.

- Furukawa, T., L. Virag, N. Furukawa, T. Sawanobori, and M. Hiraoka. 1994. Mechanism for reactivation of the ATP-sensitive K⁺ channel by MgATP complexes in guinea-pig ventricular myocytes. *J Physiol (Lond)*. 479:95-107.
- Garlid, K. D., P. Paucek, V. Yarov-Yarovoy, H. N. Murray, R. B. Darbenzio, A. J. D'Alonzo, N. J. Lodge, M. A. Smith, and G. J. Grover. 1997. Cardioprotective effect of diazoxide and its interaction with mitochondrial ATP-sensitive K⁺ channels. Possible mechanism of cardioprotection. *Circ Res*. 81:1072-1082.
- Gillis, K. D., W. M. Gee, A. Hammoud, M. L. McDaniel, L. C. Falke, and S. Misler. 1989. Effects of sulfonamides on a metabolite-regulated ATPi-sensitive K⁺ channel in rat pancreatic B-cells. *Am J Physiol*. 257:C1119-1127.
- Greer, J. J., J. C. Smith, and J. L. Feldman. 1992. Glutamate release and presynaptic action of AP4 during inspiratory drive to phrenic motoneurons. *Brain Res*. 576:355-357.
- Gross, G. J., and R. M. Fryer. 1999. Sarcolemmal versus mitochondrial ATP-sensitive K⁺ channels and myocardial preconditioning. *Circ Res*. 84:973-979.
- Grynkiewicz, G., M. Poenie, and R. Y. Tsien. 1985. A new generation of Ca²⁺ indicators with greatly improved fluorescence properties. *J Biol Chem*. 260:3440-3450.
- Haas, M. 1994. The Na-K-Cl cotransporters. *Am J Physiol*. 267:C869-885.
- Haddad, G. G., and D. F. Donnelly. 1990. O₂ deprivation induces a major depolarization in brain stem neurons in the adult but not in the neonatal rat. *J Physiol (Lond)*. 429:411-428.
- Haller, M., C. Heinemann, R. H. Chow, R. Heidelberger, and E. Neher. 1998a. Comparison of secretory responses as measured by membrane capacitance and by amperometry. *Biophys J*. 74:2100-2113.
- Haller, M., S. L. Mironov, and R. D. W. 1998b. Changes in the IR transmittance in the rhythmically active slice in the mice. *Arch.Pflügers*. 435S:R223.
- Harden, T. K., J. L. Boyer, and R. A. Nicholas. 1995. P₂-purinergic receptors: subtype-associated signaling responses and structure. *Annu Rev Pharmacol Toxicol*. 35:541-579.
- Hasbani, M. J., K. L. Hyrc, B. T. Faddis, C. Romano, and M. P. Goldberg. 1998. Distinct roles for sodium, chloride, and calcium in excitotoxic dendritic injury and recovery. *Exp Neurol*. 154:241-258.
- Heinemann, C., R. H. Chow, E. Neher, and R. S. Zucker. 1994. Kinetics of the secretory response in bovine chromaffin cells following flash photolysis of caged Ca²⁺. *Biophys J*. 67:2546-2557.
- Higgins, C. F. 1995. The ABC of channel regulation. *Cell*. 82:693-696.
- Hilgemann, D. W. 1997. Cytoplasmic ATP-dependent regulation of ion transporters and channels: mechanisms and messengers. *Annu Rev Physiol*. 59:193-220.
- Hiraoka, M. 1997. Pathophysiological functions of ATP-sensitive K⁺ channels in myocardial ischemia. *Jpn Heart J*. 38:297-315.
- Hoffmann, E. K. 1992. Cell swelling and volume regulation. *Can J Physiol Pharmacol*. 70:S310-313.
- Holthoff, K., and O. W. Witte. 1998. Intrinsic optical signals in vitro: a tool to measure alterations in extracellular space with two-dimensional resolution. *Brain Res Bull*. 47:649-655.
- Hori, N., and D. O. Carpenter. 1994. Functional and morphological changes induced by transient in vivo ischemia. *Exp Neurol*. 129:279-289.
- Horie, M., H. Irisawa, and A. Noma. 1987. Voltage-dependent magnesium block of adenosine-triphosphate-sensitive potassium channel in guinea-pig ventricular cells. *J Physiol (Lond)*. 387:251-272.
- Housley, G. D. 1998. Extracellular nucleotide signaling in the inner ear. *Mol Neurobiol*. 16:21-48.
- Hu, H., T. Sato, J. Seharaseyon, Y. Liu, D. C. Johns, B. O'Rourke, and E. Marban. 1999. Pharmacological and histochemical distinctions between molecularly defined sarcolemmal K_{ATP} channels and native cardiac mitochondrial K_{ATP} channels. *Mol Pharmacol*. 55:1000-1005.
- Hu, K., D. Duan, G. R. Li, and S. Nattel. 1996. Protein kinase C activates ATP-sensitive K⁺ current in human and rabbit ventricular myocytes. *Circ Res*. 78:492-498.
- Illes, P., and W. Norenberg. 1993. Neuronal ATP receptors and their mechanism of action. *Trends Pharmacol Sci*. 14:50-54.
- Inagaki, N., T. Gono, J. P. Clement, C. Z. Wang, L. Aguilar-Bryan, J. Bryan, and S. Seino. 1996. A family of sulfonylurea receptors determines the pharmacological properties of ATP-sensitive K⁺ channels. *Neuron*. 16:1011-1017.

- Inagaki, N., T. Gonoj, J. P. t. Clement, N. Namba, J. Inazawa, G. Gonzalez, L. Aguilar-Bryan, S. Seino, and J. Bryan. 1995a. Reconstitution of IKATP: an inward rectifier subunit plus the sulfonylurea receptor [see comments]. *Science*. 270:1166-1170.
- Inagaki, N., T. Gonoj, and S. Seino. 1997. Subunit stoichiometry of the pancreatic beta-cell ATP-sensitive K⁺ channel. *FEBS Lett.* 409:232-236.
- Inagaki, N., Y. Tsuura, N. Namba, K. Masuda, T. Gonoj, M. Horie, Y. Seino, M. Mizuta, and S. Seino. 1995b. Cloning and functional characterization of a novel ATP-sensitive potassium channel ubiquitously expressed in rat tissues, including pancreatic islets, pituitary, skeletal muscle, and heart. *J Biol Chem.* 270:5691-5694.
- Isomoto, S., C. Kondo, M. Yamada, S. Matsumoto, O. Higashiguchi, Y. Horio, Y. Matsuzawa, and Y. Kurachi. 1996. A novel sulfonylurea receptor forms with BIR (Kir6.2) a smooth muscle type ATP-sensitive K⁺ channel. *J Biol Chem.* 271:24321-24324.
- Jan, L. Y., and Y. N. Jan. 1994. Potassium channels and their evolving gates. *Nature*. 371:119-122.
- Jiang, C., and G. G. Haddad. 1997. Modulation of K⁺ channels by intracellular ATP in human neocortical neurons. *J Neurophysiol.* 77:93-102.
- Kabakov, A. Y. 1998. Activation of K_{ATP} channels by Na/K pump in isolated cardiac myocytes and giant membrane patches. *Biophys J.* 75:2858-2867.
- Kajioka, S., K. Kitamura, and H. Kuriyama. 1991. Guanosine diphosphate activates an adenosine 5'-triphosphate-sensitive K⁺ channel in the rabbit portal vein. *J Physiol (Lond)*. 444:397-418.
- Kaplan, J. H., and G. C. Ellis-Davies. 1988. Photolabile chelators for the rapid photorelease of divalent cations. *Proc Natl Acad Sci U S A.* 85:6571-6575.
- Kargacin, M. E., and G. J. Kargacin. 1997. Predicted changes in concentrations of free and bound ATP and ADP during intracellular Ca²⁺ signaling. *Am J Physiol.* 273:C1416-1426.
- Karschin, A., J. Brockhaus, and K. Ballanyi. 1998. K_{ATP} channel formation by the sulphonylurea receptors SUR1 with Kir6.2 subunits in rat dorsal vagal neurons in situ. *J Physiol (Lond)*. 509:339-346.
- Kass, I. S., and P. Lipton. 1982. Mechanisms involved in irreversible anoxic damage to the in vitro rat hippocampal slice. *J Physiol (Lond)*. 332:459-472.
- Kim, E., J. Han, W. Ho, and Y. E. Earm. 1997. Modulation of ATP-sensitive K⁺ channels in rabbit ventricular myocytes by adenosine A1 receptor activation. *Am J Physiol.* 272:H325-333.
- Kimelberg, H. K., C. L. Bowman, and H. Hirata. 1986. Anion transport in astrocytes. *Ann N Y Acad Sci.* 481:334-353.
- Kinard, T. A., G. de Vries, A. Sherman, and L. S. Satin. 1999. Modulation of the bursting properties of single mouse pancreatic beta- cells by artificial conductances. *Biophys J.* 76:1423-1435.
- King, B. F., A. Townsend-Nicholson, and G. Burnstock. 1998. Metabotropic receptors for ATP and UTP: exploring the correspondence between native and recombinant nucleotide receptors. *Trends Pharmacol Sci.* 19:506-514.
- Kirsch, G. E., J. Codina, L. Birnbaumer, and A. M. Brown. 1990. Coupling of ATP-sensitive K⁺ channels to A1 receptors by G proteins in rat ventricular myocytes. *Am J Physiol.* 259:H820-826.
- Klingauf, J., and E. Neher. 1997. Modeling buffered Ca²⁺ diffusion near the membrane: implications for secretion in neuroendocrine cells. *Biophys J.* 72:674-690.
- Konishi, M., S. Hollingworth, A. B. Harkins, and S. M. Baylor. 1991. Myoplasmic calcium transients in intact frog skeletal muscle fibers monitored with the fluorescent indicator fura-2. *J Gen Physiol.* 97:271-301.
- Koyano, T., M. Kakei, H. Nakashima, M. Yoshinaga, T. Matsuoka, and H. Tanaka. 1993. ATP-regulated K⁺ channels are modulated by intracellular H⁺ in guinea-pig ventricular cells. *J Physiol (Lond)*. 463:747-766.
- Kreisman, N. R., and J. C. LaManna. 1999. Rapid and slow swelling during hypoxia in the CA1 region of rat hippocampal slices. *J Neurophysiol.* 82:320-329.
- Krishtal, O. A., S. M. Marchenko, and A. G. Obukhov. 1988. Cationic channels activated by extracellular ATP in rat sensory neurons. *Neuroscience.* 27:995-1000.
- Larsson, O., H. Kindmark, R. Brandstrom, B. Fredholm, and P. O. Berggren. 1996. Oscillations in K_{ATP} channel activity promote oscillations in cytoplasmic free Ca²⁺ concentration in the pancreatic beta cell. *Proc Natl Acad Sci U S A.* 93:5161-5165.
- Lazriev, I. L., I. K. Svanidze, A. Tsitsishvili, and E. I. Dzamoeva. 1980. [Ultrastruct characteristics of neurons and synapses in the central cortex during circulatory hypoxia]. *Tsitologiya.* 22:139-143.

- Le Corrone, H., B. Hue, and R. M. Pitman. 1999. Ionic mechanisms underlying depolarizing responses of an identified insect motor neuron to short periods of hypoxia. *J Neurophysiol.* 81:307-318.
- Lederer, W. J., and C. G. Nichols. 1989. Nucleotide modulation of the activity of rat heart ATP-sensitive K⁺ channels in isolated membrane patches. *J Physiol (Lond).* 419:193-211.
- Leysens, A., A. V. Nowicky, L. Patterson, M. Crompton, and M. R. Duchen. 1996. The relationship between mitochondrial state, ATP hydrolysis, [Mg²⁺]_i and [Ca²⁺]_i studied in isolated rat cardiomyocytes. *J Physiol (Lond).* 496:111-128.
- Liang, B. T. 1996. Direct preconditioning of cardiac ventricular myocytes via adenosine A1 receptor and K_{ATP} channel. *Am J Physiol.* 271:H1769-1777.
- Light, P. E., A. A. Sabir, B. G. Allen, M. P. Walsh, and R. J. French. 1996. Protein kinase C-induced changes in the stoichiometry of ATP binding activate cardiac ATP-sensitive K⁺ channels. A possible mechanistic link to ischemic preconditioning. *Circ Res.* 79:399-406.
- Lim, W., S. J. Kim, H. D. Yan, and J. Kim. 1997. Ca²⁺-channel-dependent and -independent inhibition of exocytosis by extracellular ATP in voltage-clamped rat adrenal chromaffin cells. *Pflugers Arch.* 435:34-42.
- Lipscombe, D., S. Kongsamut, and R. W. Tsien. 1989. Alpha-adrenergic inhibition of sympathetic neurotransmitter release mediated by modulation of N-type calcium-channel gating. *Nature.* 340:639-642.
- Lipton, P. 1973. Effects of membrane depolarization on light scattering by cerebral cortical slices. *J Physiol (Lond).* 231:365-383.
- Liu, Y., W. D. Gao, B. O'Rourke, and E. Marban. 1996. Synergistic modulation of ATP-sensitive K⁺ currents by protein kinase C and adenosine. Implications for ischemic preconditioning. *Circ Res.* 78:443-454.
- Liu, Y., T. Sato, J. Seharaseyon, A. Szewczyk, B. O'Rourke, and E. Marban. 1999. Mitochondrial ATP-dependent potassium channels. Viable candidate effectors of ischemic preconditioning. *Ann N Y Acad Sci.* 874:27-37.
- Loffler-Walz, C., and U. Quast. 1998. Disruption of the actin cytoskeleton abolishes high affinity 3H-glibenclamide binding in rat aortic rings. *Naunyn Schmiedebergs Arch Pharmacol.* 357:183-185.
- Macouillard-Poullietier de, G., M. A. Belaud-Rotureau, P. Voisin, N. Leducq, F. Belloc, P. Canioni, and P. Diolez. 1998. Flow cytometric analysis of mitochondrial activity in situ: application to acetylceramide-induced mitochondrial swelling and apoptosis. *Cytometry.* 33:333-339.
- MacVicar, B. A., and D. Hochman. 1991. Imaging of synaptically evoked intrinsic optical signals in hippocampal slices. *J Neurosci.* 11:1458-1469.
- Mar, T. 1981. Measurement of mitochondrial volume independent of refractive index by light scattering. *J Biochem Biophys Methods.* 4:177-184.
- Martell, A. E., and R. M. Smith. 1982. Critical Stability Constants. Plenum, New York.
- Matsuura, H., and T. Ehara. 1996. Modulation of the muscarinic K⁺ channel by P2 purinoceptors in guinea-pig atrial myocytes. *J Physiol (Lond).* 497:379-393.
- Mauerer, U. R., E. L. Boulpaep, and A. S. Segal. 1998. Regulation of an inwardly rectifying ATP-sensitive K⁺ channel in the basolateral membrane of renal proximal tubule. *J Gen Physiol.* 111:161-180.
- Mercuri, N. B., A. Bonci, S. W. Johnson, F. Stratta, P. Calabresi, and G. Bernardi. 1994. Effects of anoxia on rat midbrain dopamine neurons. *J Neurophysiol.* 71:1165-1173.
- Metzger, F., C. Loffler, and U. Quast. 1997. Sulphonylurea binding in rat isolated glomeruli: pharmacological characterization and dependence on cell metabolism and cytoskeleton. *Naunyn Schmiedebergs Arch Pharmacol.* 355:141-149.
- Minamikawa, T., D. A. Williams, D. N. Bowser, and P. Nagley. 1999. Mitochondrial permeability transition and swelling can occur reversibly without inducing cell death in intact human cells. *Exp Cell Res.* 246:26-37.
- Mironov, S. L. 1994. Metabotropic ATP receptor in hippocampal and thalamic neurones: pharmacology and modulation of Ca²⁺ mobilizing mechanisms. *Neuropharmacology.* 33:1-13.
- Mironov, S. L. 1995. Plasmalemmal and intracellular Ca²⁺ pumps as main determinants of slow Ca²⁺ buffering in rat hippocampal neurones. *Neuropharmacology.* 34:1123-1132.
- Mironov, S. L., K. Langohr, M. Haller, and D. W. Richter. 1998. Hypoxia activates ATP-dependent potassium channels in inspiratory neurones of neonatal mice. *J Physiol (Lond).* 509:755-766.

- Mironov, S. L., K. Langohr, and D. W. Richter. 1999. A1 adenosine receptors modulate respiratory activity of the neonatal mouse via the cAMP-mediated signaling pathway. *J Neurophysiol.* 81:247-255.
- Mironov, S. L., and D. W. Richter. 2000. Intracellular signalling pathways modulate K(ATP) channels in inspiratory brainstem neurones and their hypoxic activation: involvement of metabotropic receptors, G-proteins and cytoskeleton. *Brain Res.* 853:60-67.
- Misler, S., D. W. Barnett, K. D. Gillis, and D. M. Pressel. 1992. Electrophysiology of stimulus-secretion coupling in human beta-cells. *Diabetes.* 41:1221-1228.
- Misler, S., and G. Giebisch. 1992. ATP-sensitive potassium channels in physiology, pathophysiology, and pharmacology. *Curr Opin Nephrol Hypertens.* 1:21-33.
- Miura, T., and A. Tsuchida. 1999. Adenosine and preconditioning revisited. *Clin Exp Pharmacol Physiol.* 26:92-99.
- Mosbacher, J., R. Maier, B. Fakler, A. Glatz, J. Crespo, and G. Bilbe. 1998. P2Y receptor subtypes differentially couple to inwardly-rectifying potassium channels. *FEBS Lett.* 436:104-110.
- Mukai, E., H. Ishida, S. Kato, Y. Tsuura, S. Fujimoto, A. Ishida-Takahashi, M. Horie, K. Tsuda, and Y. Seino. 1998. Metabolic inhibition impairs ATP-sensitive K⁺ channel block by sulfonylurea in pancreatic beta-cells. *Am J Physiol.* 274:E38-44.
- Muller, M., and G. G. Somjen. 1998. Inhibition of major cationic inward currents prevents spreading depression-like hypoxic depolarization in rat hippocampal tissue slices. *Brain Res.* 812:1-13.
- Muller, M., and G. G. Somjen. 1999. Intrinsic optical signals in rat hippocampal slices during hypoxia-induced spreading depression-like depolarization. *J Neurophysiol.* 82:1818-1831.
- Murayama, T., Y. Yakushi, A. Watanabe, and Y. Nomura. 1998. P2 receptor-mediated inhibition of adenylyl cyclase in PC12 cells. *Eur J Pharmacol.* 348:71-76.
- Nichols, C. G., W. J. Lederer, and M. B. Cannell. 1991. ATP dependence of K_{ATP} channel kinetics in isolated membrane patches from rat ventricle. *Biophys J.* 60:1164-1177.
- Nichols, C. G., E. Niggli, and W. J. Lederer. 1990. Modulation of ATP-sensitive potassium channel activity by flash-photolysis of 'caged-ATP' in rat heart cells. *Pflugers Arch.* 415:510-512.
- Nishizaki, T., and Y. Ikeuchi. 1996. Adenosine evokes potassium currents by protein kinase C activated via a novel signaling pathway in superior colliculus neurons. *FEBS Lett.* 378:1-6.
- Noma, A. 1983. ATP-regulated K⁺ channels in cardiac muscle. *Nature.* 305:147-148.
- North, R. A., and E. A. Barnard. 1997. Nucleotide receptors. *Curr Opin Neurobiol.* 7:346-357.
- O'Reilly, J. P., C. Jiang, and G. G. Haddad. 1995. Major differences in response to graded hypoxia between hypoglossal and neocortical neurons. *Brain Res.* 683:179-186.
- O'Rourke, B., B. M. Ramza, and E. Marban. 1994. Oscillations of membrane current and excitability driven by metabolic oscillations in heart cells. *Science.* 265:962-966.
- Obeidat, A. S., and R. D. Andrew. 1998. Spreading depression determines acute cellular damage in the hippocampal slice during oxygen/glucose deprivation. *Eur J Neurosci.* 10:3451-3461.
- Ohno-Shosaku, T., B. J. Zunkler, and G. Trube. 1987. Dual effects of ATP on K⁺ currents of mouse pancreatic beta-cells. *Pflugers Arch.* 408:133-138.
- Palecek, J., M. B. Lips, and B. U. Keller. 1999. Calcium dynamics and buffering in motoneurons of the mouse spinal cord. *J Physiol (Lond).* 520 Pt 2:485-502.
- Palmer, L. G., and G. Frindt. 1996. Gating of Na channels in the rat cortical collecting tubule: effects of voltage and membrane stretch. *J Gen Physiol.* 107:35-45.
- Park, J. S., M. C. Bateman, and M. P. Goldberg. 1996. Rapid alterations in dendrite morphology during sublethal hypoxia or glutamate receptor activation. *Neurobiol Dis.* 3:215-227.
- Patel, A. J., I. Lauritzen, M. Lazdunski, and E. Honore. 1998. Disruption of mitochondrial respiration inhibits volume-regulated anion channels and provokes neuronal cell swelling. *J Neurosci.* 18:3117-3123.
- Pierrefiche, O., A. M. Bischoff, and D. W. Richter. 1996. ATP-sensitive K⁺ channels are functional in expiratory neurones of normoxic cats. *J Physiol (Lond).* 494:399-409.
- Pierrefiche, O., A. M. Bischoff, D. W. Richter, and K. M. Spyer. 1997. Hypoxic response of hypoglossal motoneurons in the in vivo cat. *J Physiol (Lond).* 505:785-795.
- Pierrefiche, O., A. S. Foutz, and M. Denavit-Saubie. 1993. Effects of GABAB receptor agonists and antagonists on the bulbar respiratory network in cat. *Brain Res.* 605:77-84.
- Poenie, M., and R. Tsien. 1986. Fura-2: a powerful new tool for measuring and imaging [Ca²⁺]_i in single cells. *Prog Clin Biol Res.* 210:53-56.

- Polischuk, T. M., and R. D. Andrew. 1996. Real-time imaging of intrinsic optical signals during early excitotoxicity evoked by domoic acid in the rat hippocampal slice. *Can J Physiol Pharmacol.* 74:712-722.
- Polischuk, T. M., C. R. Jarvis, and R. D. Andrew. 1998. Intrinsic optical signaling denoting neuronal damage in response to acute excitotoxic insult by domoic acid in the hippocampal slice. *Neurobiol Dis.* 4:423-437.
- Proks, P., M. Takano, and F. M. Ashcroft. 1994. Effects of intracellular pH on ATP-sensitive K^+ channels in mouse pancreatic beta-cells. *J Physiol (Lond).* 475:33-44.
- Qin, F., A. Auerbach, and F. Sachs. 1996. Estimating single-channel kinetic parameters from idealized patch-clamp data containing missed events. *Biophys J.* 70:264-280.
- Qin, F., A. Auerbach, and F. Sachs. 1997. Maximum likelihood estimation of aggregated Markov processes. *Proc R Soc Lond B Biol Sci.* 264:375-383.
- Raju, B., E. Murphy, L. A. Levy, R. D. Hall, and R. E. London. 1989. A fluorescent indicator for measuring cytosolic free magnesium. *Am J Physiol.* 256:C540-548.
- Richter, D. W. 1982. Generation and maintenance of the respiratory rhythm. *J Exp Biol.* 100:93-107.
- Richter, D. W., K. Ballanyi, and S. Schwarzacher. 1992. Mechanisms of respiratory rhythm generation. *Curr Opin Neurobiol.* 2:788-793.
- Richter, D. W., A. Bischoff, K. Anders, M. Bellingham, and U. Windhorst. 1991. Response of the medullary respiratory network of the cat to hypoxia. *J Physiol (Lond).* 443:231-256.
- Richter, D. W., H. Camerer, and U. Sonnhof. 1978. Changes in extracellular potassium during the spontaneous activity of medullary respiratory neurones. *Pflugers Arch.* 376:139-149.
- Richter, D. W., P. M. Lalley, O. Pierrefiche, A. Haji, A. M. Bischoff, B. Wilken, and F. Hanefeld. 1997. Intracellular signal pathways controlling respiratory neurons. *Respir Physiol.* 110:113-123.
- Richter, D. W., P. Schmidt-Garcon, O. Pierrefiche, A. M. Bischoff, and P. M. Lalley. 1999. Neurotransmitters and neuromodulators controlling the hypoxic respiratory response in anaesthetized cats [see comments]. *J Physiol (Lond).* 514:567-578.
- Rorsman, P., P. Arkhammar, K. Bokvist, C. Hellerstrom, T. Nilsson, M. Welsh, N. Welsh, and P. O. Berggren. 1989. Failure of glucose to elicit a normal secretory response in fetal pancreatic beta cells results from glucose insensitivity of the ATP- regulated K^+ channels. *Proc Natl Acad Sci U S A.* 86:4505-4509.
- Rose, C. R., Y. Kovalchuk, J. Eilers, and A. Konnerth. 1999. Two-photon Na^+ imaging in spines and fine dendrites of central neurons. *Pflugers Arch - Eur J Physiol.* 439:201-207.
- Rudolphi, K. A., P. Schubert, F. E. Parkinson, and B. B. Fredholm. 1992. Adenosine and brain ischemia. *Cerebrovasc Brain Metab Rev.* 4:346-369.
- Sakmann, B., and E. Neher. 1995. Single-Channel Recording. Plenum Press, New York and London.
- Sakura, H., C. Ammala, P. A. Smith, F. M. Gribble, and F. M. Ashcroft. 1995. Cloning and functional expression of the cDNA encoding a novel ATP- sensitive potassium channel subunit expressed in pancreatic beta-cells, brain, heart and skeletal muscle. *FEBS Lett.* 377:338-344.
- Sawynok, J. 1998. Adenosine receptor activation and nociception. *Eur J Pharmacol.* 347:1-11.
- Schmid, K., A. S. Foutz, and M. Denavit-Saubie. 1996. Inhibitions mediated by glycine and GABAA receptors shape the discharge pattern of bulbar respiratory neurons. *Brain Res.* 710:150-160.
- Schmidt, C., M. C. Bellingham, and D. W. Richter. 1995. Adenosinergic modulation of respiratory neurones and hypoxic responses in the anaesthetized cat. *J Physiol (Lond).* 483:769-781.
- Schurr, A., R. S. Payne, M. F. Heine, and B. M. Rigor. 1995. Hypoxia, excitotoxicity, and neuroprotection in the hippocampal slice preparation. *J Neurosci Methods.* 59:129-138.
- Schwarzacher, S. W., J. C. Smith, and D. W. Richter. 1995. Pre-Botzinger complex in the cat. *J Neurophysiol.* 73:1452-1461.
- Shimizu, T., and M. Nakamura. 1992. Ouabain-induced cell swelling in rabbit connecting tubule: evidence for thiazide-sensitive Na^+ - Cl^- cotransport. *Pflugers Arch.* 421:314-321.
- Shyng, S., and C. G. Nichols. 1997. Octameric stoichiometry of the K_{ATP} channel complex. *J Gen Physiol.* 110:655-664.
- Smith, J. C., H. H. Ellenberger, K. Ballanyi, D. W. Richter, and J. L. Feldman. 1991. Pre-Botzinger complex: a brainstem region that may generate respiratory rhythm in mammals. *Science.* 254:726-729.
- Smith, J. C., J. J. Greer, G. S. Liu, and J. L. Feldman. 1990a. Neural mechanisms generating respiratory pattern in mammalian brain stem-spinal cord in vitro. I. Spatiotemporal patterns of motor and medullary neuron activity. *J Neurophysiol.* 64:1149-1169.

- Smith, P. A., F. M. Ashcroft, and P. Rorsman. 1990b. Simultaneous recordings of glucose dependent electrical activity and ATP-regulated K^{+} -currents in isolated mouse pancreatic beta-cells. *FEBS Lett.* 261:187-190.
- Smith, R. M., and A. E. Martell. 1975a. Critical Stability Constants: Amines. Plenum, New York.
- Smith, R. M., and A. E. Martell. 1975b. Critical Stability Constants: Amino Acids. Plenum, New York.
- Smith, T. W., R. L. Rasmusson, L. A. Lobaugh, and M. Lieberman. 1993. Na^{+}/K^{+} pump inhibition induces cell shrinkage in cultured chick cardiac myocytes. *Basic Res Cardiol.* 88:411-420.
- Spruce, A. E., N. B. Standen, and P. R. Stanfield. 1985. Voltage-dependent ATP-sensitive potassium channels of skeletal muscle membrane. *Nature.* 316:736-738.
- Spruce, A. E., N. B. Standen, and P. R. Stanfield. 1987. Studies of the unitary properties of adenosine-5'-triphosphate- regulated potassium channels of frog skeletal muscle. *J Physiol (Lond).* 382:213-236.
- Standen, N. B., J. M. Quayle, N. W. Davies, J. E. Brayden, Y. Huang, and M. T. Nelson. 1989. Hyperpolarizing vasodilators activate ATP-sensitive K^{+} channels in arterial smooth muscle. *Science.* 245:177-180.
- Stoner, C. D., and H. D. Sirak. 1969. Osmotically-induced alterations in volume and ultrastructure of mitochondria isolated from rat liver and bovine heart. *J Cell Biol.* 43:521-538.
- Tabarean, I. V., P. Juranka, and C. E. Morris. 1999. Membrane stretch affects gating modes of a skeletal muscle sodium channel. *Biophys J.* 77:758-774.
- Takano, M., D. Y. Qin, and A. Noma. 1990. ATP-dependent decay and recovery of K^{+} channels in guinea pig cardiac myocytes. *Am J Physiol.* 258:H45-50.
- Tang, L., M. Parker, Q. Fei, and R. Loutzenhiser. 1999. Afferent arteriolar adenosine A2a receptors are coupled to K_{ATP} in in vitro perfused hydronephrotic rat kidney. *Am J Physiol.* 277:F926-933.
- Terzic, A., I. Findlay, Y. Hosoya, and Y. Kurachi. 1994a. Dualistic behavior of ATP-sensitive K^{+} channels toward intracellular nucleoside diphosphates. *Neuron.* 12:1049-1058.
- Terzic, A., A. Jahangir, and Y. Kurachi. 1995. Cardiac ATP-sensitive K^{+} channels: regulation by intracellular nucleotides and K^{+} channel-opening drugs. *Am J Physiol.* 269:C525-545.
- Terzic, A., R. T. Tung, A. Inanobe, T. Katada, and Y. Kurachi. 1994b. G proteins activate ATP-sensitive K^{+} channels by antagonizing ATP- dependent gating. *Neuron.* 12:885-893.
- Thomas, S. A., and R. I. Hume. 1993. Single potassium channel currents activated by extracellular ATP in developing chick skeletal muscle: a role for second messengers. *J Neurophysiol.* 69:1556-1566.
- Thomas, T., V. Ralevic, C. A. Gadd, and K. M. Spyer. 1999. Central CO_2 chemoreception: a mechanism involving P2 purinoceptors localized in the ventrolateral medulla of the anaesthetized rat. *J Physiol (Lond).* 517:899-905.
- Thomas, T., and K. M. Spyer. 2000. ATP as a mediator of mammalian central CO_2 chemoreception. *J Physiol (Lond).* 523:441-447.
- Tokube, K., T. Kiyosue, and M. Arita. 1996. Openings of cardiac K_{ATP} channel by oxygen free radicals produced by xanthine oxidase reaction. *Am J Physiol.* 271:H478-489.
- Torres, J. E., N. R. Kreisman, and D. Gozal. 1997. Nitric oxide modulates in vitro intrinsic optical signal and neural activity in the nucleus tractus solitarius of the rat. *Neurosci Lett.* 232:175-178.
- Trafton, J., G. Tombaugh, S. Yang, and R. Sapolsky. 1996. Salutary and deleterious effects of acidity on an indirect measure of metabolic rate and ATP concentrations in CNS cultures. *Brain Res.* 731:122-131.
- Trapp, S., P. Proks, S. J. Tucker, and F. M. Ashcroft. 1998. Molecular analysis of ATP-sensitive K channel gating and implications for channel inhibition by ATP. *J Gen Physiol.* 112:333-349.
- Turner, D. A., P. G. Aitken, and G. G. Somjen. 1995. Optical mapping of translucence changes in rat hippocampal slices during hypoxia. *Neurosci Lett.* 195:209-213.
- Tusnady, G. E., E. Bakos, A. Varadi, and B. Sarkadi. 1997. Membrane topology distinguishes a subfamily of the ATP-binding cassette (ABC) transporters. *FEBS Lett.* 402:1-3.
- Ulmer, H. J., V. M. de Lima, and W. Hanke. 1995. Effects of nitric oxide on the retinal spreading depression. *Brain Res.* 691:239-242.
- Urbach, V., E. Van Kerkhove, D. Maguire, and B. J. Harvey. 1996. Cross-talk between ATP-regulated K^{+} channels and Na^{+} transport via cellular metabolism in frog skin principal cells. *J Physiol (Lond).* 491:99-109.

- Vaziri, C., and C. P. Downes. 1992. Association of a receptor and G-protein-regulated phospholipase C with the cytoskeleton. *J Biol Chem.* 267:22973-22981.
- Virsolvy-Vergine, A., H. Leray, S. Kuroki, B. Lupo, M. Dufour, and D. Bataille. 1992. Endosulfine, an endogenous peptidic ligand for the sulfonylurea receptor: purification and partial characterization from ovine brain. *Proc Natl Acad Sci U S A.* 89:6629-6633.
- Vladimirov Iu, A., and E. M. Kogan. 1981. [Mechanisms of disorders of the bioenergetic functions of mitochondrial membranes in hypoxia]. *Kardiologiya.* 21:82-85.
- Walz, W. 1992. Role of Na/K/Cl cotransport in astrocytes. *Can J Physiol Pharmacol.* 70:S260-262.
- Wang, Y., and M. Ashraf. 1999. Role of protein kinase C in mitochondrial K_{ATP} channel-mediated protection against Ca²⁺ overload injury in rat myocardium. *Circ Res.* 84:1156-1165.
- Wilken, B., J. M. Ramirez, I. Probst, D. W. Richter, and F. Hanefeld. 1998. Creatine protects the central respiratory network of mammals under anoxic conditions. *Pediatr Res.* 43:8-14.
- Xia, Y., and G. G. Haddad. 1991. Major differences in CNS sulfonylurea receptor distribution between the rat (newborn, adult) and turtle. *J Comp Neurol.* 314:278-289.
- Yabe, K., Y. Nasa, and S. Takeo. 1995. Hypoxic preconditioning in isolated rat hearts: non-involvement of activation of adenosine A1 receptor, Gi protein, and ATP-sensitive K⁺ channel. *Heart Vessels.* 10:294-303.
- Yamada, M., S. Isomoto, S. Matsumoto, C. Kondo, T. Shindo, Y. Horio, and Y. Kurachi. 1997. Sulphonylurea receptor 2B and Kir6.1 form a sulphonylurea-sensitive but ATP-insensitive K⁺ channel. *J Physiol (Lond).* 499:715-720.
- Yao, Z., and G. J. Gross. 1994. Activation of ATP-sensitive potassium channels lowers threshold for ischemic preconditioning in dogs. *Am J Physiol.* 267:H1888-1894.
- Yokoshiki, H., Y. Katsube, M. Sunugawa, T. Seki, and N. Sperelakis. 1997. Disruption of actin cytoskeleton attenuates sulfonylurea inhibition of cardiac ATP-sensitive K⁺ channels. *Pflugers Arch.* 434:203-205.
- Zawar, C., T. D. Plant, C. Schirra, A. Konnerth, and B. Neumcke. 1999. Cell-type specific expression of ATP-sensitive potassium channels in the rat hippocampus. *J Physiol (Lond).* 514:327-341.
- Zeevalk, G. D., and W. J. Nicklas. 1996. Hypothermia and metabolic stress: narrowing the cellular site of early neuroprotection. *J Pharmacol Exp Ther.* 279:332-339.
- Zimmermann, H. 1994. Signalling via ATP in the nervous system. *Trends Neurosci.* 17:420-426.

Acknowledgements

I would like to thank first of all Prof. Dr. D.W. Richter for giving me the opportunity to work on this project, for providing me with the necessary work environment and for his constant support throughout.

I am also greatly grateful to Prof. Dr. W. Felsch for his interest in this thesis and for representing it at the physics department of the University of Göttingen.

I wish to thank PD Dr. Mironov for answering all my questions and helping me with the experimental setup.

My special thanks go to Hella Timmermann and Nicole Hartelt for their expert technical assistance and also to Jürgen Huhnold for his innovative technical contributions.

Finally, I would like to thank Andreas Karschin for the collaboration with the single cell PCR experiments.

Lebenslauf

- 16.02.1970 geboren in Hannover
Eltern: Herbert Haller
Dr. Karin Haller
- 1976-1986 Schulbesuch in Hannover
- 1986-1988 Besuch der St.-Felix-School, England (A-levels)
- 1988-1990 Oberstufe und Abitur an der Leibnizschule, Hannover
- Okt.1990 Immatrikulation in Physik an der Universität Göttingen
- Okt 1992 Vordiplom Physik
- 1993/1994 einjähriger Studienaufenthalt an der University of California, San Diego im Rahmen des Education Abroad Program der Universität Göttingen
- 1995-1996 Diplomarbeit am Max-Planck-Institut für biophysikalische Chemie in Göttingen unter Anleitung von Prof. Neher. Thema: "Untersuchung zweier kinetischer Komponenten bei der Sekretion in chromaffinen Zellen"
(angestellt als wissenschaftliche Hilfskraft)
- Mai 1996 Diplom Physik
- seit WS 1996 Doktorarbeit im II. Physiologischen Institut der Universität Göttingen unter Anleitung von Prof. Richter.
(angestellt als wissenschaftliche Mitarbeiterin)